# DEVELOPMENT OF LABORATORY SPINE WITH ARTIFICIAL MUSCLES

Being a Thesis submitted for the Degree of PhD

In the University of Hull

By

Amit Swamy

September 2007

Success comes to those who think they can succeed.

Experiences teaches reasoning,
Reasoning with justification is hard rock.

Their can be many failures, but only one success in each journeys we make.

# ACKNOWLEGMENTS

I would really like to acknowledge this research to my friend called JESUS who helped me to devote my time in study and achieve something thoughtful. The important parameters to my motivation are my parents with my lovely brother in India and especially my granny up their in heaven; have all been the real strength behind my success. The success of this research is a small gift that I would give my most loving and never trying feet of my Dad and mom, who are still fighting hard for their bread.

Another most important aspect of my research is my supervisor Dr Michael Fagan, who has been the right hope and guide without his directions and support I would have never made it this far.

This research is not a one mans makeover its indebted to the following people, firstly Dr Catherine Dobson for her encouraging words, John in the mechanical workshop for all help provided and understanding my drawings, Ernie for keeping pace with solving computer problems and lastly Mike Poole and Design Enterprise Centre for permitting me to use their machines. There is also that special person who makes me feel like I am a beginner in whose dreams I have perfected the art of improving and every Pico-second miss her (mi breath Neelu).

# DEVELOPMENT OF LABORATORY SPINE WITH ARTIFICIAL MUSCLES

There is an increasing demand for spinal surgery and a growing number of new spinal implants and surgical procedures being offered by orthopaedic companies. However, the testing of spinal implants and spinal instrumentation is problematic, with testing in cadavers and animals becoming increasingly difficult and both having significant limitations.

Thus the aim of this research is to develop an artificial laboratory spine that will have the same physical and biomechanical properties as the human spine. Validation of computer model is difficult hence an active artificial laboratory spine is being developed. A number of spinal elements have been produced and are being investigated, including an artificial intervertebral disc with different material properties to allow it to simulate different clinical conditions.

The study is the first of its kind with the characteristics of the disc material that have been assessed in the laboratory, artificial muscles and spring elements and with normal physiological movements compared and validated from the reported literature. The model was used to investigate the potential of Shape Memory Alloy wires to act as artificial muscles and to control the movement of the spine. It is anticipated that the laboratory spine will have a number of other applications, in particular in the assessment of spinal instrumentation and testing.

An actual geometry laboratory spine is also generated with suitable manufacturing technique for intervertebral disc, which has an accurate surface profile to fit between the two vertebral bodies above and below it, is discussed in this thesis.

# GLOSSARY

| | |
|---|---|
| **Austenite** | Higher temperature phase with strained crystallographic structure. |
| **Coronal plane** | 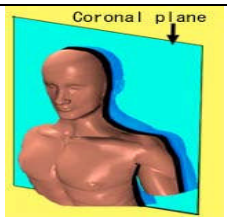  Plane which vertically divides body back and forth and perpendicular to sagittal plane (Reference planes, 2007 ) |
| **CT** | Computerised tomography - non-invasive radiological imaging technique. |
| **Extension** | Backward bending of the body. ( Gray and Pick,1987) |
| **Fascicule** | Bundles of nerve and muscle fibre. |
| **Flexion** | Forward bending of the body. ( Gray and Pick,1987) |
| **Foramen** | The natural opening in the intervertebral body walls. |
| **Forward bias time** | The time to heat the wire, to the strained condition. |
| **Least square error method** | Method for calculating the best fir curve to a set of data points. |
| **Lateral bending** | Bending side by side of the body. ( Gray and Pick,1987) |

| | |
|---|---|
| **Lordosis** | Inward or outward curvature formed by the vertebral bodies, i.e. S-curve of the healthy lumbar spine. |
| **Martensite** | Lower temperature phase with the relaxed crystallographic structure. |
| **Modelling** | Theoretical representation simulating the behaviour or activity of systems (biological or otherwise). |
| **Pseudo-elastic** | Elastic under certain conditions for example when heated. |
| **Reverse bias time** | The time to cool the wire, back to reach its original condition. |
| **Sagittal plane** | 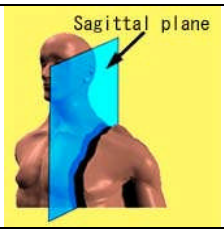  Plane which vertically divides body into right and left section. (Reference planes, 2007 ) |
| **SMA** | Shape Memory Alloy. |
| **Stereolithography (STL)** | A computer controlled method of producing dimensionally accurate models by the curing of a photo-sensitive resin by a laser. |
| **Stimulation frequency** | Twitch of muscle. Response to stimulus. |
| **Transverse plane** | 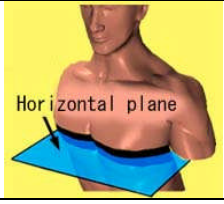  Plane that is parallel to the ground and perpendicular to sagittal plane. (Reference planes, 2007 ) |
| **Torsional movement** | Rotation of the body. (Gray and Pick,1987) |
| **Via points** | Cross over points used for muscle attachments. |
| **Y-displacement** | Displacement taken in Sagittal plane measured in Y axis. |

# INDEX

Declaration

Acknowledgements

Abstract for “Development of laboratory spine with artificial muscles”.

Glossary.

Table of contents.

## Table of contents

**Chapter 1 Introduction……7**

1.1- Research background.

1.2- Overview of thesis.

**Chapter 2 The lumbar spine……..10**

2.1 – Introduction.

2.2 – The lumbar spine structure.

2.3 – Intervertebral disc structure.

2.4 – Ligaments and musculature surrounding the lumbar spine

2.5 – Biomechanics of lumbar spine.

2.6 – Stability of lumbar spine.

2.7 – Lower back pain and spinal disorders.

2.8 – Cadaveric testing of lumbar spine.

2.9 – Discussion.

**Chapter 3 Review of relevant technology……..44**

3.1 – Introduction.

3.2 – Computer model of the lumbar spine.

3.3– Artificial muscles.

3.4 – Shape memory alloy as muscles

3.5– Control for shape memory wires.

3.6 – Testing of mechanical disc.

**Chapter 4** **Development of laboratory spine with active muscles……...65**

4.1 – Introduction.

4.2 – Geometrical modelling of simplified laboratory spine.

4.3 – Material selection and properties.

4.4 – Properties of SMA as artificial muscles.

4.5 – Development of active muscle for simplified geometry model.

4.6 – Designing of the control circuit for the active muscles

4.7 – Assembly of the simplified geometry model.

4.8 – Discussion.

**Chapter 5** **Comparison and validation of computer model and experimental models……95**

5.1 –Introduction.

5.2 – Development of simplified laboratory spine with active muscles.

5.3 – Performance of simplified model.

5.4 – Discussion.

**Chapter 6** **Modelling and development of an accurate geometry spine model……107**

6.1 – Introduction.

6.2 – Accurate geometry modelling.

6.3 – Manufacturing of intervertebral disc.

6.4 – Discussion

**Chapter 7** **Discussion……112**

7.1 – Introduction.

7.2 – Simplified laboratory spine.

7.3 – Actual geometry spine.

**Chapter 8** **Conclusion……...117**

**Chapter 9 Future work……..120**
**References……..121**
**Appendix……133**
**Presentation ……..140**

# CHAPTER 1
# INTRODUCTION

## 1.1 Research background

National Health Services quotes that 'lower back pain is one of most common diseases after cough and cold, is seen almost in every 4 out of 5 individuals' (NHS report, 2002). It has been one of the most prominent issues, as it reduces the work efficiency of an individual resulting in either inconsistent approach for work (improper concentration) or permanent bed rest. According to the CSAG (1993), an estimated 2 million people suffer from chronic low back pain in the United Kingdom costing the economy approximately 6 millions which accounts to the production loss and reduction in work efficiency of individuals. The TSSA report (2001) shows over 119 million days lost due to registered disability caused by lower back problems. This figure includes only people who claimed benefits as a result of their backs so the total estimate including short spells could be nearer to 180 million lost working days. Also lower back pain affects all kind of people irrespective of sex or age; this can be explained by the survey conducted by Back Care (2004).

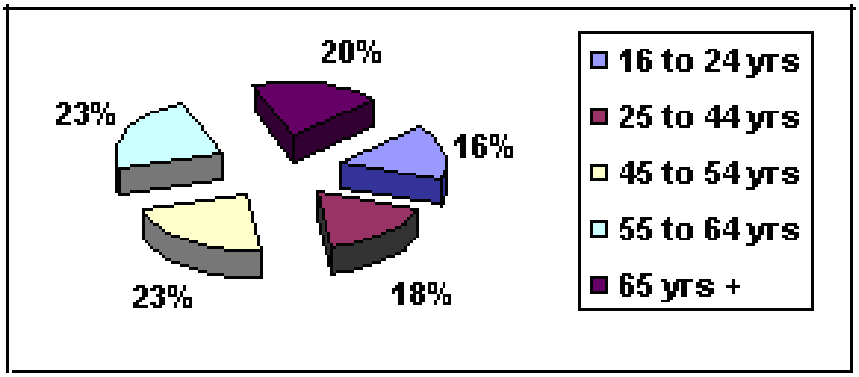


**Figure 1.1 Percentage age distribution of lower back pain problem. (Back Care, 2004)**

At present surgeons can frequently cure and alleviate lower back pain using a number of different techniques available to them. But it is the initial diagnosis that can be very problematic due to the intricate and interesting 3-D skeletal structure and its

multiple degrees of freedom. The best imaging techniques cannot provide sufficient detail of the spine with realistic loads. Also animal models are proposed for *in vitro* mechanical testing, but due to the high cost involved and ethical issues, this is now becoming increasingly difficult. So, the purpose of this research project is to develop a patient specific laboratory spine with artificial muscles that can apply realistic forces. A laboratory spine with muscles could then be used to represent numerous physiological conditions and test spinal devices.

## 1.2 Overview of thesis

The development of laboratory spine necessitates a fundamental knowledge of bone biology and biomechanics. These issues are covered in Chapter 2, where the lumbar spine structure, intervertebral discs, musculature and biomechanics are outlined.

Previous techniques are investigated in Chapter 3, where the various simulation and modelling techniques adopted by other researchers are discussed individually and then collectively with regard to their relevance to the current work. The intervertebral disc is a critical component of the spine. So, a simplified model of an intervertebral disc was developed and subjected to compressive flexion and torsional loading. The effects of material were also investigated and the results compared with the experimental data. In Chapter 4, the development of the model with a simplified geometry is then outlined, considering in particular material selection and testing, selecting the muscle architecture and identifying the control parameters for the artificial muscles. An FE model to assist in the development and validation of the simplified spine model is presented in Chapter 5.

Chapter 6 consists of an accurate geometry model developed from the actual data and the lumbar curve. Complex intervertebral disc fits exactly in between the two lumbar vertebrae. This was a very time consuming part of the project, but vital to the long-term success of the laboratory spine. The results of the validation of the finite element models and for the actual geometry spine are discussed in Chapter 7. The whole project is concluded in Chapters 8 and 9, highlighting the main points, discussing the relevance to other work and drawing out implications for further development and improvement of the work.

Finally, a list of the publications arising from this research is included for reference purposes. Thus, the main objectives of this work were:

1. To develop an artificial laboratory spine with active muscles that could be used to test spinal devices and instrumentation.

2. To compare and validate a finite element model to predict the resultant changes in the disc behaviours, which could be used in the later optimization of the laboratory spine.
3. To model a control system that can control individual muscles in the spine.
4. To observe the behaviour of the simple spine and compare it with the performance of actual human spine reported in the literature.
5. To develop an accurate geometry spine model and develop a method to manufacture physiologically reasonable vertebral bodies and intervertebral discs.

# CHAPTER 2

# THE LUMBAR SPINE

## 2.1 Introduction

The lumbar spine is one of the most intricate and complex structures in the human body, which must be fully understood for this research. Therefore, this chapter presents key anatomical information on the vertebrae, intervertebral discs, ligaments and musculature, and discusses musculoskeletal architecture and lumbar geometry in particular with respect to biomechanics of spinal movement.

The lumbar spine is a mechanical structure whose principal function is to provide controlled movements, encase the spinal cord and transfer loads from the head and trunk to the pelvis. The spine involves 24 individual vertebral bodies and two fused bodies supported on the pelvis, with intervertebral discs to transfer loads from one vertebra to another. The spinal column as shown in figure 2.1 consists of 7 cervical vertebrae C1 to C7, 12 thoracic vertebrae T1 to T12, 5 lumbar vertebrae L1 to L5 with two fused sacral vertebrae and coccyxeal vertebral bodies.

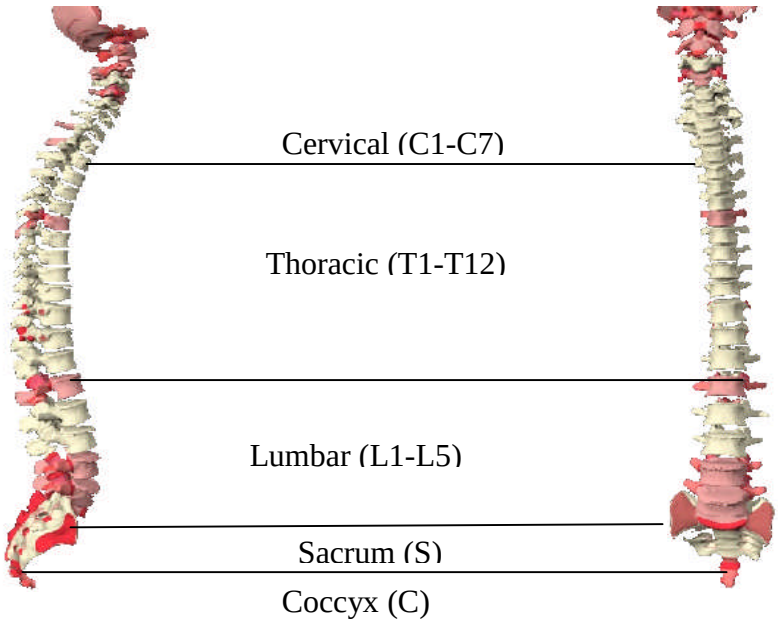


**Figure 2.1 Lateral and anterior views of the human spine. (Modified from Back.com, 2001)**

The entire spinal column as shown in the lateral view of figure 2.1, maintains an S-shaped curve. The lower region of the curve, consisting of five vertebral bodies acts as functional unit called the lumbar spine, where each adjacent pair of vertebrae and interposed intervertebral disc is known as a motion segment.

## 2.2 The lumbar spine structure

### 2.2.1 Characteristics of the lumbar vertebrae

A vertebral body as described by Gray et al. (1987) is a thin ring of dense cortical bone, which is thinner in its centre and thicker at its ends (figure 2.2), and surrounds a core of light, spongy, cancellous tissues. It has a greater diameter in the sagittal plane than the frontal plane. Each vertebral body consists of various processes, pedicles, facet joints and a vertebral cavity for the spinal cord and spinal nerves, as shown in figure 2.2

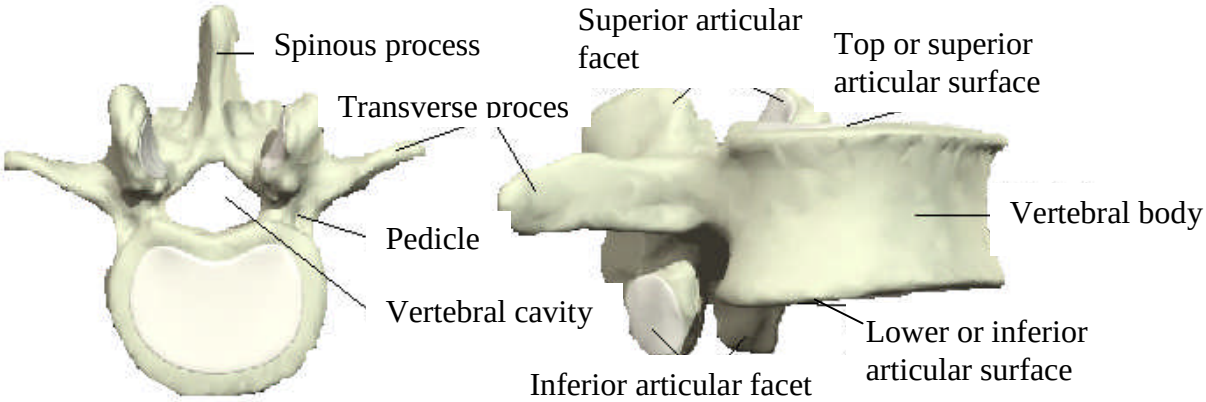


**Figure 2.2 Key features of a lumbar (L2) vertebral body.**
**(Modified from Noordeen et al, 2001)**

The lumbar vertebrae are the largest segments of the movable part of the vertebral column, with the lumbar region being comprised of five lumbar vertebrate – L1 to L5 (figure 2.1). Detailed descriptions of the anatomy of the vertebrae can be found in all standard textbooks on human anatomy and physiology.

Flexion, extension and some torsional motion is possible in the lumbar spine, with the torsional movement limited by the facets, which are oriented at right angles to the transverse plane, as shown in figure 2.2, and described in Gray et al. (1987) and Yang and Kam (2002) for lumbar vertebral bodies. The load sharing between the facets and the disc during motion varies with the position of the spine. The loads on

the facets are greatest (about 30% of the total load) when the spine is hyper-extended but are also high during forward bending coupled with rotation, Gray et al (1987).

### 2.2.2 Lumbar geometry

The normal erect stance is accomplished by having the popularly known 'S' curve observed in healthy individuals in the sagittal plane. In toddlers, when they begin to sit, the spine has a cervical shape 'C' as shown in figure 2.3, which transforms into an 'S' curve, when they start sitting and standing. The posterior lumbar concavity tends to increase in women during later months of pregnancy, due to the fetal load (Snell, 2004).

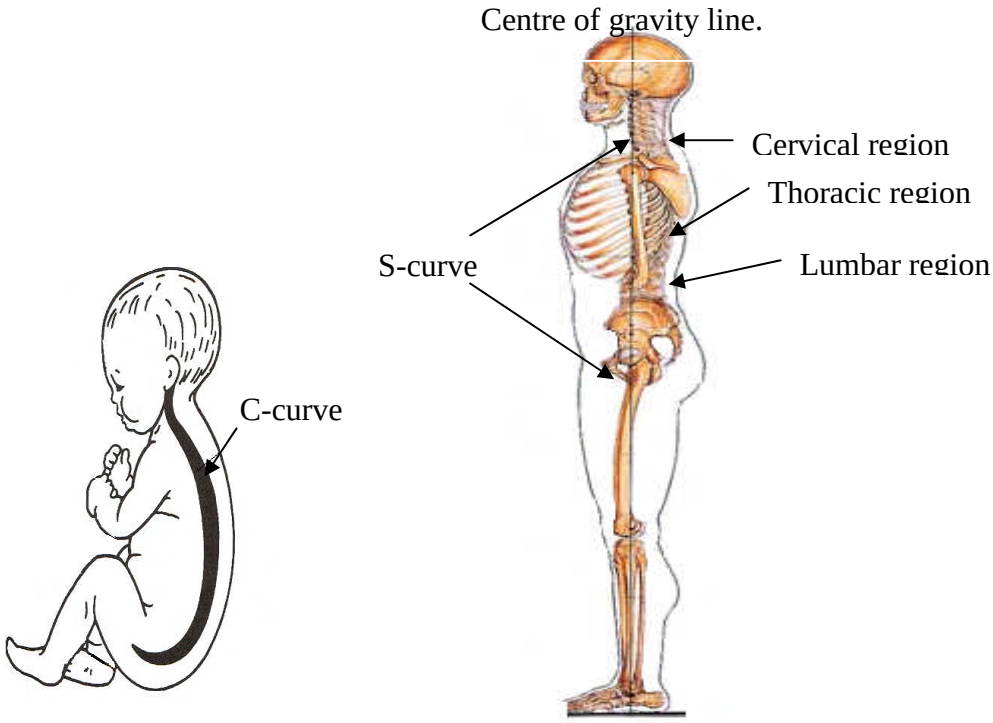


**Figure 2.3 Toddlers having 'C' shaped curve and adult having 'S' shaped curve about the centre line**

Thus each vertebral body in the lumbar region is inclined in a backward direction, as shown in figure 2.3 (Luder, 1993 and Gregg, 2000) allowing minimum muscle effort to maintain the vertical line passing through the centre of gravity. The lumbar curves play a very important role in the design of the spine. It allows the proper spacing between each and every vertebrae as shown in figure 2.4.

According to Schmorl et al. (1971) the lumbosacral disc (L5 - Sacrum) is wedge shaped, unlike the other lumbar invertebral discs and inclined downwards and forwards, with the angle formed between the vertebral body and sacrum typically 33$^{o}$.

Among the various techniques for measuring the geometry of the lumbar spine, the most common method used by radiographs is the Cobb angle. In this method the angle between the inferior and superior endplates of two adjacent vertebrae is measured.

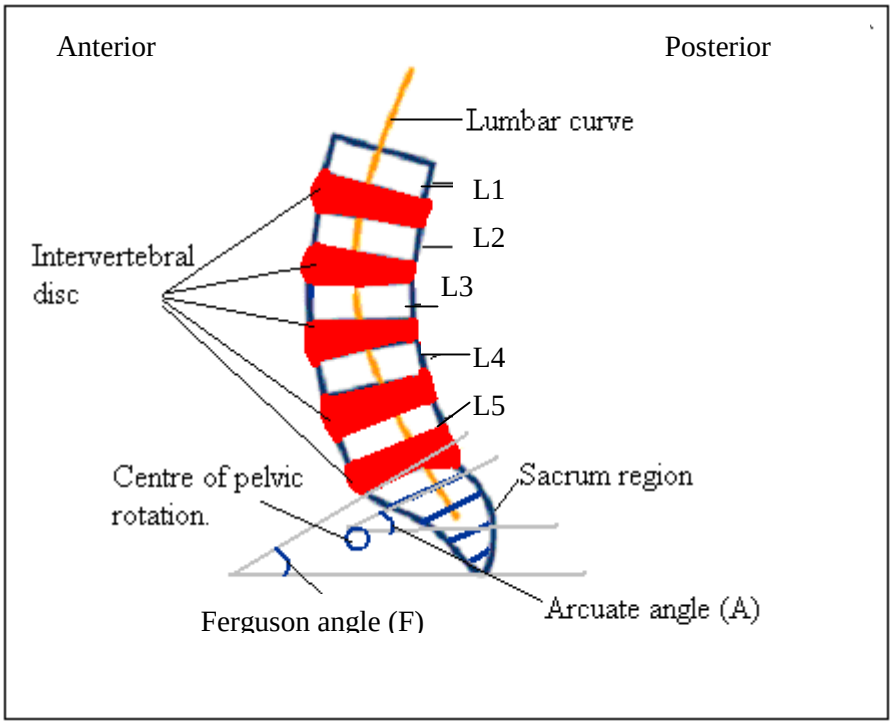


**Figure 2.4 Lumbar geometric curves.**

The other common technique is the RRA (Relative Rotational Angle) in which the angle is measured from the facet joints (considered as the point of rotation). Among these various techniques the Cobb angle is commonly preferred due to its simplification and its non dependency upon any parameter.

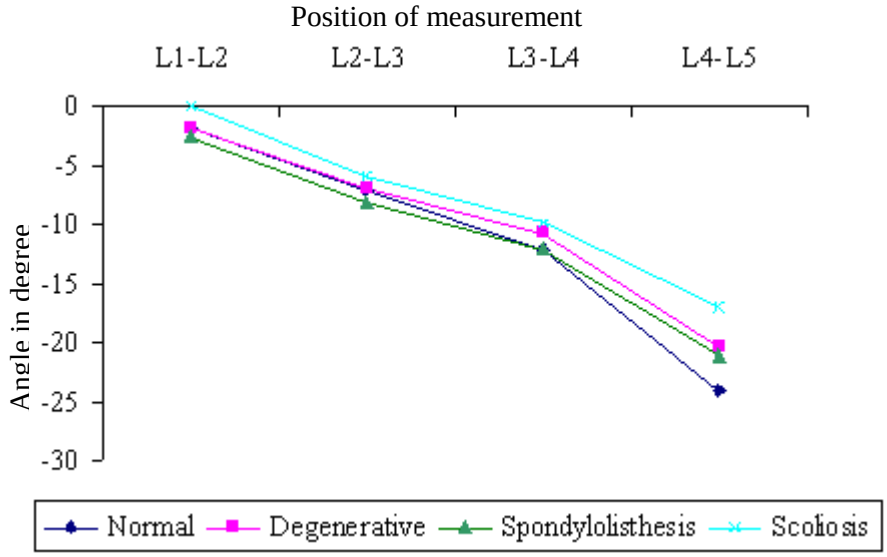


**Figure 2.5 Cobb angles of the lumbar spine for normal and diseased conditions**

The two most common conditions affecting a major part of the population are spondylolisthesis and spondylolysis. These defects are observed especially in the L5-S1 and L4-L5 regions. Spondylolysis is defined as a defect or fracture of the lamina between the two facets of the vertebral bodies and spondylolisthesis can be explained as translation between adjacent vertebral bodies. The mechanisms responsible for these failures are repetitive spinal flexion, combined flexion and extension operations, forcible hyperextensions and sudden lumbar spinal rotations. The variations in lordosis for normal and diseased conditions such as degenerative disc and spondylolisthesis have been studied. Figure 2.5 shows Cobb angles measured in static position for designing the actual geometry spine discussed in Chapter 6. The various angles of the spine are compared in normal, degenerative (disc disease) and spondylolisthesis. For example the Cobb angles shown in figure 2.5 of the spine at various positions are compiled in Table 2.1.

| | **L1-L2 ($^o$)** | **L2-L3 ($^o$)** | **L3-L4 ($^o$)** | **L4-L5 ($^o$)** | **L5-S1 ($^o$)** | **L1-S1 ($^o$)** | **T12-L1 ($^o$)** | **T12 S1 ($^o$)** | **F ($^o$)** | **A ($^o$)** |
|---|---|---|---|---|---|---|---|---|---|---|
| a Normal * | -1.9 | -7.2 | -12 | -17 | -24 | -62.1 | - | - | - | - |
| a Degenerat* | -1.9 | -6.9 | -10.6 | -16.7 | -20.4 | -56.5 | - | - | - | - |
| a Spondylol* | -2.5 | -8.1 | -12 | -21 | -23 | -66.4 | - | - | - | - |
| a Scoliosis* | 0 | -5.9 | -9.9 | -17 | -24 | -56.8 | - | - | - | - |
| b Normal~ | 3.2 | 7.9 | 12.3 | 16.7 | 33.0 | - | 3.1 | 65.4 | 39.4 | 48.9 |
| b Acute~ | 3.0 | 8.4 | 12.5 | 16.6 | 35.1 | - | 1.6 | 70.0 | 44.6 | 53.4 |
| b Chronic~ | 0.3 | 5.3 | 9.6 | 14.3 | 30.1 | - | 2.2 | 57.0 | 38.2 | 47.4 |
| b Pathology~ | 1.7 | 6.5 | 11.1 | 15.8 | 32.6 | - | 1.1 | 58.0 | 36.5 | 44.4 |

**Table 2.1 Angles of the spine at different spine levels.**

In measurements '+' is anterior side for measurement and '-'is posterior side for measurement of the angles.
Type of variation in measurement technique, 'a' Cobb angle, 'b' Relative Rotational angle.
* Jaink et al. (1998).
~ Jackson et al (1998).

Knowledge of the normal curve of the lumbar spine according to Bogduk and Twomey (1997) is important for diagnosis of lower back pain. In Gracovetsky et al. (1987) a high lordosis corresponds to an angle of L5-S1 which is greater than 40$^o$, a healthy lumbar spine corresponds to an angle less than 40$^o$. A healthy individual can adjust lumbar lordosis significantly by rotating the pelvis with hip extensors. In recent

studies, it has been shown that forward tilting of the pelvis and an increase in lumbar lordosis reduces the loads on the lumbar region during erect sitting (Yang and Kam, 2002).

## 2.3 Intervertebral disc structure

### 2.3.1 Introduction

The bodies of the lumbar vertebrae are separated by intervertebral discs that are compressed between two bodies, as shown in figure 2.6, and allow motion of the spine but also act as shock absorbers. Each disc is connected to the superior and inferior surfaces of the adjacent vertebral bodies and consequently takes its cross-sectional shape from these vertebrae, and together they form a functional spinal unit.

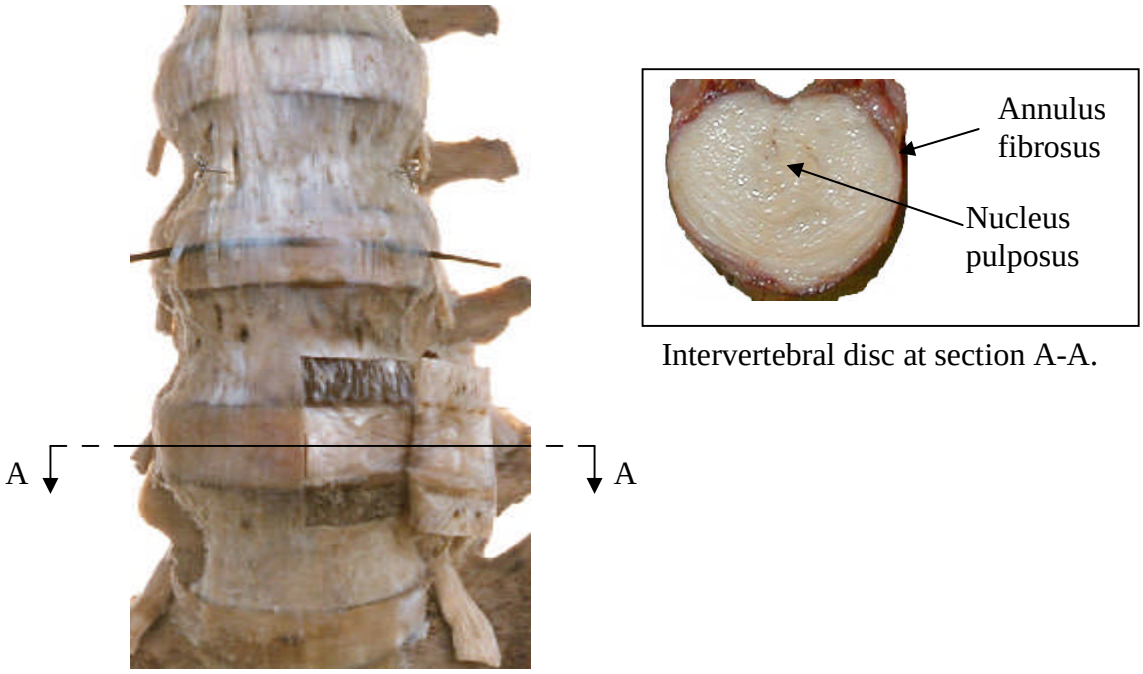


**Figure 2.6 Lumbar vertebral bodies from a cadaver, showing the intervertebral discs. (Modified from Noordeen et al, 1997)**

### 2.3.2 Intervertebral disc structure

The discs vary in shape, size and thickness in different parts of the spine, being oval in the cervical and lumbar regions and circular in the thoracic region. The discs are largest in the lumbar spine as they sustain the largest loads. The lumbar intervertebral discs are kidney shaped, that are compressed between two vertebral bodies. The disc thickness also varies in different regions, and is generally wedge shaped in the cervical and lumbar regions, being thicker in the front of the disc, thus giving these sections their characteristic geometric curves, as shown in figure 2.4. In the thoracic

region the intervertebral discs are more uniform in thickness. Generally, the discs in the human spine vary in thickness between 6 and 18mm.

Each disc consists of two basic components, the nucleus pulposus and annulus fibrosus as shown in figure 2.6. The annulus fibrosus is composed of fibro-cartilage, which consists of collagen fibres arranged in a highly ordered pattern, having 10 to 20 concentric layers (called lamellae) in a disc. The lamellae contain a criss-cross arrangement of fibres lying between 30 – 65$^{o}$ to the sagittal plane as shown in figure 2.7, in order to withstand bending and torsional loads. This annulus encapsulates a soft, pulpy, highly elastic nucleus pulpous. The nucleus pulposus has loose fibres of proteoglycan-collagen suspended in a mucoprotein gel, having a consistency of jelly.

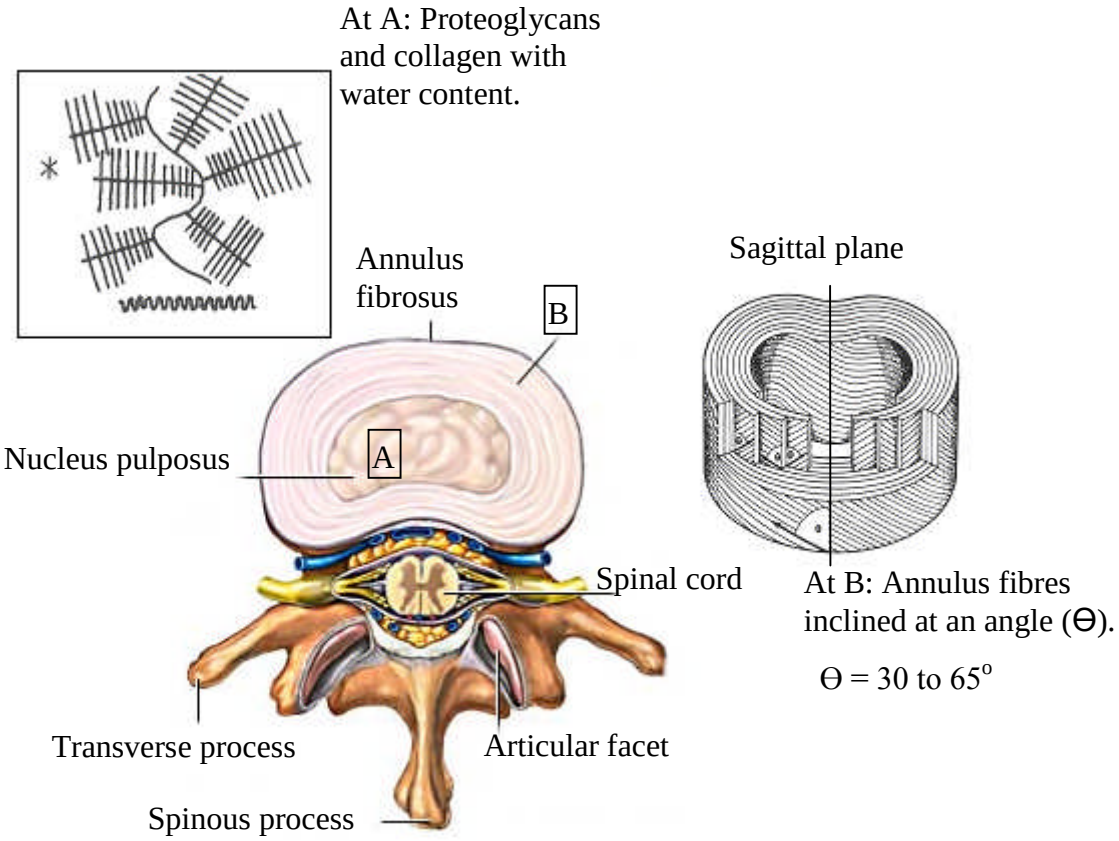


**Figure 2.7 Parts of the intervertebral disc. (Modified from Martini et al, 2001).**

As suggested by researchers the accurate fibre orientation was a complexity, Bogduk and Twomey (1997) discussed an envelope surrounding the intervertebral disc as shown in figure 2.7 which has different set fibres i.e. annulus fibrosus which is layered. Each layer of fibre has different orientation of fibres that ranges from 30 to 60$^{o}$. The intervertebral discs are relatively flexible, so that when an axial load is applied to a disc, the external forces are resisted in several ways, including an elevated nucleus pressure. Bogduk and Twomey (1997) observed that the end-plates, which

are attached to the top and bottom surfaces of the vertebral bodies, play a very important role in the load transfer. The nucleus pulposus consists of proteoglycans and collagen with water content. If the annulus is healthy and intact, the end-plates experience a high pressure, during load transfer from one vertebral body to another. So that, in a steady state of hydration, the proteoglycans (long chain like protein polymers) contained in the nuclei balances the applied stresses as shown in figure 2.8. If the applied stress increases, water is driven out of the disk until a new equilibrium is reached, stabilizing the force and transmitting to the next vertebral joint (Van et al, 1997).

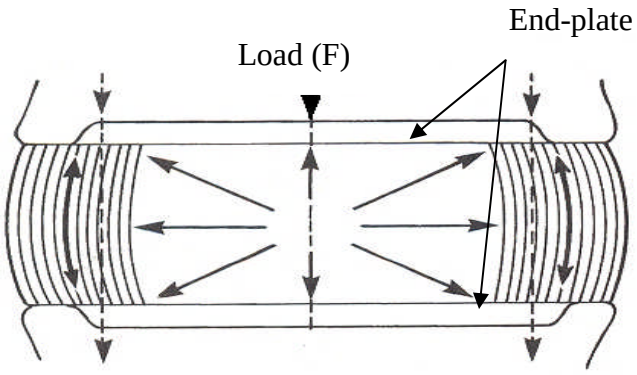


**Figure 2.8 Intervertebral disc loading.**
**(From Bogduk and Twomey, 1997)**

The intervertebral discs receive some fluid supply through movement, from which they get nutrients, but also the discs expand while at rest allowing them to soak up further nutrient rich fluid. Flexion, extension, and lateral flexion of the spine produces mainly tensile and compressive stresses in the disc, whereas rotation and translation produces mainly shear stresses (Bogduk and Twomey, 1997). In the normal equilibrium position, the nucleus has an inherent positive pressure, while during loading of the spine, the disc acts hydrostatically, allowing a uniform distribution of pressure throughout the disc (Gray et al, 1987). In the lumbar spine the tensile stress seen in the posterior part of the disc, has been estimated to be four or five times the applied axial compressive load, as the criss-cross fibers of annulus fibrosus are tensed. When the transverse process of the vertebral body is inhibited by repetitive loading configurations performed by muscles through movements or poor posture, the discs becomes thinner and more prone to injury. This may cause gradual degeneration of the structure and loss of function of the disc over time.

The amount of water, in the nucleus changes throughout the day depending on activity (Yang and Kam, 2002). For an average individual, the water content is approximately 70 to 90%, but this decreases with ageing. The gradual hardening of

the nucleus then causes the disc to be less able to adapt to compressive loads and the annulus fibrosus gets weaker and is prone to tearing, which causes chronic pain. A herniated disc occurs when some of the nucleus protrudes through an injured annulus and exerts pressure on the sensitive spinal nerves. According to Bogduk and Twomey (1997) the pressure exerted on the intervertebral disc is transmitted from one motion segment to the other. The movement of the vertebral body is shown in figure 2.9 which moves in the direction of the applied force. The loading is concentrated at one end of the disc in the direction of force, causing it to compress while the other face is in tension.

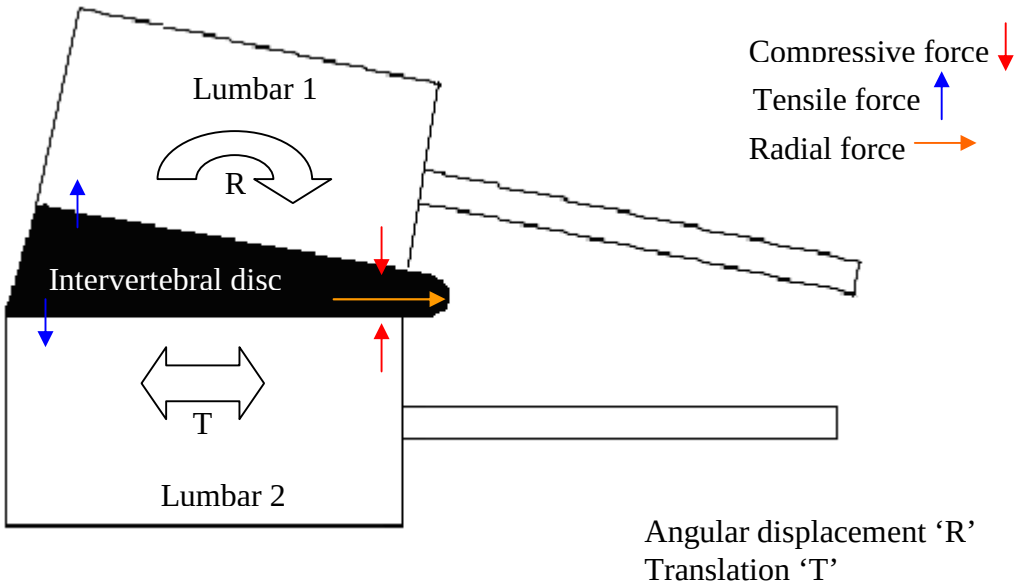


**Figure 2.9 Loading for simplified intervertebral disc.**
**(Adapted from Bogduk and Twomey, 1997)**

## 2.4 Ligaments and musculature surrounding the lumbar spine

### 2.4.1. Ligaments

Ligaments are strong fibrous soft tissues that are collagenous, viscoelastic and tension sustaining bands. They are attached to the vertebral bodies, and surround each of the intervertebral discs, with uni-axial fibres arranged along the axis of the ligaments. The seven ligaments associated with the spine are shown in figure 2.10.

The *anterior* and *posterior longitudinal ligaments* are composed of long and short bands of fibres that connect the front and back of the vertebral bodies and the intervertebral discs. The main function is to resist flexion and extension, to support the intervertebral disc and protect the anterior region against tensile loads.

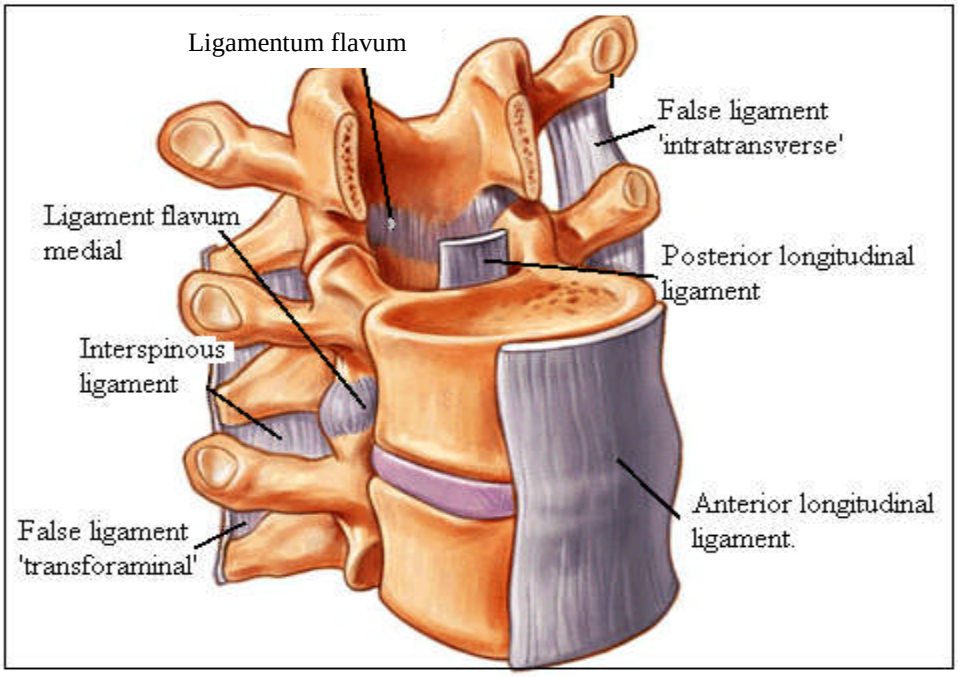


**Figure: 2.10 Ligaments surrounding L1 and L2.**
**(Modified from Spine Universe, 2004).**

The *ligamentum flavum* connects the anterior aspects of the inferior and superior articular processes of adjacent vertebrae, and resists the separation of the vertebrae. The ligaments are highly elastic and become increasingly thick and strong towards the lumbar spine, pre-stressing the discs to maintain an upright position of the spine and provide resistance to flexion (Nachemson and Evans, 1968).

The *illliolumbar ligament* connects only the transverse process of the fifth lumbar vertebrae to the ilium. Its basic function is to protect the intervertebral disc between fifth vertebrae and sacrum, and resist forward, backward and lateral bending of the fifth vertebrae.

The *inter-spinous* and *supra spinous ligaments* pass through the spinous processes, and combine at different levels depending on the relative position within the spine. They also connect with the supra spinous ligaments and the ligament flavum to provide stability of the spine.

The *inter-transverse ligament* connects the transverse processes and has a significant influence on lateral bending and axial rotation.

The *capsular ligaments or ligament flavum medial* are the shortest ligaments surrounding the zygapophyseal (facet) joint. They have a complex geometry and constrain the translatory motion of the articular process with respect to the adjacent vertebral body.

The *false ligament intratranseverse* connects the upper transverse processes of the vertebral bodies. As the name suggests it is not a true ligament, but acts as a membrane or bands of fascia to protect the vertebral bodies against excessive movements observed in flexion and extension.

Thus, consecutive vertebrae and the sacrum are held together by the ligaments, in particular the *supra-spinous*, *inter-spinous*, *inter-transverse* and *ligamentum flava*.

### 2.4.2 Muscle structure

Muscles are contractile organs in the body, which are attached (via tendons) to the vertebral bodies to produce movement and stabilize the spinal structure.

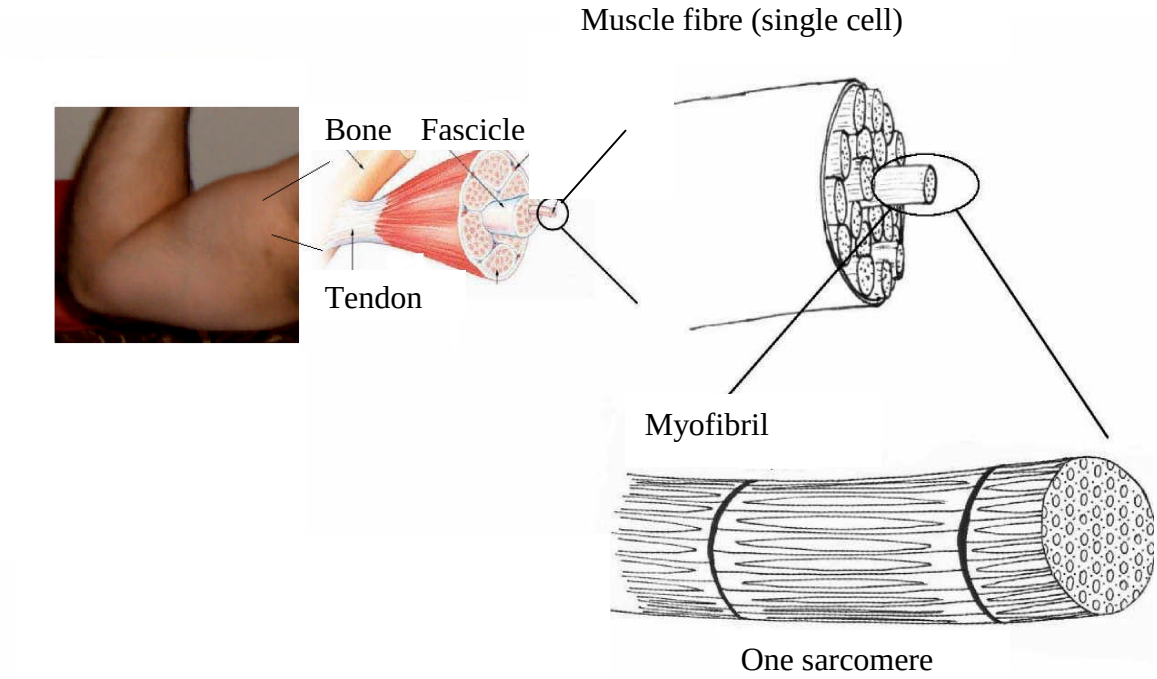


**Figure 2.11 The skeletal muscle structure (Modified from Fung and Pinto, 1993).**

Each muscle consists of bundles of fibres 20 to 100 microns in diameter, which are surrounded by connective tissues, as shown in figure 2.11. Each fibre, termed a myofibril, consists of a string of sarcomeres, where the total number of sarcomeres within a fibre depends on the muscle fibre length and diameter. The sarcomeres are separated by thin partitions called Z-lines (or disks), and consist of thin filaments of actin (in A-bands) connecting thick myosin filoments (in I-bands), as shown in figure 2.12. The filaments of the I- and A-bands interleave in a hexagonal structure, and on stretching or compressing of the muscle fibre, the A-bands remain at a constant length, while the I-bands expand and contract.

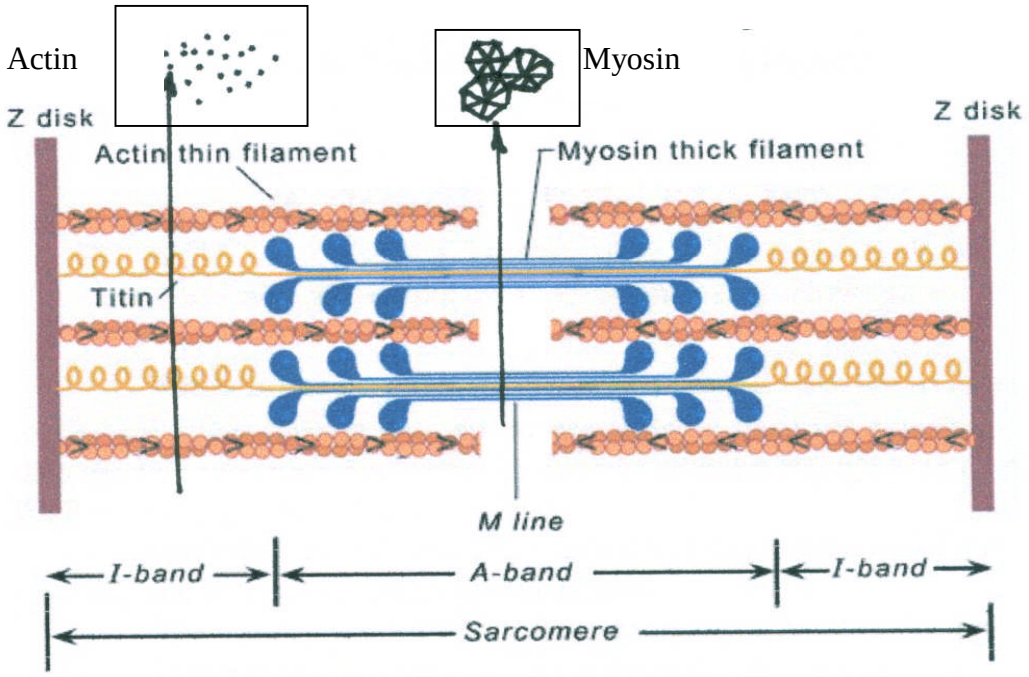


**Figure 2.12 Skeletal muscle contains a regular array of actin and myosin (Modified from Martini *et al*, 2001)**

The lumbar postural muscles, which stabilize the spine, are dominated by slow twitch muscles, which are surrounded by fast twitch muscles. The fatigue endurance i.e. the cycle life of slow twitch muscles plays a very important role in the biochemical function of the tissues. The fast twitch muscles overlap i.e. muscles are not connected directly to the vertebral bone and are fast to respond, while the slow twitch muscles are connected to the vertebral bones and are slow response more load bearing muscles. The biological structure varies for both fast and slow twitch muscles i.e. the fast twitch muscles have more myosin filaments. In the simplified spine models developed in this research only the slow twitch muscles, which are attached to various transverse and spinous processes of vertebral bodies, are considered (Chapter 4).

The study of muscle architecture discussed in Gray and Pick (1987) showed adaptability of the muscle due to the series arrangement within each fascicle. The total distance of fascicle shortening is equal to the sum of shortening of the individual sarcomeres, which suggests that muscle architecture has a profound effect on the muscle force generated. The Hill model (Hill, 1938) of muscle architecture states that a very long muscle will produce more force than a short muscle depending on the

tension in the muscle, and according to Lieber (2005) the length tension relationship is dependent on the interlocking contractile filaments.

The vertebral bones and the tissues such as the intervertebral discs, ligaments and muscles of the spinal column are aligned in such a way to create a protective canal that provides support to the spinal cord. The outer most layers that enclose the spinal nerves are known as the dura-mater, which is a very tough membrane that prevents cerebrospinal fluid from leaking out from the central nervous system. The space between the dura-mater and the spinal canal is called the epidural space, and is important in the treatment of low-back pain, because medications such as anaesthetics and steroids are injected into this space in order to alleviate pain and inflammation of the nerve roots.

### 2.4.3 Musculoskeletal system of the lumbar spine

The lumbar spine contains five moderately large vertebrae, which sit above each other as shown in figure 2.13.

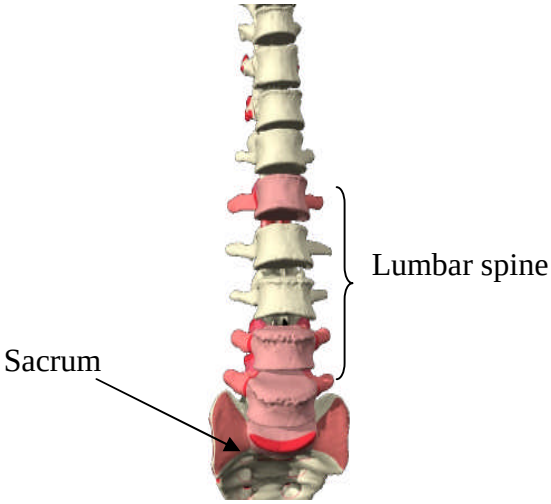


**Figure 2.13 Structure of lumbar spine with vertebral bodies.**
**(Modified from Noordeen et al, 2001)**

The transverse and spinous processes acts as attachments for muscles and ligaments in the lumbar spine and also encase and protect the lower spinal cord and lumbar nerve roots. For simplification purposes, the flexor and extensor muscles of the lumbar spine can be classified depending on their functional abilities, as shown in figure 2.14, where the classification is based on the grades of muscles depending on their positions and functions (Gray *et al*, 1987).

The extensor and flexor muscles are attached directly or indirectly to the processes of the vertebrae, and can be classified into different grades of muscles,

which fill the vertical gap posterior to the transverse processes and lateral to the spinous processes.

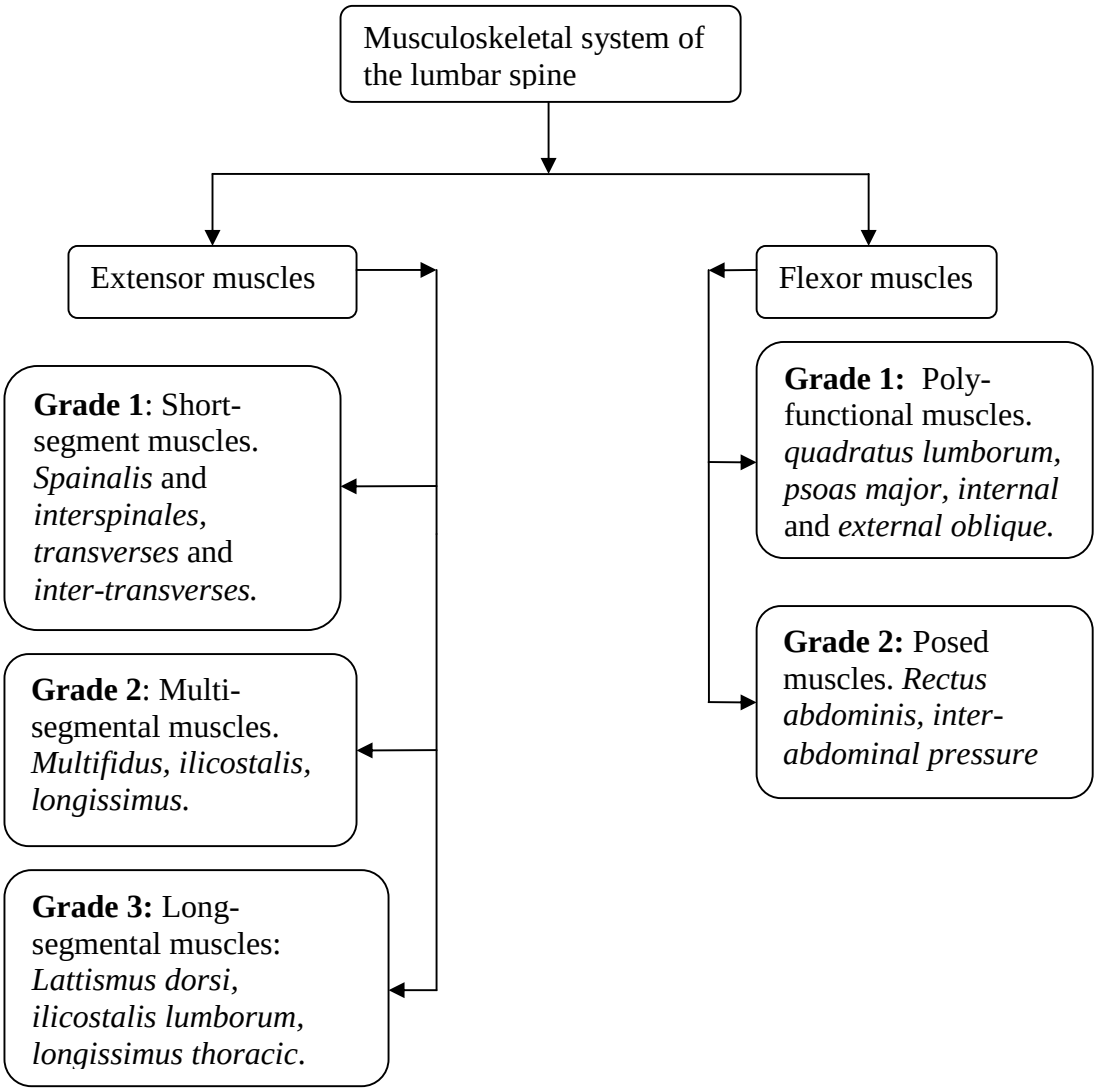


**Figure 2.14 Simplified classifications of lumbar muscles (Gray *et al* , 1987).**

The different classifications can be seen in the cadaveric cross-section in figure 2.15. The Grade 1 extensor segmental muscles, such as *supra-spainalis* and *interspinales*, *transverses* and *inter-transverses*, are short muscles that act as antagonistic pairs for each intervertebral disc rotations as shown in figure 2.16. The *interspinales* lie on the spinous processes and connect to the spinous process of the adjacent lumbar vertebrae. The *transverses* and *intertransverses* are connected to the transverse processes that act as fine tune or antagonistic pairs for imbalanced movements.

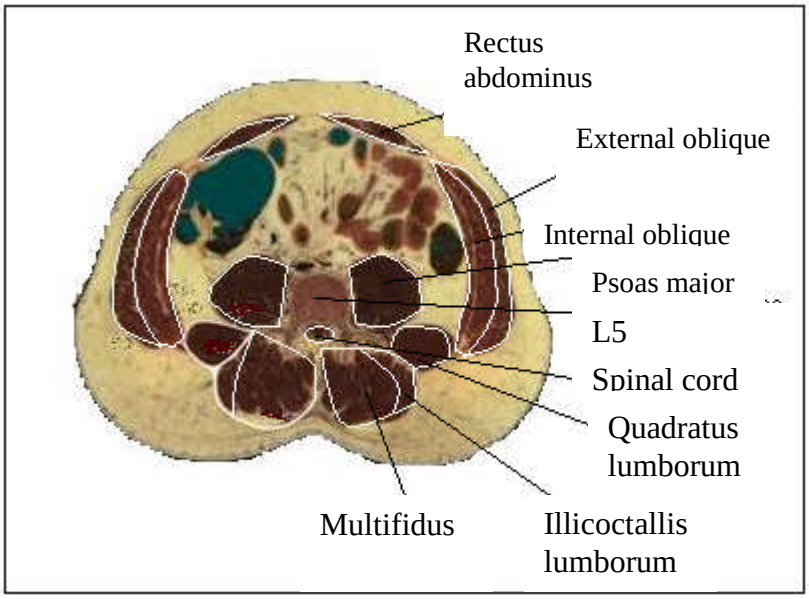


**Figure 2.15 Cadaveric cross-sections of lumbar vertebrae (L5). (Modified from Noordeen et al, 2001)**

The Grade 2 extensor multi-segmental muscles have multiple attachments depending on their physical positions and are the *multifidus*, *ilicostalis*, *longissimus*. Van et al (1997) describe the *multifidus* muscle as having a number of bundles of muscle fibres (fasciculi), which are attached to the spinous processes of each vertebra, and form one of the largest of the back muscles, as shown in figure 2.16. The *longissimus* runs from L1 to the Sacrum with some fascicles connected to the transverse processes of vertebral bodies. The Grade 3 extensor muscles lie lateral to the *multifidus* and are observed as a flat sheet of collagen fibres and muscles are responsible for the major movements of the vertebral bodies, of lifting and lowering.

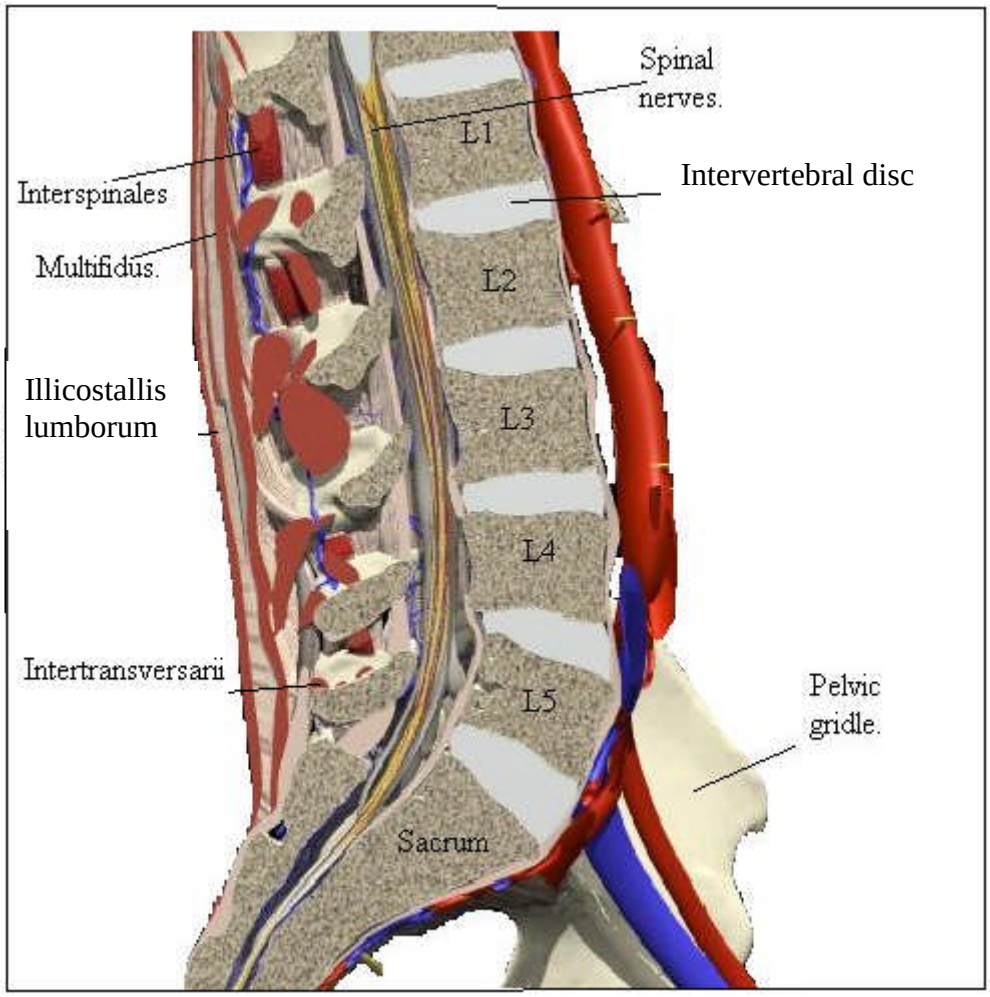


**Figure 2.16 Extensor muscles of lumbar region in sagittal plane.**
**(Modified from Noordeen et al, 2001)**

The *flexor* muscles attach to the anterior location of the spine generally in the abdominal parts, as shown in figure 2.17. The Grade 1 *flexor* muscles are called poly-functional muscles due to the multiple functions that they perform, and include the *quadratus lumborum*, *psoas major*, *internal* and *external oblique*.

The *psoas major* is divided into different fascicles, with each fascia originating from the vertebral bodies (Bogduk et al, 1997). They start from thoracic 12 (T12) and are attached to the transverse and spinous processes of the lumbar vertebrae. The *psoas major* is attached to the trochanter with an intersection point on the pelvis. The *quadratus lumborum*, contributes towards lateral flexion, as well as providing support during respiration. The *quadratus lumborum* originates from the 12$^{th}$ rib (as shown in figure 2.17) and connects the transverse processes of upper four lumbar vertebrae to the *crista iliaca.*

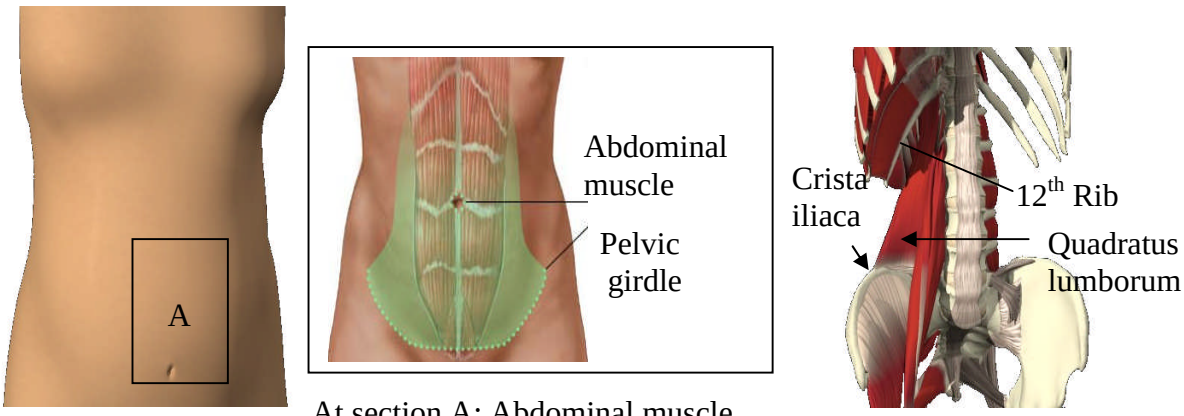


At section A: Abdominal muscle

At section A: Ribs and muscle.

**Figure 2.17 Anterior flexor muscles.**
**(Modified from Noordeen et al, 2001 and 1997)**

The Grade 1 flexor muscles are shown in figure 2.17; muscles which are connected to the abdomen (i.e. *rectus abdominis*), *quadratus lumborum* and the abdominal pressure. This abdominal musculature and the intra-abdominal pressure have a combined effect on flexure of the spine, where the flexor muscles support the extensor muscles by parallel or antagonistic activation during movements.

There are many sources of reference which describe the anatomy and function of the spine in detail; for example: Bogduk *et al* (1997), Dean and Pegington (2002), Gray *et al* (1987), Molly and Blume (2001), Schmorl and Junghanns (1971), Van *et al* (1997).

## 2.5 Biomechanics of the lumbar spine.

### 2.5.1 General biomechanics

The study of spinal biomechanics involves the study of movements of the spine, intervertebral discs and musculature surrounding the bones. The range of motion between the vertebral bodies is determined by the discs and partly by the size of articular processes. Also according to Hoppenfeld (1976), the interlocking articular processes and tightening effect causing pretension of the ligaments and muscles in the lumbar spine, controls the range of joint motions. The maximum movement is observed at the L5-S1 joint, which has the thickest disc. The lumbar spine has two basic types of motion – translation and rotation as shown in figure 2.18.

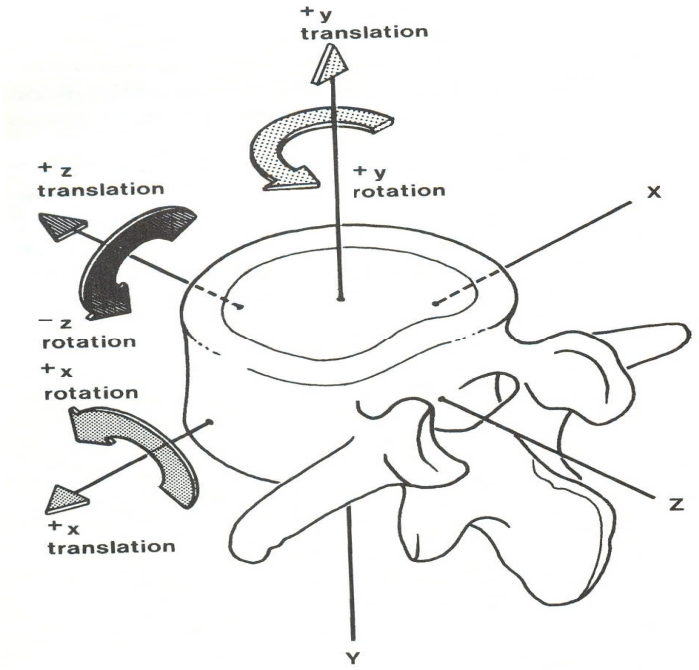


**Figure 2.18 Axes and direction of movements of vertebral body (Adapted from Bogduk and Twomey, 1997)**

Forward and backward motions are observed in the Sagittal plane (i.e. formed by Y-Z axis) and sideways bending movements are noticed in coronal plane (i.e. formed by Y-X axis).

The translation and rotation of vertebral bodies caused by loading is affected by the intersegmental stiffness provided by the intervertebral disc that is reacted by ligaments (acting as spring elements) to control or limit the spinal motions. The study by Cholewicki et al (1999) shows that skeletal muscle stiffness is directly proportional to muscle force. Thus an increase in stiffness and stability is provided by muscular contractions, and flexing of the spine can be controlled by pelvic motion and the lumbar curve and its surrounding musculature. In this way, Gracovetsky et al (1987) proposed that the normal lumbar curve has a minimal compressive stress at all intervertebral joints.

### 2.5.2 Musculature biomechanics

Ligament biomechanics

When a load is carried on the back, the muscles are heavily loaded and have to contract with a large application of force in order to lift the load. When no load condition is applied, they can contract more quickly. Thus the amount of energy required is more when carrying a given load for the same activity, such as walking or climbing stairs.

The ligaments act as mechanical force stabilisers and dampers to support the unbalanced forces of the muscles and can be controlled by antagonistic actions as shown by opposing arrows in figure 2.19

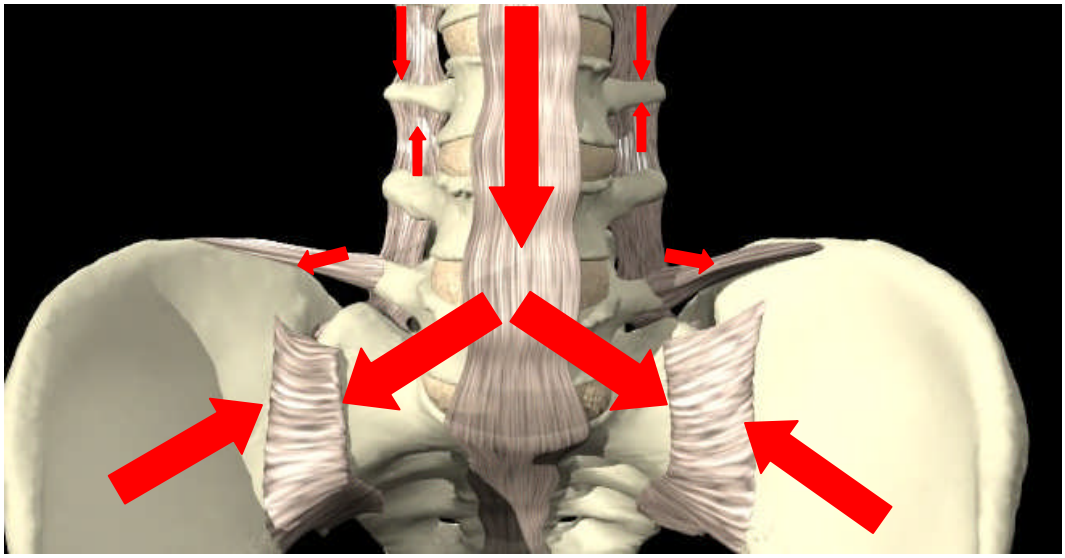

**Figure 2.19 Stabilizing force ↓ showing the biomechanics of ligament moment . (Adapted from Noordeen et al. (2001) as suggested by Bogduk and Twomey (1997))**

The structural characteristic of a ligament can be expressed in mechanical terms as a strong, tough and flexible band, which can prevent yielding under the most severely applied forces. The study in Bogduk and Twomey (1997) shows that changes in the ligament attachment strengths are due to the rapid remodelling of bone, near the developmental stages.

Musculature biomechanics

The muscles work symmetrically in antagonistic pairs. The extensor and flexor muscles are shown in figure 2.20. The muscular force required to perform lifting is derived from the actions of the hip extensors transmitting force to the upper extremities through the use of trunk muscle with stabilizing lingamentous system. Thus, at each motion segment the force gathered by the muscles and supporting ligaments is equal to the force due to be lifted (Gracovetsky et al 1987).

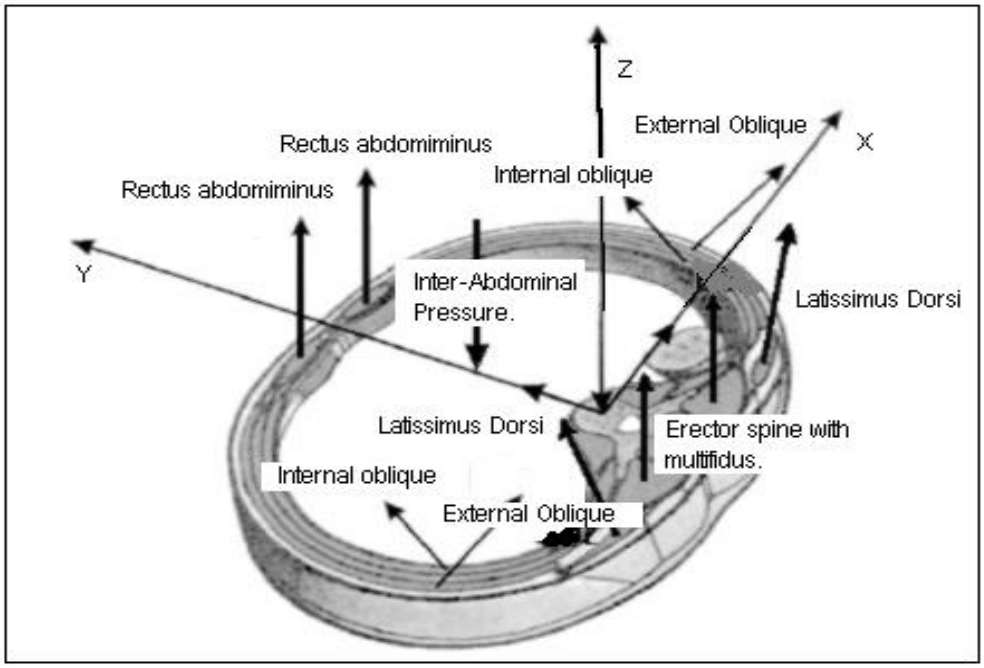


**Figure 2.20 Biomechanics of muscles. (Reproduced from Benner et al 1962)**

The lumbar fasciae form two fibrous layers in the lower back. When active, the muscle may pull the fasciae tighter and limit the initial movement available between adjacent vertebrae of the lower back while the other muscle acts in an antagonistic manner, which can prevent injury to intervertebral discs. Thus musculature of the lumbar spine is capable of several possible actions such as flexion (forward bending), extension (backward bending) and rotations (lateral bending), which include multiple tasks performed by a single muscle group depending upon activity. The movements of the vertebral bodies also include the minor vertebral body movement, postural movements like bending forward and backward, sideways movements and twisting. Table 2.2 aims to document the effects of tension on the lumbar fasciae for movement of the lumbar vertebrae and intervertebral bodies during segmental motion analysis for development of the simplified spine models.

| | Target muscle | Location | Task |
|---|---|---|---|
| 1. | Interspinales and intertransversii | Internal posterior | Minor posterior sagittal rotation and fine tune for imbalanced forces |
| 2. | Multifidus, latissimus dorsi, illiocostallis. | Posterior | Postural control with standing and sitting moment. |
| 3. | Lattismus dorsi, ilicostalis lumborum, longissimus thoracic. | Posterior | Extension involving lifting, lowering and pull up pulls down moments. |
| 4. | Quadratus lumborum, psoas major, internal and external oblique. | Anterior and sides | Side moments, rotations and postural moments of body. |
| 5. | Rectus abdominis, inter-abdominal pressure | Anterior | Postural control with standing and sitting (antagonistic manner), bending and arching the lower back. |

**Table 2.2 Functional abilities of muscle groups**.

The loading of the lumbar spine is due to external loads, gravitational forces and contracting lumbar muscles, exerting a longitudinal compression that raises the pressure in the intervertebral discs. When standing, forward bending causes an increase in disc pressure which further increases if load is lifted, flexed and rotated. In addition to these loads on the disc, the muscle activity increases in proportion to the loads.

The muscle can be triggered to change from a passive state to an active state, which can apply a force that may increase, decrease or remain the same depending on the external load applied. The elastic nature of the connective tissues means that it will regain its length when stretched and released. The muscle with considerable mass has greater fibre angles, greater cross sectional area, an active and steep passive force and length relationship (Mow and Hayes, 1997). The overall force output is a function of the inclination of the muscle fibres. The resting position for any skeletal muscle is referred to as the tone of any muscle i.e. the ideal pretension in the muscle fibres. To avoid fatigue different muscle groups are relaxed and contracted, controlled by asynchronous discharge of nervous impulses depending on the loading configurations. This is described by Snell (2004) and is accomplished by actuating an increasing number of motor units to cause contraction while reducing the activity of motor units that antagonise the motion thus causing relaxation.

For the antagonist motion of the muscles, the fibres can be considered to be of approximately equal length and uniform thickness. This model can be explained with the extensor muscle force as shown in figure 2.21. The extensor muscle force on the vertebral body '$F_m$' acts at an angle, which can be resolved into two vectors, with '$F_1$'

acting on the axis of the vertebral body, providing compression on the intervertebral bodies and '$F_2$' parallel to the upper face of the vertebral body applying shear on the joints.

As the muscles have a tendency to store energy at low speed and then release the energy at high speed, this could cause permanent deformation to invertebral disc. Thus '$F_2$' could produce a translation movement and protrusion.

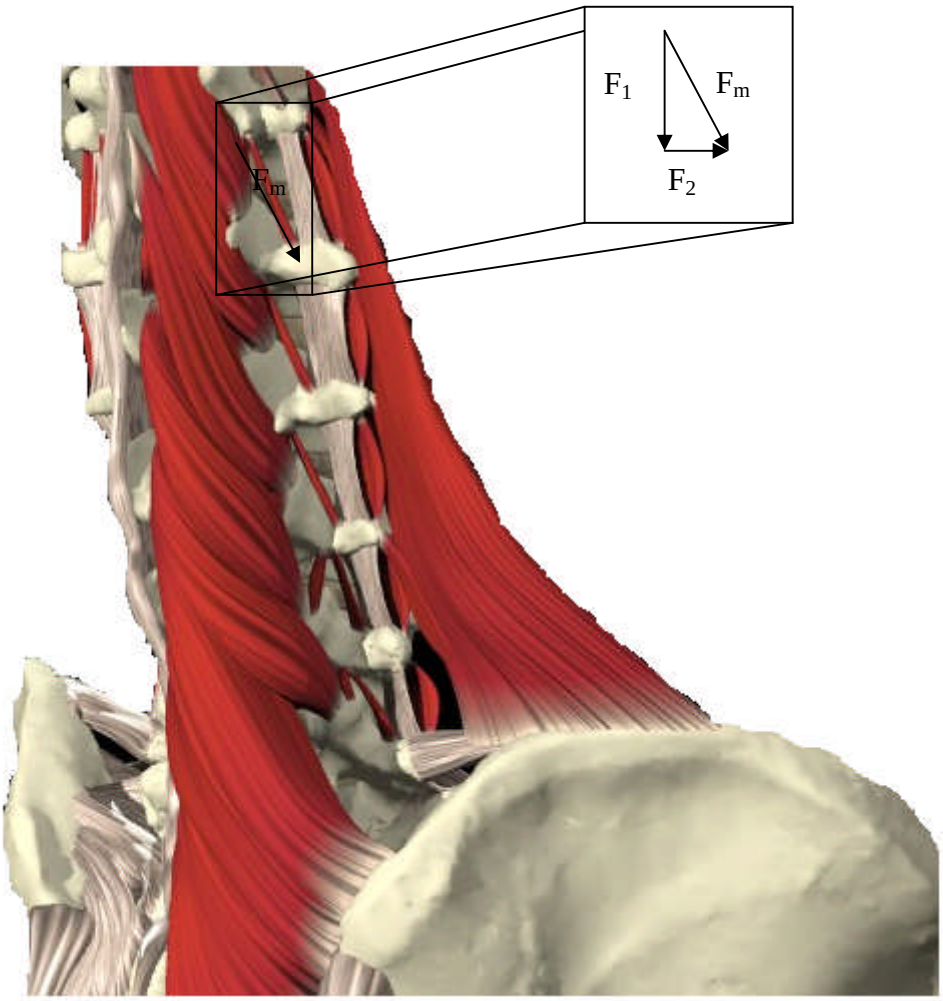


**Figure 2.21 Intersegmental muscle mechanics for lumbar vertebral bodies. (Adapted from Noordeen et al. 2001 as discussed in Bogduk and Twomey, 1997)**

The type of loading and the range of motions observed for each vertebral body depend largely on the thickness of the intervertebral disc, shape and direction of articular processes and the stretched tissues surrounding the spinal structure. For the lumbar region the following movements are observed for the lumbar spine (Gray and Pick ,1987)

- In flexion i.e. forward bending in the sagittal plane, the anterior ligaments are relaxed, the intervertebral disc is compressed anteriorily by the load. In this

movement the *posterior ligament, ligamentum flavum and interspinous ligaments* are stretched.

- In extension i.e. backward bending in sagittal plane, *the posterior ligament, ligament flavum and interspinous ligaments* are relaxed and the intervertebral disc is compressed posterior by the load and the anterior ligaments are fully stretched.
- In lateral bending i.e. side bending, the intervertebral disc is compressed at the sides and intertransverse and capsular ligaments on the opposite side of load are stretched.
- Rotation or twisting i.e. torsional movements having combination of flexion or extension with lateral bending, the intervertebral bodies and ligaments cause resistance to motion depending on the direction of load.

Thus the main function of the muscle is providing stabilization under various loading conditions. The various loading conditions of the spine can be classified as Type 1: Ground muscles – the basic muscles attached to the processes of the vertebral bodies that are responsible for particular moments; Type 2: Resister muscles – the muscles attached to the vertebral body in more than one location that work in opposition to the standard ground muscle moments; Type 3: Factor muscles – muscles that cross several vertebral bodies before they reach the joint at which the actuation takes place.

## 2.6 Stability of lumbar spine

This section discusses how the tissues that surround the lumbar geometry work together to create a balance in stiffness and stability. Lumbar stability can be explained by considering the lumbar tissues, which provide the stiffness for resisting the loads during involuntary movements.

### 2.6.1 Importance of stability

The spinal muscles have a segmental pattern of attachment that is architecturally well suited to maintaining stability in the lumbar spine as discussed in Jemmett et al (2004) and Panjabi et al (1989). The stability of the lumbar spine is of prime importance for an efficient system. The muscle provides continuous energy during different loading conditions (Potvin et al, 2005). Muscle stiffness plays a very important role in stabilization, because the muscle with higher stiffness stores more energy. Thus spinal stability requires a muscular system capable of controlling segmental motions and

maintaining a normal nucleus neutral zone (NZ) as shown figure 2.22. The nucleus neutral zone is the centre position while the elastic zone (EZ) is the loaded position of the nucleus of the intervertebral discs.

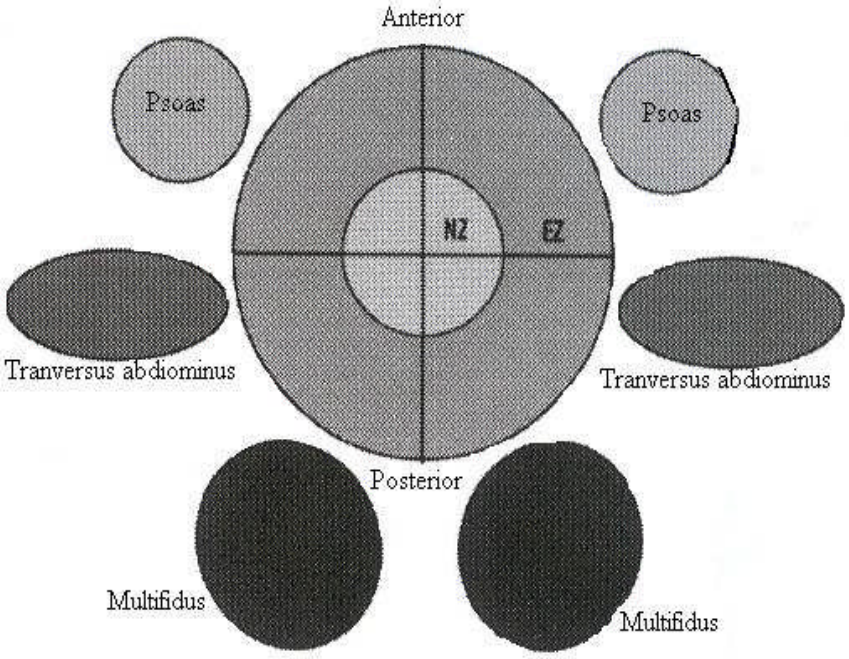


**Figure 2.22 Architectural relationship of lumbar intervertebral disc with stability (Jemmett et al, 2004).**

The flexibility of a lumbar spine is defined as the slope of the tangent of the linear portion of its torque-angular rotation graph as shown in figure 2.23. The nucleus neutral zone is defined between zero and the point on the rotation axis which is intersected by the tangent line. The stability of a model i.e. the return of the nucleus to the initial position can be tested by using a spirit level as was observed by Jermett et al (2004) and Panjabi (2003). The initial position of the bubble can be termed as a neutral position and the area in which the bubble moves is called as elastic zone as shown in figure 2.23.

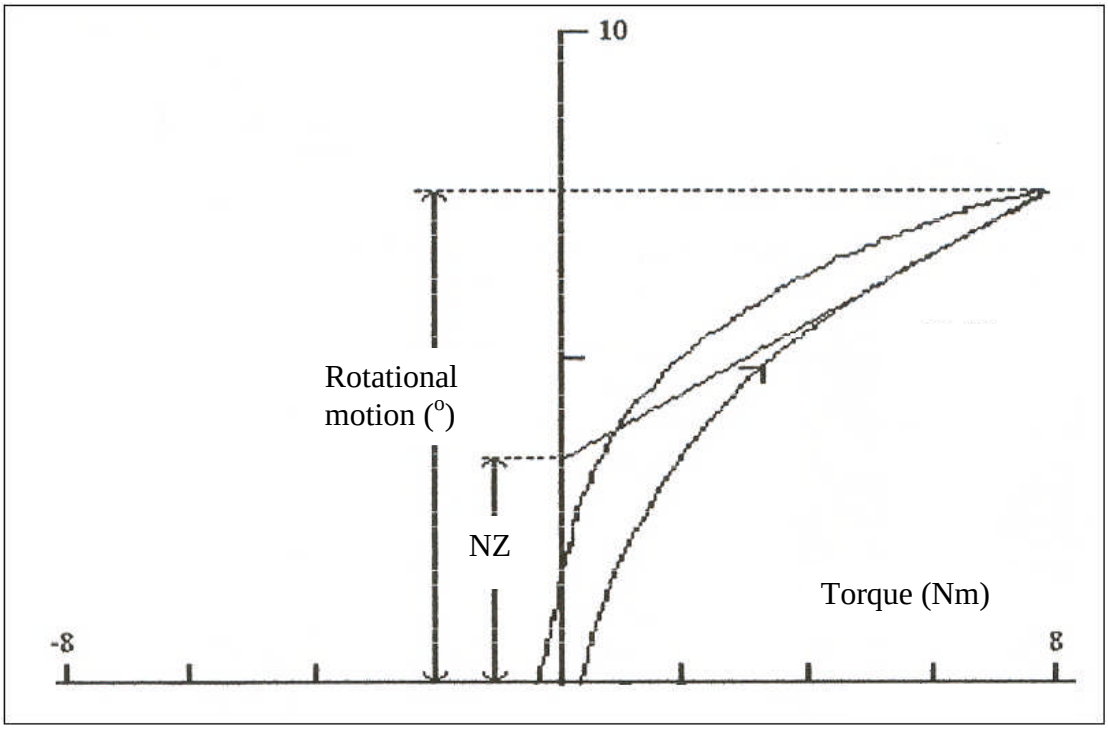


**Figure 2.23 Rotational motion and torque curve ( Adapted from Spencier et al, 2006)**

The nucleus neutral zone as described above, proposes a theoretical range of motion defining the mechanical stability of the lumbar spine. Panjabi (2003) discusses the stability with respect to pain and no pain groups. The study is based on the schematic model shown in figure 2.24.

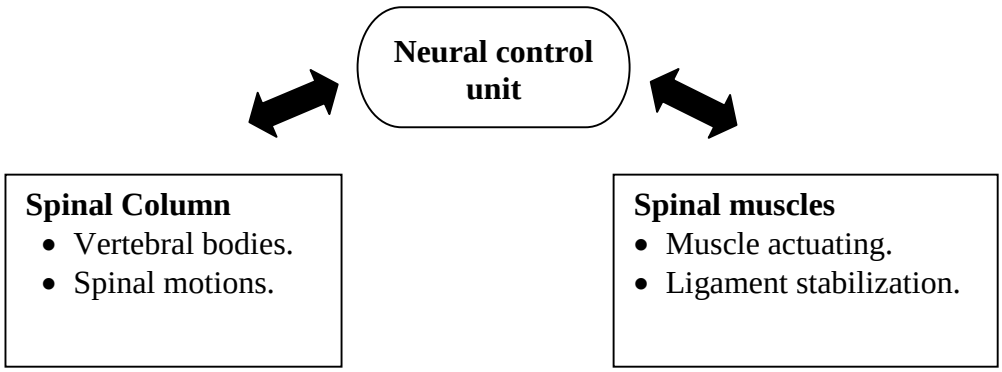


**Figure 2.24 The spinal stabilizing system. (adapted from Panjabi, 2003)**

Panjabi's model considers spinal motions with muscle activation controlled by a programmed neural control unit. For a given load, the necessary balance information is transformed into the muscle actions, with muscles working in tandem to stiffen the spine and control perturbations.

The study by Iida et al (2002) suggests that the posterior and anterior ligaments do not participate in the segmental stability of the lumbar spine. This statement was challenged by Panjabi et al (1989) who suggests that the ligamental stiffness provides

a necessary resistance to the intervertebral discs during translation. A prolonged consistent loading of the passive tissues decreases the stiffness and increases the deformations. The thoracic region of the spine has a relatively high stability because of the stabilizing effects of the ribs and the rib cage. This region extends from the first thoracic vertebra (T1) down to the level of twelfth thoracic vertebra (T12). Additional stabilizing effects are provided by the orientation of the articulating processes and the oblique arrangement of the spinal processes. Hence a significant force is required to cause a fracture or dislocation in this region as compared to the lumbar vertebral regions. The lumbar region can be considered more flexible and a transitional zone between the thoracic and sacrum region. The neutral position for a lumbar spine in a 2D sagittal plane is a function of posture with the pelvic girdle. The analysis by Jorgensen et al (2003) suggest that the grade 2 and 3 extensor muscles and grade 1 and 2 flexor muscles (discussed in Section 2.4.3), do not have uniform lengthening, which affects the spinal stability.

Stability in a mechanical system can be explained as equilibrium of a body to a state of resting with load(s) acting on the body. Thus the applied force must equal the reactions produced. The mechanical stability in a system also plays a significant role in its long-term resistance to fatigue due to high-induced stresses. Thus a mechanical system with moving parts, for example an engine that produces vibrations, will be stabilized by dampers, springs, fillers and cushioning materials, which will bear minimal loads, but produce resistance to mechanical fatigue.

Each fascicle in the functional spinal unit can be considered to provide mechanical stabilization for the naturally unstable human spine. The stability of a human lumbar spine can be studied as an alternating mechanical system, with switching muscular activity to maintain equilibrium of the mechanistic model. This for the stable lumbar spine, discussed in McGill et al (2000), indicates that for an efficient system, endurance training of the muscles surrounding the lumbar geometry is very important.

Muscle tone is considered as important when considering the stability of the lumbar spine. Weinstein et al (1995) used seven cadaveric lumbar spine models to study the different loading configurations, and concludes that the muscle forces required for standing are higher than in sitting posture and the forces in erector spine muscles are much larger in flexion than in extension.

The vertebral bodies with the tissues can be visualised as a mechanically stable system when the system is in equilibrium. The study by Jemmett et al (2004) proposed that inter-segmental stiffness of the lumbar spine is required to maintain the neutral zone.

Cholewicki et al (1999) suggests the lumbar spine can be considered to be an inverted pendulum with linear springs representing the abdominal, and erector spine muscles are shown in figure 2.25.

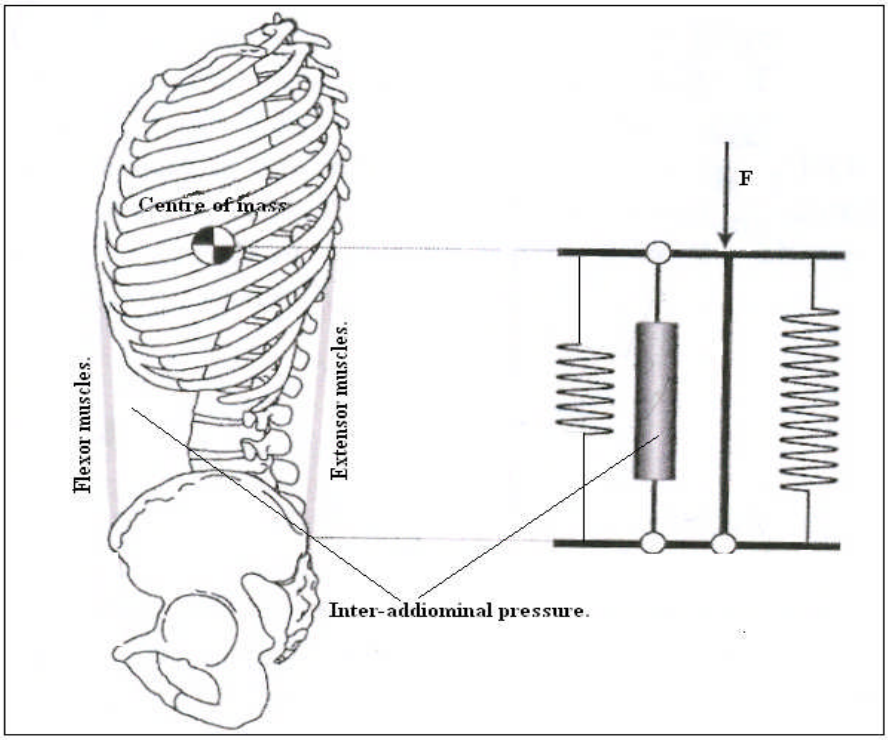


**Figure 2.25 Muscle modelled with intra-abdominal pressure.**
**(Adapted from Cholewicki et al, 1999)**

The abdominal pressure shown in figure 2.25 consists of a pneumatically actuated piston with compressed air to stabilize the spine. The study discusses stability produced by antagonistic flexor-extensor co-activation and abdominal muscle activation by inter abdominal pressure generation.

## 2.7 Lower back pain and spinal disorders

Lower back pain is one of the most common patient complaints, observed equally in men and women. Lower back pain discussed by Whiting and Zernicke (1998) is classified into two basic types, chemical and mechanical. Chemical irritation is associated with biochemical effects causing tissue damage. In contrast mechanical irritations are a result of over stretching connective tissues and possibly rupture of the intervertebral discs.

Tissue abnormalities are classified into disc damage, ligament failures and muscular pains. Nerve root syndrome is characterised by pain arising from the nerve root impingement due to herniated discs, which result from spinal disc degeneration. After thinning, the nucleus pulposus herniates out of the central cavity against the nerve root. Sciatica is a compressive neuropathy involving the sciatica nerve; which travels down through the buttocks and divides into the two legs. This pain is extremely severe as the nerve gets trapped between the ventral canals of the vertebrate and may cause pain or a paralytic complication in legs. As the lumbar vertebrae are located between the pelvis and upper torso, the degree of stresses endured by the lumbar spine is great and can cause trapping of nerve as shown in figure 2.26. These high degrees of stress result in frequent lumbar vertebral subluxations, misalignments and improper motion patterns of the lumbar vertebrae.

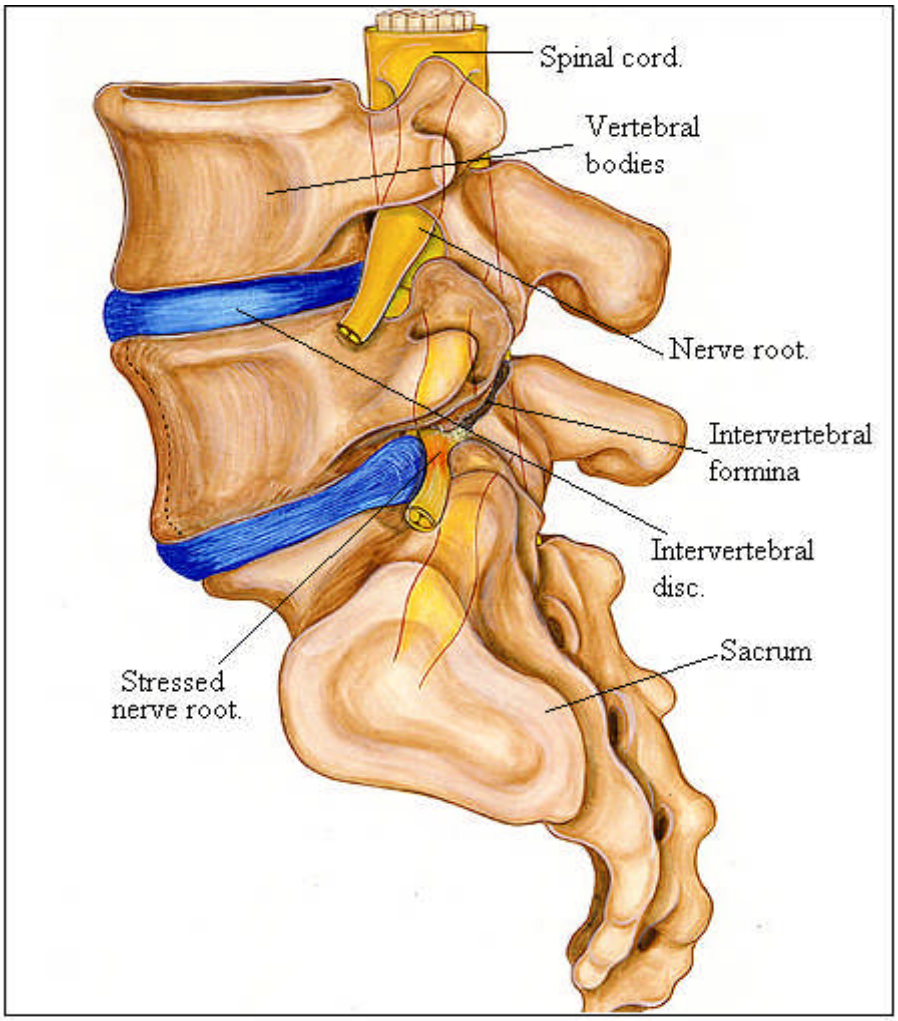


**Figure 2.26 Lumbar bone and spinal cord with nerve root pain.**
**(Adapted from Spine Universe, 2004)**

The tissues in the form of muscles and ligaments require adequate exercise to maintain strength and healthiness to bear different loads. Muscle strength and

flexibility is necessary to maintain the neutral spinal positions with a natural lumbar curve. Poor muscle strength (for example, weak abdominal muscles) causes flexor muscles to tighten causing imbalances in posture and uneven distribution of loads; thus causing the loss of stability and lower back pain. Sometimes, physical therapy and exercise regimens can be very effective in reducing back pain and minimising the need for surgery by strengthening the flexor, extensor and oblique muscles (Spine-health, 2005). Other diseases of the lumbar spine include bone abnormalities such as osteoporosis which increases the fracture risk for the vertebrae. The combination of disc degeneration and osteoporosis on vertebral bodies observed by Polikeit et al (2004) caused changes in strain distribution and compressional stiffness which eventually resulted in changes to the loading of the bones.

## 2.8 Cadaveric testing of the lumbar spine

### 2.8.1 Cadaveric models

Cadaveric modelling involves experimentation on human and animal lumbar spine samples that were removed during autopsy, and can provide invaluable validation of the computer models.

Brown et al (1957) carried out several types of mechanical tests on human cadaveric motion segments, and reported on disc bulge data acquired under pure axial compression, axial tension and combined bending. The data was collected using dial gauges to measure both the anterior and posterior bulges. Their study concluded that in the posteriolateral bulges the removal of pressure had no effect on the disc bulge, thus indicating that no special relation exists between intradiscal pressures and disc bulge. However this statement was questioned by Shirazi-Adl et al (1984) who used a finite element model to show that the bulge increased with increasing intradiscal pressure.

Pearcy (1985) reported on the range of maximum motions observed in loaded sheep discs, as summarised in Table 2.3. These movements of the vertebral bodies were observed with the entire musculature surrounding the bones.

| Levels | Direction of rotation | Maximum range of motion ($^o$) |
|---|---|---|
| L1- L2 | Extension | -5 |
| L2-L3 | Extension | -1 |
| L3-L4 | Extension | -2 |

**Table 2.3 Maximum range of motion (Adapted from Pearcy, 1985)**

Mow and Hayes (1997) reported on lumbar spine movements derived from radiographic studies of intersegmental movements of human spines. The study considered a cadaveric arrangement of the entire lumbar spine with the musculature performing extensions and torsions. The results of motion segments is shown in Table 2.4, which presents the average maximum intersegmental rotations.

| Level | Extension ($^o$) | Torsion($^o$) |
|---|---|---|
| L1-L2 | 5 | 1 |
| L2-L3 | 3 | 1 |
| L3-L4 | 1 | 2 |
| L4-L5 | 2 | 2 |
| L5-S1 | 5 | 1 |

**Table 2.4 Maximum intersegmental rotations of lumbar bodies. (Mow and Hayes, 1997)**

The *in vitro* dynamic mechanical testing of lesions in sheep discs has been discussed by Thompson et al (2004), with specific disc degeneration being related to changes in mechanical function of the disc. The effect of concentric and radial tears was examined experimentally as shown figure 2.27. He observed that they can disrupt the inter-lamellar bonds of the annulus, reducing the disc's ability to move, and any hysteresis (which is a result of fluid movement) can indicate an altered stress distribution in the disc. Furthermore during lateral bending, any affected portion of the annulus that was under tension would reduce the number of fibres resisting the motion. When the mechanical response after creation of the tears, was compared to the undamaged response, it showed that the nucleus, was unaffected by the disc lesions.

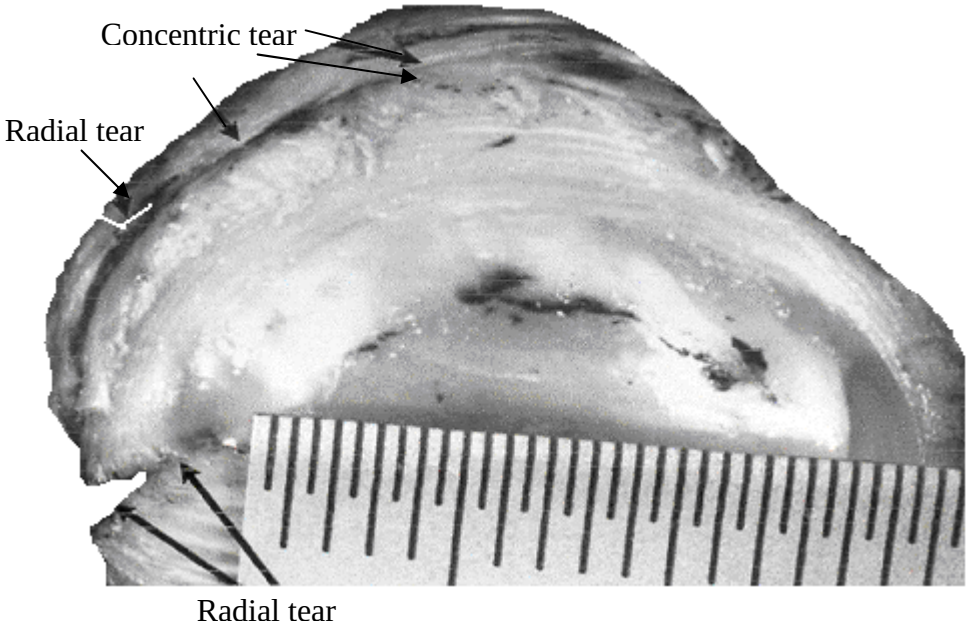


**Figure 2.27 Concentric tear and radial tear of the annulus. (Thompson et al, 2004)**

The result of experiments discussed by Seroussi et al (1989) showed that denucleated discs experienced an inward bulge in flexion and extension. Heidari et al (2004) used a cadaveric model to show movements of the vertebral bodies which causes loading that influences the collagen fibre. Thus this causes imbalance within the annulus fibrosus which alters the shape of the spinal curve resulting in destabilization of the vertebral bodies. The study also indicated that for healthy individuals during growth, the curve become more severe having displacements in the vertebral bodies, which increases the fibre elongation.

The study conducted by Fazey et al (2006) reported on the path followed by the nucleus during various types of movements as shown in figure 2.28. They observed that factors such as the surrounding tissues, the joint geometry and bone structure all influenced the path followed by the nucleus.

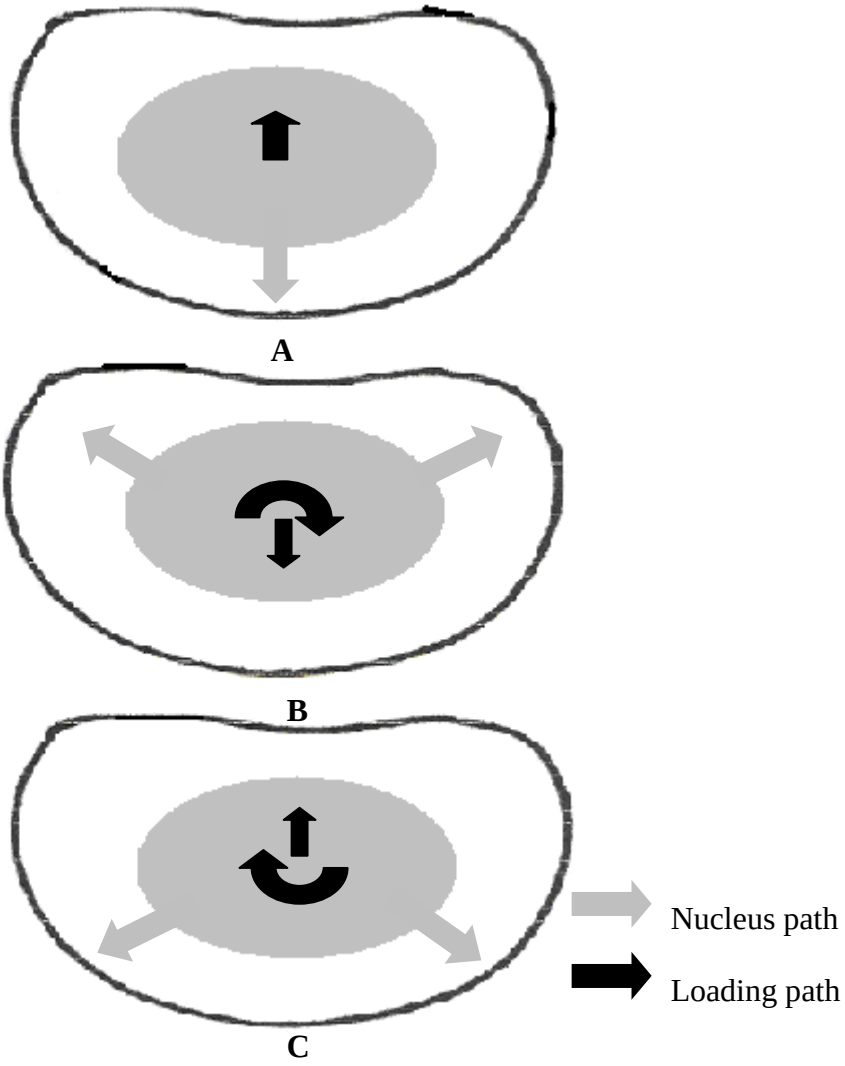


**Figure 2.28 Nucleus path followed during different loading**
**(A) shows movements in flexion or extension, (B) shows left rotation in flexion, (C) shows left rotation in extension. (Fazey, 2006)**

The respiratory system was investigated by Shirley et al (2003), and found to affect the posterior stiffness of the lumbar spine, influencing factors including trunk muscle and inter-abdominal pressure which vary with breathing. The study concluded that the stiffness of the lumbar spine increases with effort of the abdominal muscles in expiration. This destabilizes the lumbar spine extensor muscles thus causing increase in stiffness, due to the antagonistic pair of muscle activation.

## 2.9 Discussion

The lumbar spine is a complicated structure with very complex musculature and control. The entire human lumbar spine with all geometrical complexity physiologically performs all movements of the body. These movements are generated from the biomechanical movements of the different vertebral bodies connected to the

lumbar spine that as explained causes different behaviour of the intervertebral discs.

A very complex architecture of muscles and ligaments surrounds the vertebral bodies. The physiological movements are caused by different muscle activation connected to various processes of the vertebral bodies. The muscles considered in the lumbar spine model of Shirazi-Adl et al (2002) had extensor and flexor muscles modelled with different processes of lumbar vertebral body as shown in figure 2.29.

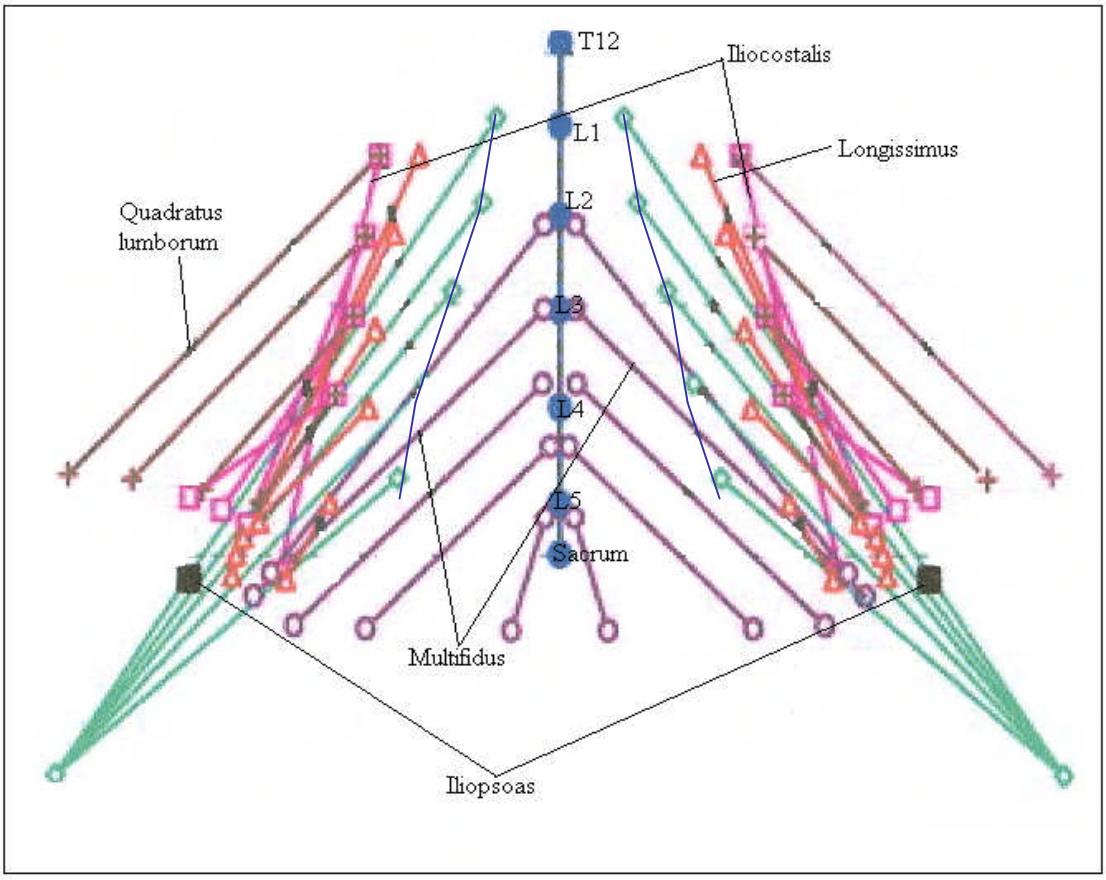


**Figure.2.29 Artificial muscle attachments.**
**(Modified from Shirazi-Adl et al, 2002)**

The use of cadaveric tissue to examine the biomechanical characteristics of individual components or sections of the spine is fraught with difficulties. Firstly, the method of storage will affect the results of the tests and the general condition of the sample. Secondly, it seems highly unlikely that the properties of dead tissue will be representative of living tissue, hence range of motion data, should be treated with caution. This may also explain why there is often variability between different researcher's results. Finally, the effect of diseases will affect the properties hence the source of material also needs to be considered carefully.

# CHAPTER 3
# Investigation of relevant technology

## 3.1 Introduction

This chapter gives an introduction to the key technologies relevant to the work carried out in this thesis – namely the development of the artificial laboratory spine. This includes a brief overview of computer modelling, artificial muscles and physical modelling. The artificial muscle modelling section considers architecture and recruitment patterns for optimal response of the model. Further, the chapter considers stability issues of the simplified geometry system, considering the vertebral motions and the activation control.

## 3.2 Computer model of the lumbar spine

### 3.2.1 Finite element modelling

Finite element analysis is a common engineering method for analysing static, dynamic and transient problems in which the geometry is divided into a finite number of elements whose behaviour can be specified in terms of equations and constraints of the boundary conditions and loading.

Belytschko et al (1974) modelled the intervertebral disc as two discrete volumes with separate material properties for the annulus and the nucleus. Kulak et al (1976) used a parameterised version of the annulus using average orthotropic properties for concentric sub-regions with the nuclei assumed to be incompressible and in a hydrostatic state.

Later models used composite or poroelastic properties for the discs. In the composite models the annulus was modelled using concentric lamellae with a nucleus. For example Shirazi-Adl et al (1984) developed a three dimensional non-linear finite element model of intervertebral disc with collagenous fibres embedded in ground substance, while the nucleus was modelled as an incompressible fluid as shown in figure 3.1

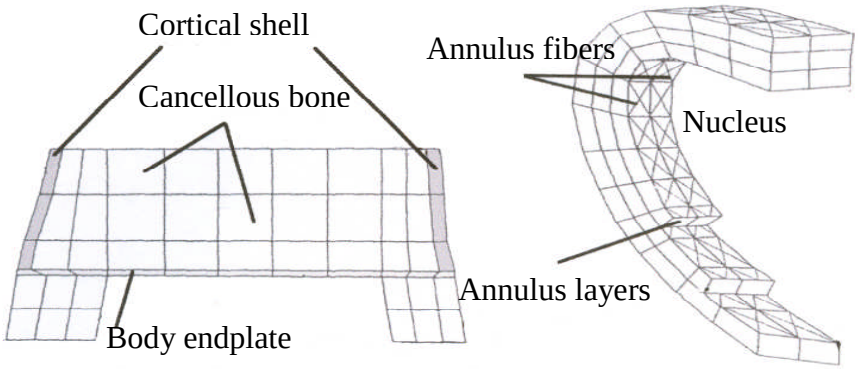


**Figure 3.1 Model of vertebral and intervertebral body (Shirazi-Adl et al, 1984)**

The poroelastic approach considers osmotic pressure effects and poroelastic swelling to simulate general hydration and dehydration of the disc behaviour. The model formulated by Simon et al (1985) shown in figure 3.2 concluded that the osmotic pressure could cause a change in response of the vertebral body movement. The direction of the nucleus for a normal disc in compression has a steady distribution of force as compared to the denucleated disc, which causes a concave shape at the walls of the annulus fibrosis.

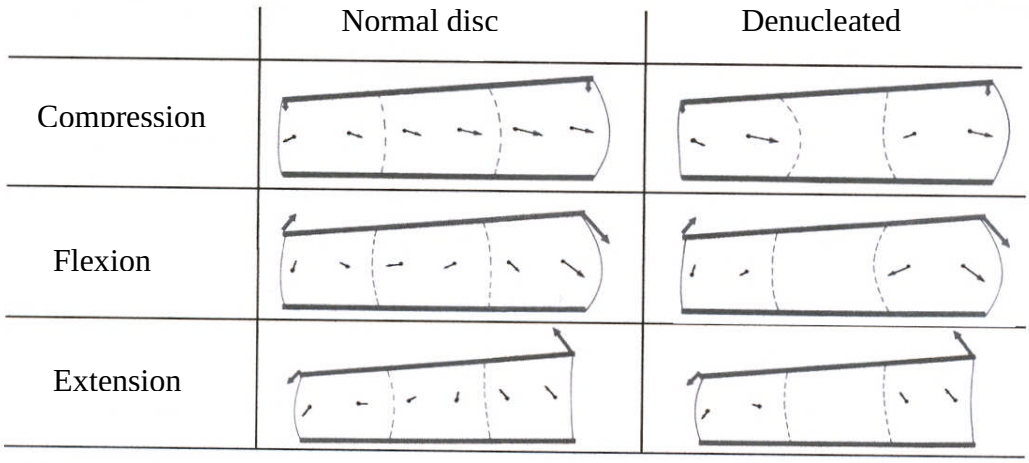


**Figure 3.2 Intervertebral disc bulge for normal and denucleated cadaveric discs. (Adapted Seroussi et al, 1989)**

Researchers like Lavaste et al (1992) created models of the entire lumbar spine from anteroposterior and lateral radiographs, as shown in figure 3.3, and examined variations in parameters such as facet spaces and disc fibre properties.

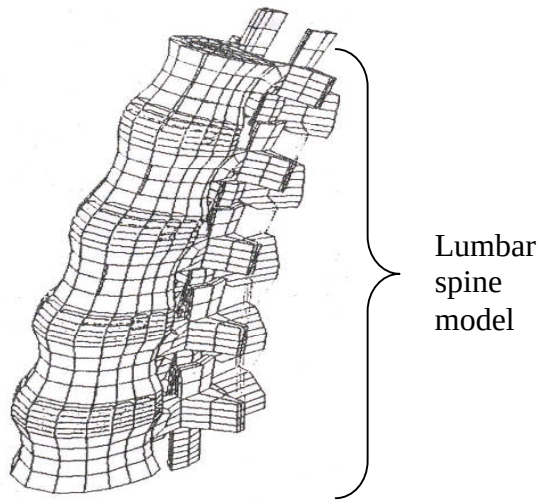


**Figure 3.3 A-three dimensional model of lumbar spine. (Lavaste et al. 1992)**

The model discussed by Najarian et al (2005) of the vertebral body and intervertebral disc included a cortical shell, cancellous core, endplates, pedicle, transverse processes, and spinous process with the intervertebral disc having nucleus pulposus and annulus fibrosus. Figure 3.4 shows their model generation using spline curves for the L4-L5 motion segments.

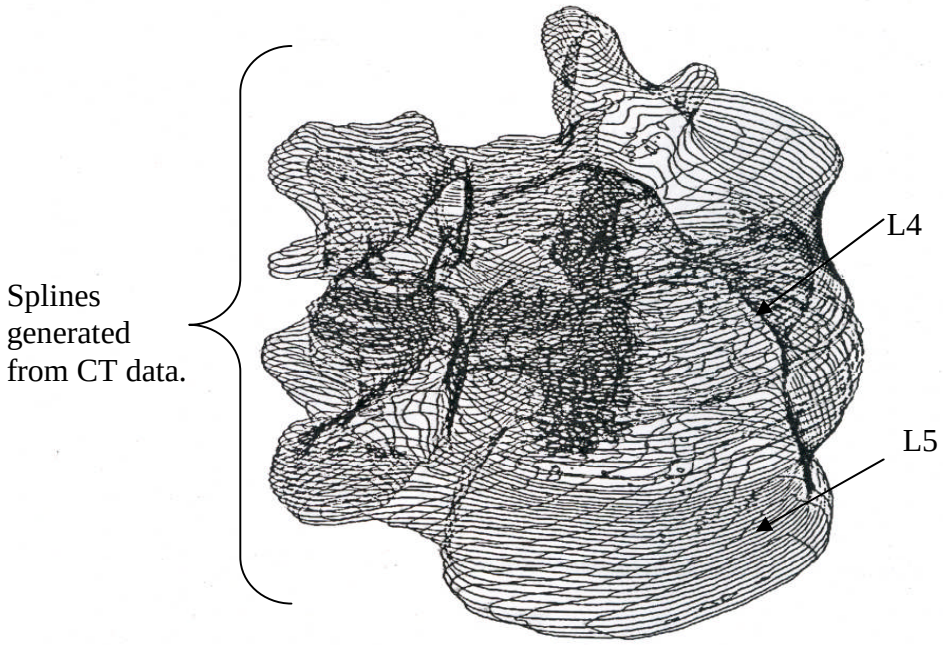


**Figure 3.4 Modelling of L4-L5 motion segments using splines curves.**
**(Najarian et al, 2005)**

Najarian's model also included anterior and posterior longitudinal ligaments with supraspinous and transverse ligaments to support the intervertebral disc. The results indicated a high concentration of stresses in the pedicles and the anterior section of the vertebral body. They concluded that damage to the intervertebral body

is a function of load, type of moment and its extent, with the highest stress concentrated on the vertebral arch and the pedicle areas. They also found that the posterior longitudinal ligament undergoes higher stresses during lateral bending while the supraspinous ligament experiences the highest stresses in extension.

Siddall (2003) generated a finite element model of the lumbar spine with intervertebral discs using CT data. Models of L1, L2 and L3 with their intervertebral discs were analysed. The structure of the disc was similar to that used by Shirazi-Adl et al. (1984) in Table 3.1 and as shown in figure 3.5. Fagan et al (2002) created a finite element model of the spine with a generic non-linear model of the intervertebral disc that was subjected to compressive, flexion and torsional loads. The effects of both material and geometric non-linearities were investigated for the three loads and were compared with the experimental data. The results showed that the non-linear geometry assumption had a significant effect for the compression-loading regime, while the non-linear materials options did not. (Fagan et al, 2002)

| | **Fibre** | | **Annulus** | | **Nucleus** | |
|---|---|---|---|---|---|---|
| | **$E_f$ (MPa)** | **$\mu_f$** | **$E_a$ (MPa)** | **$\mu_a$** | **$E_n$ (MPa)** | **$\mu_n$** |
| **Linear** | 500 | 0.3 | 4.0 | 0.45 | 4.0 | 0.499 |
| **Non linear** | 750 | 0.2 | 4.0 | 0.45 | 4.0 | 0.499 |
| **Ranges considered** | 200-1000 | -- | 1-5 | -- | 1-5 | -- |

**Table 3.1 Properties of materials used in Siddall's model (Siddall, 2003)**
**(E – elastic modulus and μ – Youngs modulus )**

The intervertebral disc consisted of a ground substance with embedded fibres. The angle for most of the fibres was about 30 to 65 $^{o}$ to the sagittal plane was modelled as cable elements in tension. The nucleus pulposus was modelled as an incompressible solid with properties given in Table 3.1.

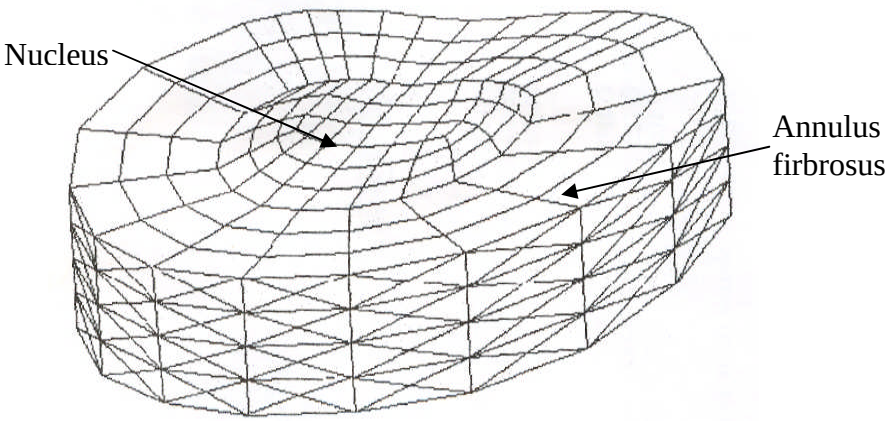


**Figure 3.5 The intervertebral disc (Siddall, 2003)**

In a later model developed by Shirazi-Adl et al (2002), each vertebra was modelled as two independent rigid bodies. One represented the main anterior body and the other the pedicles with the bony posterior elements. They used the same disc model that they developed previously.

Compression is one of the most common physiological loading conditions of the intervertebral discs. The intervertebral disc tends to deform due to the daily activities and postural movements, which increase with ageing. Molly and Blume (2001) explained the aging effect has an increasing Young's modulus of the nucleus *i.e.* decreased water content of the nucleus causing it to become stiffer due to dehydration. The younger spine has greater displacements that are partially due to the fact that there is more water in the nucleus at that time, allowing the nucleus to compress. As the water content decreases with age, so the ability of the nucleus to compress decreases. Thus these aged discs cannot properly support the loading.

Rohlmann et al (2006) developed a model of the lumbar spine and included the extensor muscles and abdominal muscle (i.e. flexor muscles). They used it to examine spinal distraction devices as shown in the figure 3.6.

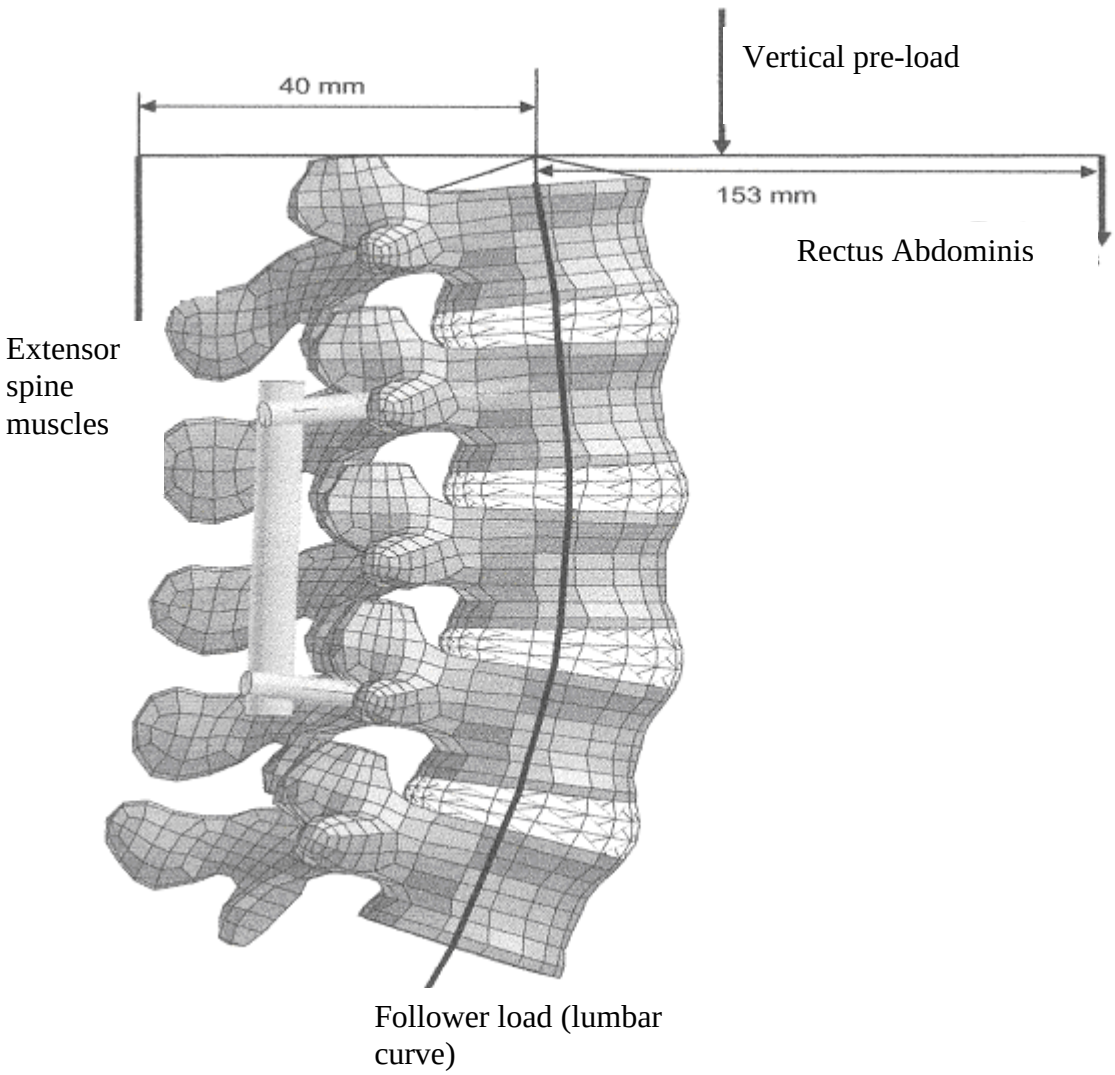


**Figure 3.6 FEM of the lumbar spine with extensor and flexor muscles (Rohlmann et al, 2006)**

A combined finite element and optimization approach was used by Goel et al (1995) to study the role of the muscles that were modelled as cable elements across the L3-L4 segment.

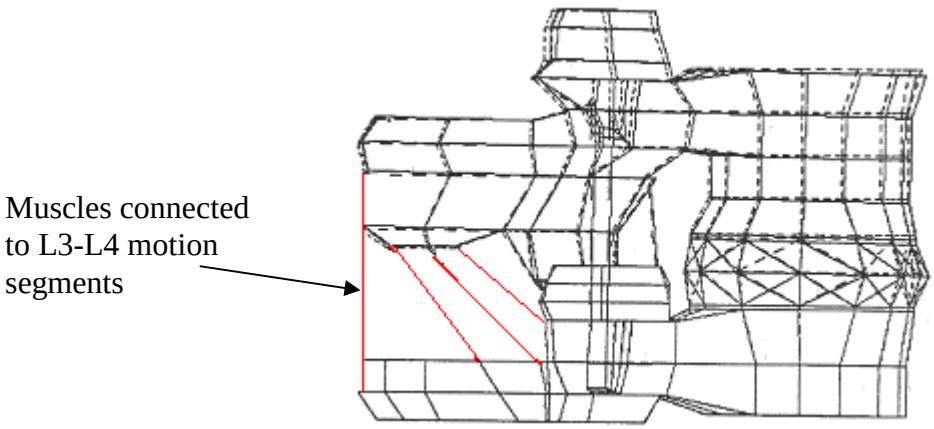


**Figure 3.7 Muscle activity model. (Modified from Goel and Gilbertson, 1995)**

The results showed that muscles affected the translation and rotation of the motion segments as expected, as illustrated in figure 3.7, which shows the movement of the L3-L4 motion segment. The finite element (FE) study reported by Yamamoto et al (1989) concluded that excessive extension in the lower region of the lumbar spine might lead to spondylolysis.

### 3.2.3 Other computer models

Another computer model developed using the software Anybody, (Anybody, USA) was discussed by Zee et al (2006). It had five segments with individual muscles, where the stiffness produced to resist movements between two segments was calculated as the product of cross-sectional area and specific muscle tension. The model assumed no abdominal pressure or ligament support and neglected the intertransversarii and inter-spinal ligaments. It concluded that the presence of multifidus, iliocostalis lumborum, oblique and psoas major muscles leads to a decrease in both stresses for the vertebral and intervertebral bodies, and stabilization effect which balances the forces in the lumbar spine.

## 3.3 Artificial muscles

The muscles in the human body convert chemical energy to mechanical energy. The live muscle cells are capable of adopting a variety of shapes and can carry out coordinated and directed movements that depend on the bone geometry and activities required. The muscles in the human body are a bunch of fibres, which contract and expand depending upon the control.

In this section, ideas for artificial muscle are discussed, with the aim of creating a similar force-length relationship to represent the actual musculature. Also the different control methodologies are introduced.

### 3.3.1 Artificial muscle types

The ligaments and muscles for the physical model essentially need to be elastic bands and force actuators respectively, depending upon the actuation process and functions. Various options are possible including magnetostrictive materials, electrostrictive materials, shape memory materials and simple mechanical mechanisms. Each of these options is now reviewed.

Magnetostrictive materials.

Magnetostriction is a property of a magnetostrictive material which can undergo a change in physical dimension due to a change in the state of magnetization. The history of magnetostriction begins in early 1840, when James Prescott Joule identified the change in length of an iron sample as its magnetization changed, which is now known as the Joule effect (Wayman et al 1983).

The most common form of magnetostrictive material available in commercial quantities, is Terfenol-D which contains two rare earth elements, terbium (Tb) and dysprosium (Dy). The magnetostriction can be modified in two ways, firstly by raising the level of Tb so enhancing the magneto-elastic performances and secondly by slightly reducing the amount of iron content (Fe) which increases the magnetization. A recent development with composition $Tb_{0.3}7Dy_{0.7}Fe_{1.95}$ has a slight excess of rare earth material at grain boundaries, so that the material is less brittle than normal. The material has Young's modulus between 25-35 GPa (Zhou and Xu, 2001).

The operation of magnetostrictive materials like Terfenol-D can be understood using a simple ellipse model as shown in figure 3.8. The material may be thought of as an ellipse where the magnetization runs along the major axis. Applying a field to the ellipse has the result of rotating the magnetization in the direction of the field and subsequently producing a change in shape.

The disadvantages of magnetostrictive materials as discussed by Heremans (1983) are that they are expensive with a large magnetic field that makes the control complicated. Also, the relatively small displacements (albeit produced with a large resultant force) require large amplifications.

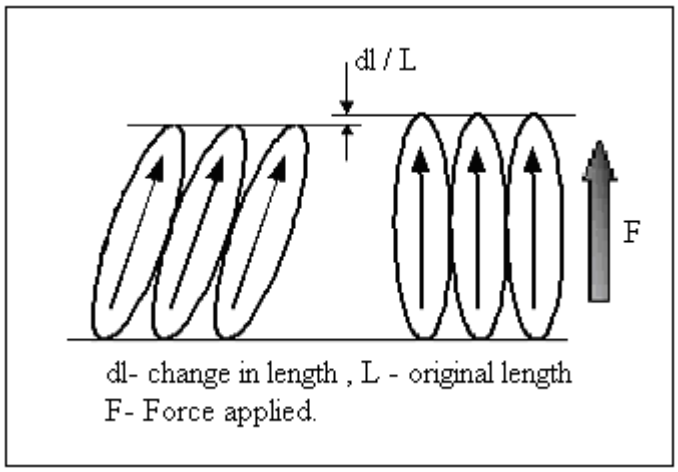


**Figure 3.8 Magnetostrictive materials showing change in length (Zhou and Lau, 2001)**

Electrostrictive materials

Electrostriction is a property of dielectric materials in which they form an elastic deformation when placed in an electric field. Non-piezoelectric materials, particularly barium titanate, can be used as electrostrictive materials. The electrostrictive response is highly dependent on the level of applied stress and output strain (Cohen, 2001), with large strain behaviour being the result of a $90^{o}$ domain switching, leading to a macroscopic polarization, and change in macroscopic strain. The degree of strain depends on the grain orientation (Steuwer et al, 2006). Thus domain switching can form the basis of large strain actuation in a crystal as shown in figure 3.9.

The disadvantages of electrostrictive materials are that they are slow in response and have a low electromechanical efficiency (Cohen, 2001). Also thermal expansion due to resistive losses can cause very high disturbances to outputs in various applications.

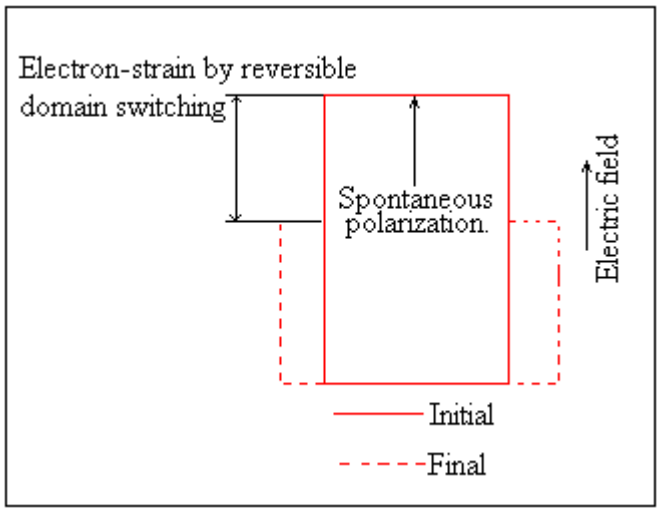


**Figure 3.9 Domain switching for electrostrictive polymers. (Steuwer et al, 2006)**

Shape memory alloys

Shape memory alloys are materials which have the ability to change to a predetermined shape when heated and return to their original shape when cooled. The phase change can be achieved by electric heating. When the material is heated it undergoes a change in crystal structure which causes the change in the length of the material. The shape memory material most commonly used is an alloy of nickel and titanium materials, known as Nitinol. These materials as described by Gilbertson et al

(2003) have very good electrical and mechanical properties, long fatigue life, and high corrosion resistance. The small size of the wires similar to muscle fibres also appear attractive for use as artificial muscles.

The other types of artificial muscles include mechanical mechanisms, including rack and pinion gears, levers, pneumatic muscles and hydraulic muscles. However these are likely to be large in size but would be mechanically efficient.

Among the alternatives discussed above the shape memory alloy was suggested as artificial muscle due to their sizes and constrain in space available for muscle attachment. Also the shape memory wires are like single fibres similar to that of actual muscles, thus are an ideal choice for shape memory wires was made as artificial muscles.

### 3.3.2 Comparison of artificial muscle options

The artificial muscle options that could be controlled electronically are compared in Table 3.2, with some of their key properties.

| **Property** | **Magnetostrictive materials** | **Electrostatic material** | **Shape memory alloys** |
|---|---|---|---|
| Maximum strain (%) | 0.24 | 5 | 8 |
| Maximum stress (MPa) | 28 | 43 | 200 |
| Work density($KJ.m^{-3}$) | 9210 | 2000 | 6450 |
| Maximum efficiency (%) | 2 | -- | 5 |
| Life cycle | $10^7$ | -- | $10^7$ |
| Elastic modulus (MPa) | 25 | 400 | 5150 |

**Table 3.2 Comparison of artificial muscles.**
**(Steuwer et al, 2006; Zhou and Xu, 2000; Gilbertson, 2003).**

Work density is the amount of work generated in one actuator cycle per unit volume of actuator. Efficiency is the ratio of work generated to input work supplied. Life cycle is the number of cycles or strokes the materials can endure. Thus a shape memory alloy appears the best option for muscle due to its the high life cycle, comparable modulus of elasticity and enhanced efficiency of performance.

## 3.4 Shape memory alloy as artificial muscles

### 3.4.1 Introduction

The shape memory alloy (SMA) popularly known as Flexinol or Nitinol is an alloy of nickel and titanium, developed by Naval Ordinance Laboratory. When a current is passed through a shape memory wire heating it to its activation temperature, the wire changes shape to that which it has been trained to remember i.e. the linear contractions and expansions. Thus it could be used to mechanically mimic actual muscles as linear elements. Gilbertson et al. (2003) comment that the wire simply reduces in length, conserving its volume and getting thicker by 4 to 8 %. Shape memory alloys, when cooled from the high temperature austenite form, undergo a phase transformation in which their crystal structure becomes weaker and transforms into its low temperature martensite form as shown in figure 3.10.

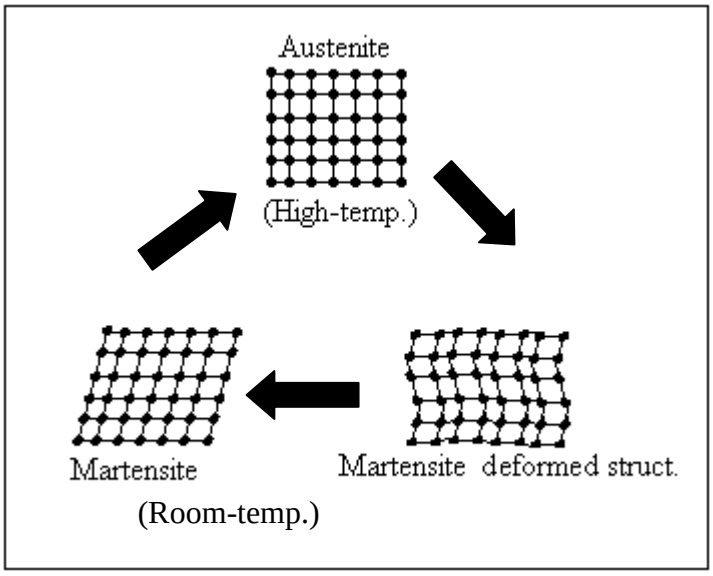


**Figure: 3.10 Mechanics of the shape memory effect.**
**(Gilbertson, 2003)**

The phase transformation occurs over a narrow range of temperature, although the start and finish of the transformation actually spreads over a much larger range as experimentally demonstrated in Chapter 4 and the hysteresis occurs because the temperature curves for heating and cooling do not overlap. However, for Nitinol wires of very small diameter ranging from 25 µm to 375 µm, the hysteresis is almost negligible as cooling below the martensite temperature is almost instantaneous. Therefore, contraction and relaxation of the wire depends solely upon the temperature of the Nitinol wire.

The unique properties of shape memory wires include pseudo-elastic

behaviour and a shape memory effect that can be used in many different fields of science and engineering. Biocompatibility of these alloys also makes them suitable for application to medical problems, as discussed by Machado et al (2003), as orthopaedic implants, cardiovascular devices, surgical instruments as well as orthodontic devices.

### 3.4.2 The shape memory effect.

In the martensite phase there is an absence of stress, and it is stable at low (i.e. room) temperature. For the austenite phase, higher stresses are caused due to the increased temperature. Initially the shape memory wire should be subjected to tensile loading in order to provide some fraction of pre-strain, to a certain percentage of its original length to regain its initial position, as discussed by Shu et al. (1997).

A study conducted by Nae et al (2004) states that when the applied stress is relieved from a shape memory alloy the material returns to the austenite phase that then assumes the crystalline cubic shape. As shown in figure 3.11, the decrease in temperature increases the length of the wire. This phenomenon is called pseudo-elasticity or super-elasticity. Deforming pseudo-elastic material results in the formation of a martensite crystal. The pseudo-elastic behaviour of the shape memory alloy can also generate a large amount of non-resilient deformation and so that it can recover its original shape at the end of the loading process.

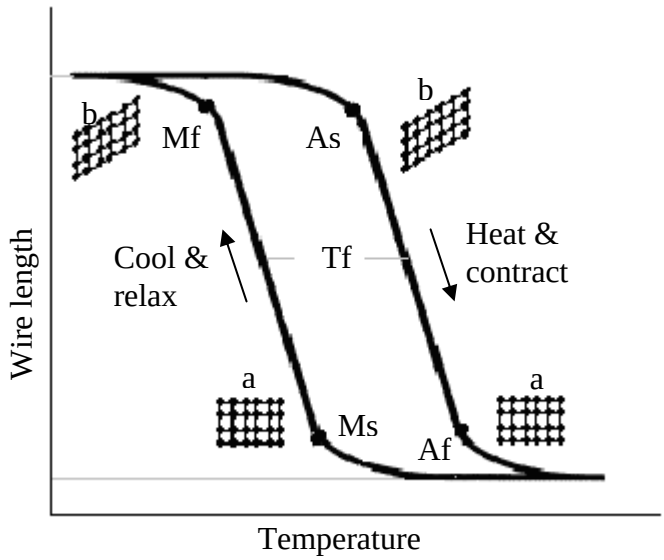


**Figure 3.11 Wire lengths vs. Temperature. (Adapted from Gilbertson, 2003)**

Mf – Martensite finish temperature (wire fully relaxed), Ms – Martensite start temperature (wire begins to relax), As – Austenite start temperature (wire begins to contract), Af – Austenite finish temperature (wire fully contract), a – Martensite form, b-Austenite form.

According to a study by Ma et al (2004) the inherent property of the material occurs as a result of the crystalline phase transformation as shown in figure 3.11 which occurs between the low temperature martensite and high temperature austenite phases. Thus when the wire is heated above the austenite start temperature by passing an electrical current through it, the SMA attempts to contract to its original length, thereby applying an actuation force. The force exerted by each wire depends on its composition and size. Larger diameter wires with larger lengths will exert more force than smaller ones having the same composition. The trained force applied to reset the wire to its original length is directly proportional to the biasing force applied by the elastic elements of the wire. The activation and relaxation temperature for Nitinol alloys can fall in a range between -200 to 110 $^{o}$C depending on the formulations of the alloy, with differences of less than 1% in ratio of the component metals in the alloy, greatly affecting the actual transition temperature
(Ma et al, 2004).

### 3.4.3 Properties of shape memory wires.

Shape memory alloy wires experience a change in length, which is proportional to temperature. This effect occurs over a narrow range of temperature. If the heat is below the material's annealing point, the crystallographic structure of the shape memory wires changes, which can cause damage to the wire and if is excessive it will cause the wire to overheat and melt. To prevent the wire from over heating Gorbet and Russell (1995) and Madill (1993) recommended that intermittent heating at a constant current should be applied, so that the wire is deprived of higher transient currents. The speed and strength of the wire contraction depends upon how fast the temperature of the wire is increased and decreased. According to the Dynalloy (2004) technical characteristics, the current should always be supplied in steps of shorter duration for the safety of wires. SMA springs can be designed such that they exert a precise force, but according to the study conducted by Velazquez and Pissaloux (2005) they can only apply a uni-directional tensile force and cannot directly apply a compressive force. Thus it is necessary to provide a biasing force to make it return to its initial position. This opposing force, used to stretch the wire back to the original length, is termed the bias force or return stroke.

The contraction time is directly a function of the current input. According to

Ma et al (2003) during its free moment an SMA actuator can generate 8% strain for single use and 5% strain for repeated operations with similar electrical resistance.

According to Gilbertson (2000) the maximum recommended recovery stress can be defined as the largest force a wire can exert when heated to protect and preserve the factory training; for Nitinol this is about 150 MPa i.e.

$$\text{Maximum force (N)} = \text{Maximum Recommended stress} \times (\pi/4d^2).$$

Table 3.3 modified from Madden et al (2003) shows a comparison between the actual muscle and the shape memory muscle.

| **Property** | **Mammalian skeletal muscle.** | **Shape memory muscle wire.** |
|---|---|---|
| Max. strain (%) | > 40 | 8 |
| Max. stress (MPa) | 0.35 | 200 |
| Work density ($KJ.m^{-3}$) | 1037 | 6450 |
| Efficiency (%) | 40 | 5 |
| Elastic modulus (MPa) | 10 – 60 | 5150 |

**Table 3.3 Comparative studies of mammalian muscle and shape memory alloy as muscle.**

Menciassi et al. (2004) conducted a study in which shape memory alloy wires were used to actuate a mechanical artificial earthworm. The SMA mechanism was inserted into the silicone shell and the disks, which were used to attach the wires, were glued to the internal part of the shell. The drivers and control of the SMA consisted of a sequential contraction of the modules, where each of modules was actuated by a square periodic signal, controlled by a microprocessor.

### 3.4.4 Improving the response of SMA wires

The Dynalloy technical specifications (2004) show that the shape memory response can be improved by optimising the cooling of the wire - by using the natural environment, forced air, heat sinks, liquid coolants and Peltier elements. In the model developed by Shu et al (1997) the temperature of the wire was increased by either a surrounding hot water bath or by resistive heating with an electrical current. In both the cases the temperature of the shape memory alloy was the driving factor, showing that the method of heat transfer needs improvisation. The optimization of the characteristics of shape memory wire discussed by Gorbet and Russell (1995) depended on two factors, i.e. limits on the heating current, to protect the wire, and

relaxation speed which is the cooling of the wire. The stress strain curves during austenite phase and martensite phase are shown in figure 3.12.

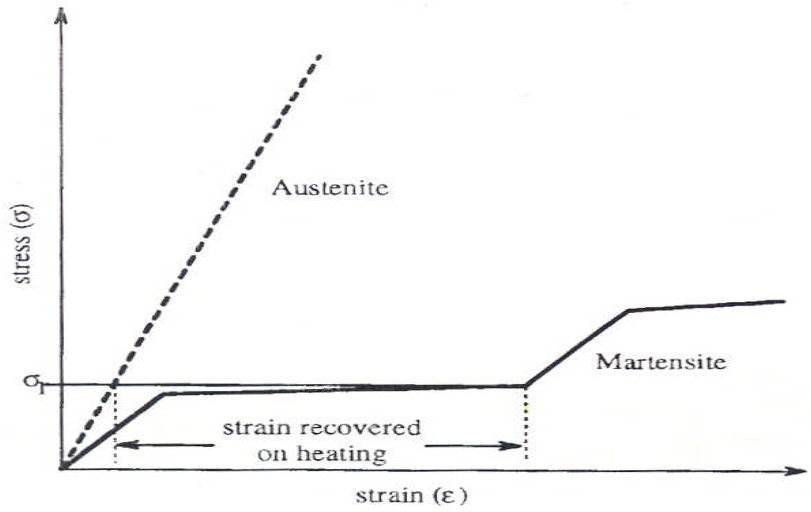


**Figure 3.12 Temperature phase for austenite and martensite curves. (Gorbet and Rusell, 1994)**

In the control mechanism studied by Holman and White (1993) the amount of heat generated was proportional to the volume of the wire, while the heat dissipated was proportional to the surface of the body exposed to the atmosphere. The property to dissipate heat was used to increase the cooling effect of the shape memory alloy actuator response, by using mechanical heat sink as heat exchangers, as shown in the figure 3.13. The heat sink shown in figure 3.13 can alter positions depending on the movement of the mobile link connected to the washer. The sink absorbs heat from the wire and due to larger surface area the convection is maximum. The movement of the mobile link shown in figure 3.13 helps the contact of the heat sink with the heated wire to absorb heat.

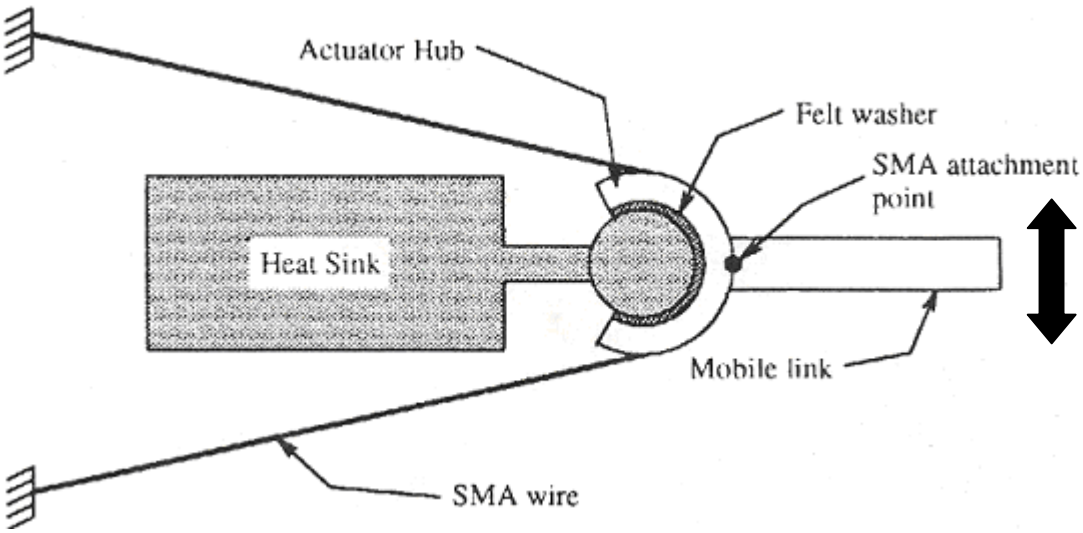


**Figure 3.13 Mechanical heat sink (Gorbet and Russell, 1994)**

The other techniques for cooling SMA wires can be achieved most effectively by using a Peltier element. In this system dissimilar metals held at different temperatures, develop a micro-voltage at the material junction in a phenomenon called the 'Seebeck effect'. Alternatively, when a voltage is applied a temperature difference between the junctions is seen. Thus the inverse of the 'Seebeck effect' results in a heat pump called a Peltier element. The main advantages of using a Peltier element is its compactness, as it is a solid state heat extraction device with no liquids, and is free from refrigerants such as chlorofluorocarbons.

The only disadvantage of using Peltier elements is that the hot surface should be in complete contact with the peltier element for it to extract heat. Bhattacharyya et al (1995) and Lagoudas and Bhattacharyya (1998) commented that the Peltier element cannot be used for applications where the wires have a very small area.

Nae et al (2004) used forced convection for the heat transfer from shape memory wires wires, which is also an effective technique for reducing the temperature. Figure 3.14 compares the natural free convection (coefficient $h_n$ =1.5 $W/m^2K$) and forced convection (coefficient, $h_f$ = 150 $W/m^2$ K) when experimentally measured for a 100 μm shape memory wire. Hyo and Lee (2003) discussed that the speed of response for using a computer-programmed fan with a K type thermocouple can increase shape memory alloy wrapped around the wire.

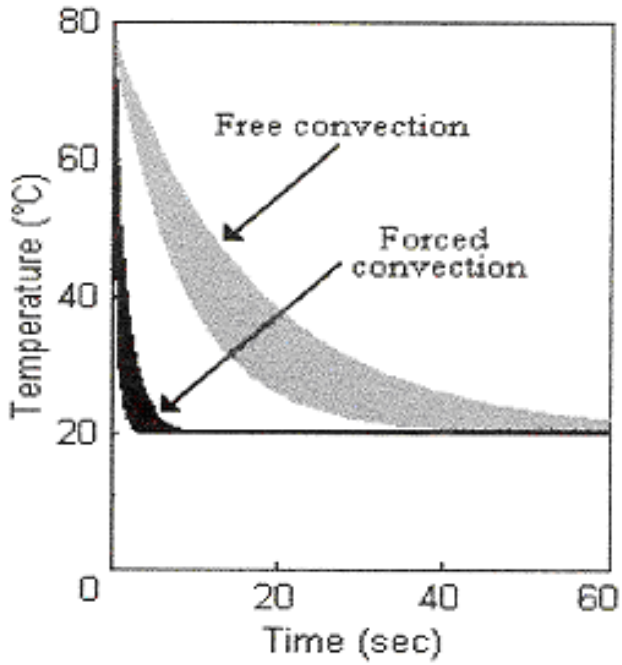


**Figure 3.14 Comparison for responses of free and forced convection. (Velazquez and Pissaloux, 2005).**

Kuribayshi (1991) proved that the maximum stable frequency response of an actuator was achieved when the wire was placed in a forced air environment and a very high current was passed into the wire to heat the wire quickly and then switched off.

Power produced by a shape memory alloy model can be calculated by using the second law of thermodynamics and Carnot cycle. The integral gives work-done to cause displacement from one position to another.

$$\Delta W = \int P dv = \rho C V \frac{dT}{dt} = W_s - |W_q| \qquad (1)$$

The above equation (1) is the amount of energy transferred from one system to another in which: W is the work done, ρ is the density of SMA, C is the specific heat capacity, V is the volume of SMA wire, $W_s$ is the work supplied to the shape memory wire, $W_q$ work processed by heat transfer. This is calculated from;

$$W_q = Q_{cd} + Q_{cv} + Q_{rd}$$

where $Q_{cd}$ is the heat transfer due to conduction which can be neglected (Velazquez and Pissaloux, 2005), because shape memory wire has low internal resistance and experiences a uniform temperature distribution; $Q_{rd}$ is the heat transfer due to radiation which can be neglected (as only one set of wire is actuated with a time interval and also the shape memory wire has a constant current passing through it for heating); $Q_{cv}$

is the heat transfer due to convection. This last term can be calculated by considering a cylindrical model of the wire with a given length, exposed to the atmosphere. This can be expressed as;

$$Q_{cv} = qw = hc(t_w - t_b)$$

where, $t_w$ is the wire temperature.

$t_b$ is the bulk temperature.

$$hc = k/d \times Nu.$$

where, hc is the heat transfer coefficient which can be given by $W/m^2\ ^oK$, k is the thermal conductivity of material and d is the diameter of the wire studied under convection.

The non-dimensional (Nu) Nusselt number for laminar flow is a function of the boundary conditions which can be expressed in terms of the Prandtl and Reynolds numbers (Rohsenow and Hartnett, 1973). The above calculations can be used for the calculation of the force produced by a single wire or a bundle of wires. This is used in Appendix C for calculating the force and heat transfer coefficient.

## 3.5 Control for shape memory wires

### 3.5.1 Controlling shape memory wires

The control of electrically operated actuators depends on the force and time response, which must be analyzed and optimized in the design (Velazquez and Pissaloux, 2005). A simple circuit constructed using a DC power supply cannot be implemented easily as a control system, as the shape memory wire needs constant heating, and to save the wire from overheating a regulated supply is always preferred.

A helicopter with adaptive control by shape memory wires designed by Roglin et al (1996) had a switching ‘on and off’ control channel, thus transmitting on and off signals to the actuator. Further, they showed that the strength of the input can easily controlled by pulse width modulation. The concept of pulse width modulation can be explained by figure 3.15 in which the muscle wire operates for an ‘on and off’ sequence of operations. Since SMA control consists of constant heating and cooling cycles, the efficiency of the response was also altered with a varying current. A simple ‘pulse width modulation circuit’ rapidly turns the power on and off to control the average current flowing through a muscle wire. The name pulse width modulation suggests that the current supplied is in the form of square pulses, whose width can be

changed as per the user interface connected. Ma et al. (2003) and Achuthan et al (2001) conclude that the relationship between the force generated by an antagonistic SMA actuator and the normalized electrical resistance for shape memory wire is linear. Thus, actuating Nitinol wire using the pulse width modulation has distinct advantages.

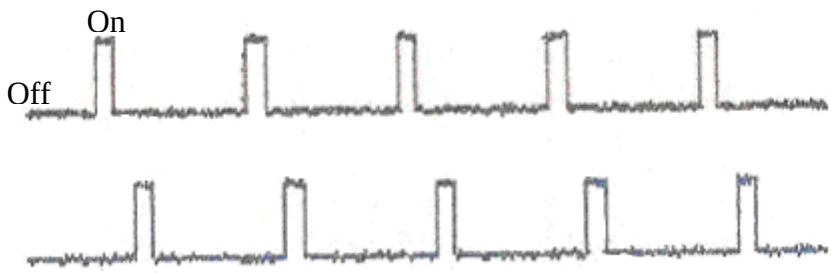


**Figure 3.15 Pulse seen rising for the actuating model with different muscle actuations (Menciassi et al, 2004)**

The oscillating on and off of the power allows more even heating of the wire and allows better control of the Nitinol wire for longer periods of time, without causing heat damage to the crystalline structure of the shape memory alloy.

## 3.6 Testing of mechanical discs

The long-term aim of this research is the development of an artificial laboratory spine that will have the same physical and biomechanical properties as that of the human spine, and will eventually be made available for testing of new implants, instrumentation and procedures. In particular, this work considers the development of intervertebral discs for the laboratory spine and active muscles that will be able to move the spine in a physiologically reasonable way to analyse the disc behaviour.

Intervertebral disc prostheses usually comprise of two metal plates and a cushion interposed between the plates as shown in figure 3.16. The cushion includes a compressible body having two ends in contact with the plates. The two ends of the disc geometry have one end that is freely displaceable to the plate and the other fixed. Thus the prosthesis imitates and approximates the mechanical properties of a healthy natural intervertebral disc.

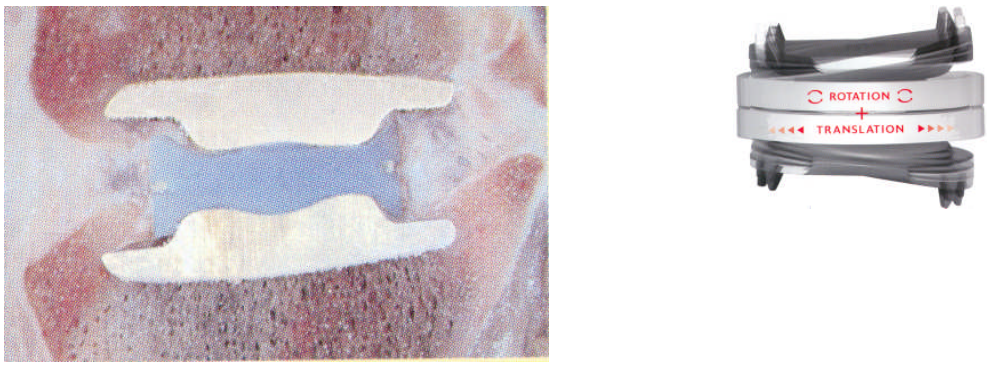


**Figure 3.16 Mechanical discs with translation and rotation.**
**(Modified from Valdevit and Errico, 2004)**

A disc such as this was tested in the laboratory spine. Other potential applications of the laboratory spine include the investigation of certain surgical techniques. For example, the technique used by surgeons to repair the vertebral bodies using bone cement known as vertebroplasty. For this work the vertebral bodies would need to have properties representative of the actual vertebrae, so that when cement was injected into them, they would stiffen in a realistic way.

Another application includes analysing the vertebral body displacements during fusion of adjacent vertebrae when the disc is too damaged to repair.

# CHAPTER 4

# DEVELOPMENT OF A LABORATORY SPINE WITH ACTIVE MUSCLES

## 4.1 Introduction

The entire development of the laboratory spine was phased into the simplified geometry spine and actual geometry spine. This chapter discusses the basic design and development of the simplified physical laboratory spine. The simplified geometry spine was designed to physically test the properties of material, design a control system and physiologically control the movements of the vertebral bodies by reducing the geometrical complexity of the actual lumbar geometry. In particular, the design data considers the simplification of geometry applied to the vertebral and intervertebral bodies, with further simplification of designing the muscles and elastic elements. The control of these artificial muscles is also discussed below. The reference data is mentioned in Chapters 2 and 3 from the in vivo and cadaveric human lumbar spine and tissue modelling.

## 4.2 Geometrical modelling of simplified laboratory spine

The simplified laboratory spine was developed with a simplified vertebral body design, PU-foam intervertebral discs, springs acting as ligaments and shape memory wires acting as artificial muscles discussed in this section.

The geometry of the simplified vertebral bodies is shown in figure 4.1. They have a solid cross-section and representative spinous and transverse processes, as shown in figure 4.1, where the dimensions are chosen so that the overall geometry was representative of the natural vertebral body (figure 4.1A). The actual geometry of the main body for the lumbar vertebrae was simplified as a circular shape for manufacturing and design simplification, thus the diameter of the vertebral body was idealised as 50 mm for the main body.

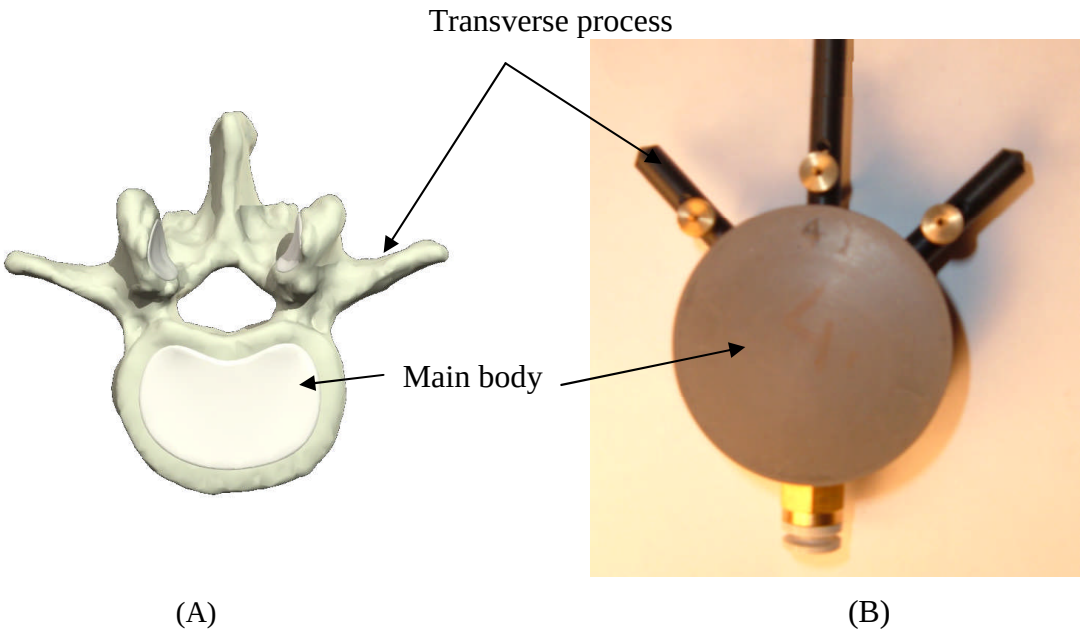


**Figure 4.1 Simplified geometry vertebrae with protruding processes.**

The spinous processes represented by the black protruding parts on the simplified model, were positioned so that they formed an angle of 45$^{o}$ with the transverse process as seen in the actual geometry vertebral bodies and had several holes drilled along their lengths in which the muscle wires were located. The intervertebral discs were circular and designed to fit the vertebral bodies, with an internal cavity of diameter 25 mm.

## 4.3 Material selection and properties

Vertebral bodies

The vertebral bodies of the physical model were manufactured from Acrylonitrile-butadiene-styrene (ABS) P400. This was chosen because ABS is tough, resilient and easily moulded. The Young's modulus for actual vertebral bodies ranges from 1.2 to 5 GPa (Langrana and Garske, 2003) while the Young's modulus for the simplified vertebral bodies is 1.5 GPa. Also the same material was used in the Fusion Deposition Moulding, as discussed later in Chapter 6 to manufacture the accurate geometry vertebral bodies.

Intervertebral discs

As in the natural spine, the vertebral bodies are much stiffer than the intervertebral discs, the material used in the manufacture of the discs is critical to the artificial spines. Therefore a number of different materials were considered, as summarised in

Table 4.1, which compares the values from the data sheets provided by the respective companies was determined experimentally.

| **Name of material** | **Manufact.** | **Hardness (Scales)** | **Tensile Streng. (MPa)** | **Tensile modulus (MPa)** | **General characteristic and method of manufacturing** | **I.D.** |
|---|---|---|---|---|---|---|
| AD 25 A/B | ACC | 29 (A) | 5.2 | - | Room temperature cure, Non corrosive, tear resistance. | ACC AD 25 A/B |
| RTV 940 | ACC | 38-42 (A) | >4.4 | - | High tensile strength, high hardness, fast curing process. | ACC RTV 940 |
| Silcoset 101 | ACC | 55 (A) | 4.13 | - | Cure at room temp, can be used at higher temp. | ACC Silcoset 101 |
| Silicone foam | Zotefoam | 1-5 | 2.41 | - | Extremely flexible applications. | Zotefoam Silicone foam |
| PU-foam | TW-foams | 0-1 | -- | 15-30 | Extremely flexible and easy for making shapes and cheap. | Foam |

**Table 4.1 Comparison of potential materials for the intervertebral discs**.

The hardness scale (i.e. the resistance to permanent indentation) played an important role in the selection of the material (further details of the different constituents of the different materials and their casting processes are included in Appendix A and B). The intervertebral disc moulded from silicone rubber was manufactured using silicone foam material and rubber material, where the ratio of rubber used in the silicone foam dictated the stiffness of the intervertebral disc. Among the various materials shown in the Table 4.1 the most suitable material for the disc was PU-foam, which was affordable, easily fabricated in different shapes without change in properties and with hardness between 0 to 1. The materials with higher hardness have a very high Young's modulus and have very low compression strength. The elastic modulus of the different materials was measured using a Q800 DMA (Dynamic Mechanical Analyser) – (TA Instruments, USA) shown in figure 4.3.

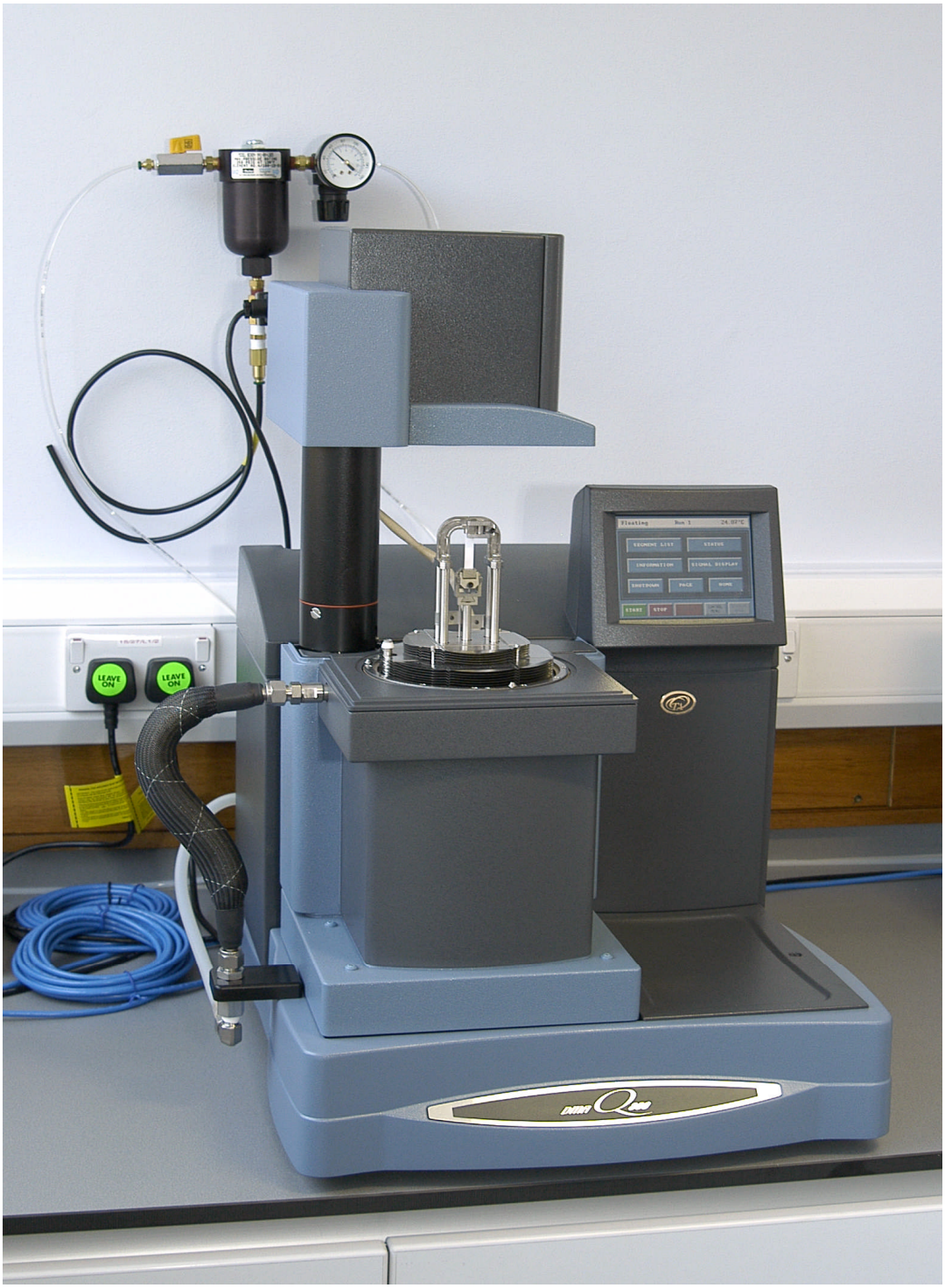


**Figure 4.3 Dynamic Mechanical Analyser (DMA).**

Samples of the foam materials and SMA wire were tested in TA instruments DMA (Q800) and DSC (Q100) (Differential Scanning Calorimeter) – (TA Instruments, USA) to determine the thermal contraction characteristic and temperature at which the phase change occurred respectively. The stress-strain graphs produced by the DMA for the different materials with similar size samples and uniform load of 1N/sec for 5 minutes were obtained as shown in figure 4.4.

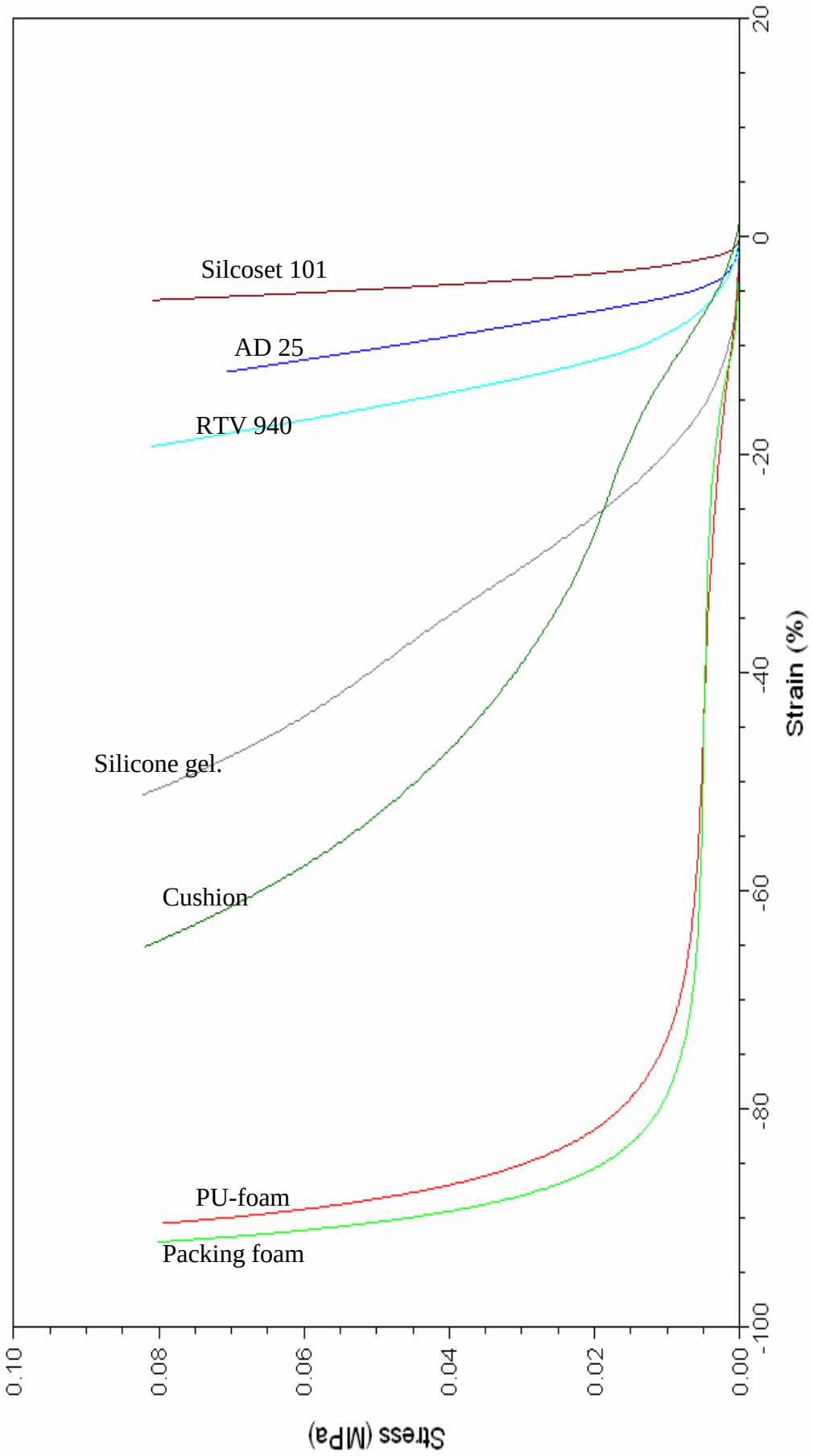


**Figure 4.4 DMA analyses for material selection of intervertebral disc.**

Thus test results show that PU-foam has better compressive properties and has a lower elastic modulus i.e. the slope of stress and strain curve. The properties observed above shows that Silicoset 101 discussed by Siddall (2003) as intervertebral disc has lower compressive properties than PU-foam.

These properties were further tested with an experimental analysis in which a PU-foam sample was compressed and the corresponding changes in stress and strain were measured and compared with DMA results, as shown in figure 4.5.

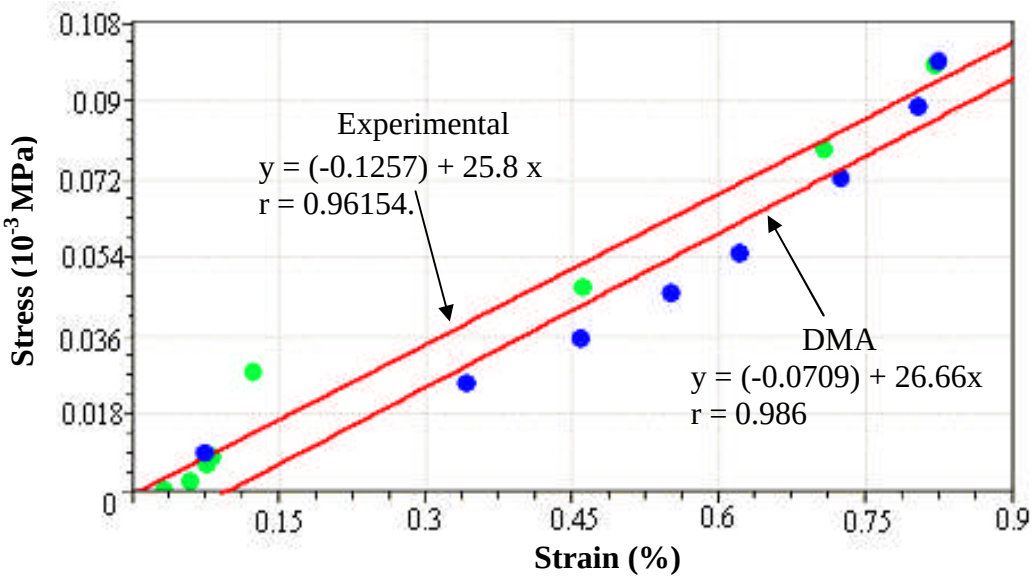


**Figure 4.5 Experimental and DMA analyses for calculation of stress strain behaviour for PU-foam.**

A best-fit line fitted through the data points (r = 0.986) showed that the slope (i.e. the Youngs modulus) was 26.67 MPa

<u>Improving properties for intervertebral disc material</u>

According to the literature an intervertebral disc (Section 2.3) has a nucleus surrounded by criss-cross fibres which varies the stiffness of the disc. Figure 4.6 shows various results from constructions of the intervertebral disc with free PU-foam sample i.e. without a cloth, straight fibre PU-foam sample and cross fibre PU-foam samples that were analysed. An angular displacement was observed with loading supplied by the artificial muscles. Among the various fibre constructions a PU-foam wrapped with a cross fibre shows repeatable displacements and better compressive and torsional properties. Thus showing that the displacement between each motion segment is repeatable (with different test numbers) with cross fibre wrapped cloth PU-foam sample.

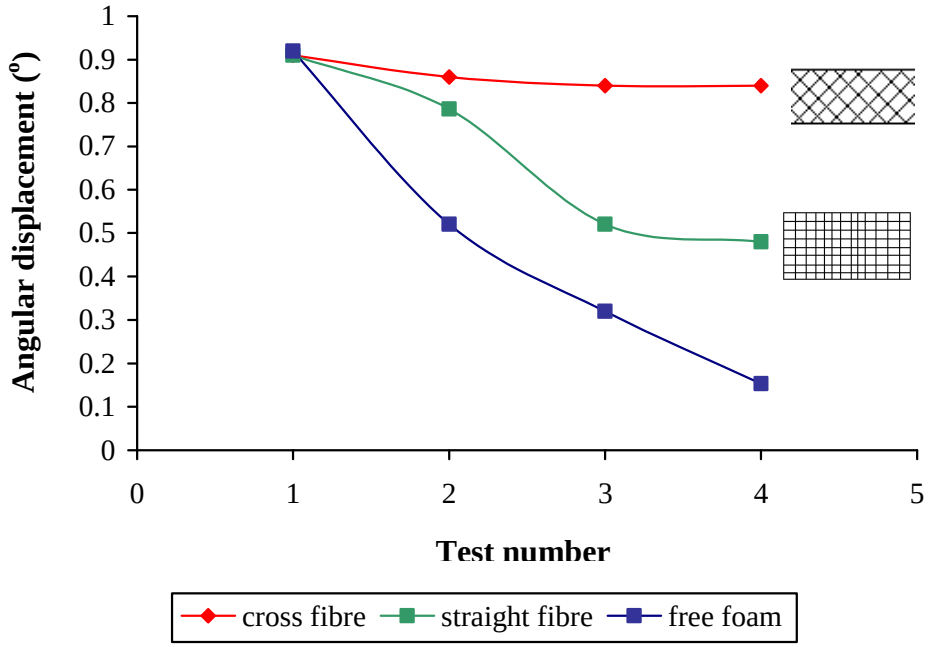


**Figure 4.6 Angular displacement observed for intervertebral disc with various constructions**

Thus torsional and compressive strength in the simplified model was made very effective by a cloth with 45° criss-cross fibres, wrapped around the PU-foam. The cloth was attached to the model by designing a jig to hold the vertebral bodies as shown in figure 4.7 so that each disc was placed in equal compression, which acts as pre-loaded springs. Grant and Hayward (1998) showed that a pre-loaded compressive spring is a very effective for system stability, which was similar to the compressed foam.

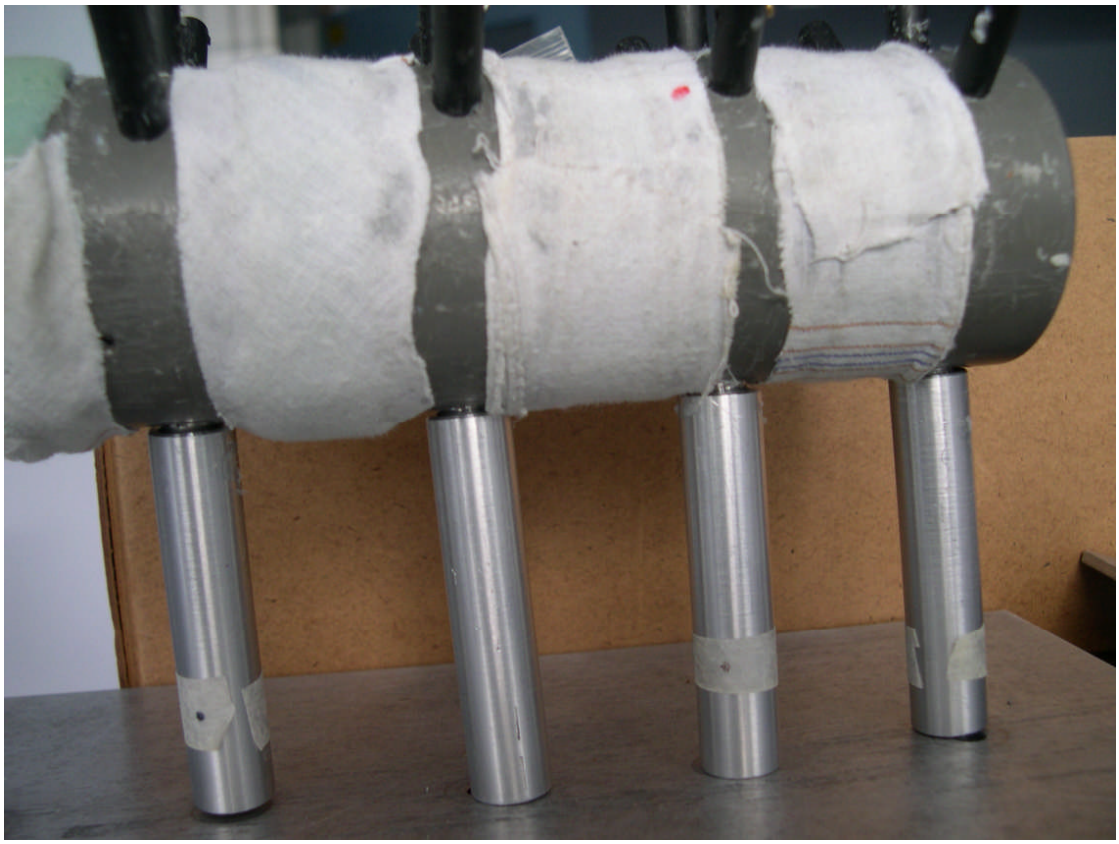

**Figure 4.7 Jig for holding the vertebral bodies.**

The radial pressure on the nucleus and the annulus gives the disc additional resilience. Thus considering the resilient behaviour of the disc and repeatability in the simplified spine model a PU-foam disc with cross fibre cloth was used.

## 4.4 Properties of SMA as artificial muscles

The muscles in the lumbar spine work against each other in order to maintain the spine's stability, as discussed in Chapter 3. The artificial muscles should mimic the muscular function as closely as possible in terms of force exertion capacity, architecture of muscle, strength to weight ratio and speed of response. The other important characteristic of the artificial muscle is the load stabilizing ability under various loading conditions.

When heated the shape memory alloy has an extremely high power to weight ratio as discussed in Section 3.5 and with a suitable preload and retracting force it can regain its original position. The attachment points of the muscle wires on the ABS vertebral bodies used a turnbuckle arrangement, where the screws were hollow, allowing the wires to pass through them and attach to an electrical connector at the head of each. Unscrewing the screw allowed the wires to be tensioned (this is equivalent to the 'tone' of the natural muscle). The wires were then attached between

the spinous and transverse processes as shown in figure 4.8, passing through brass bushes in the intermediate processes (to protect the ABS plastic).

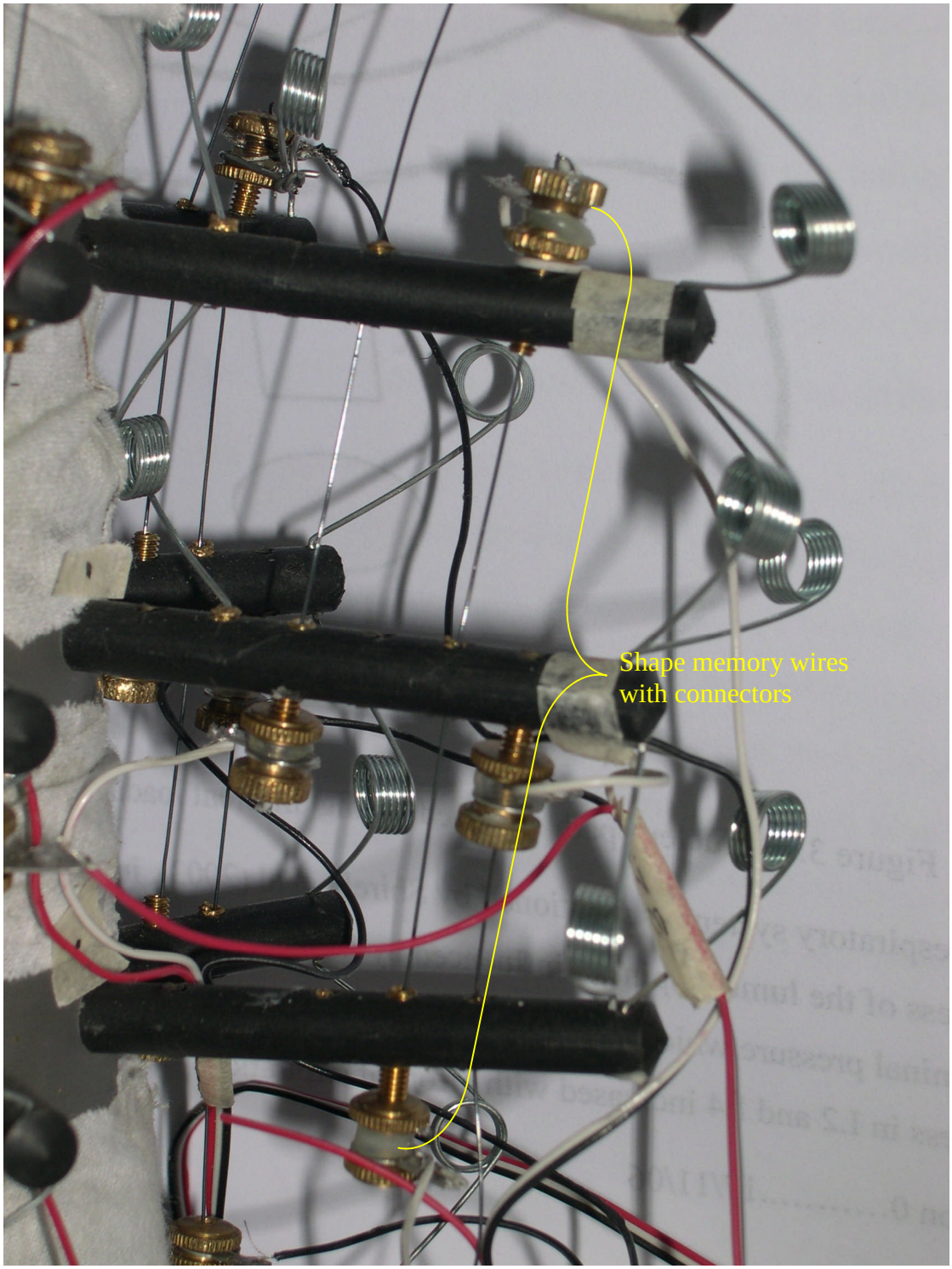


**Figure 4.8 Connectors with pretension in wires.**

Basic force properties

The shape memory alloy used for the artificial muscles exhibits a complex behaviour, which depends on its the geometry, its pre-tension, applied temperature and the

applied cooling. To determine the properties of the Nitinol SMA used in this work a test rig was constructed to measure the amount of force exerted by different length and sizes of wire. Firstly a clamp was designed to hold wire of size 50µm up to 375µm in diameter. This was then used in the experimental set-up shown in figure 4.9, where a spring balance measured the force generated in the wire. Power was applied to the wire by two 1.5V D-type batteries. The force produced by these different diameter wires of different lengths is shown in figure 4.10. The lengths are increased by increasing strands *i.e.* 1 strand = 100 mm length of wire.

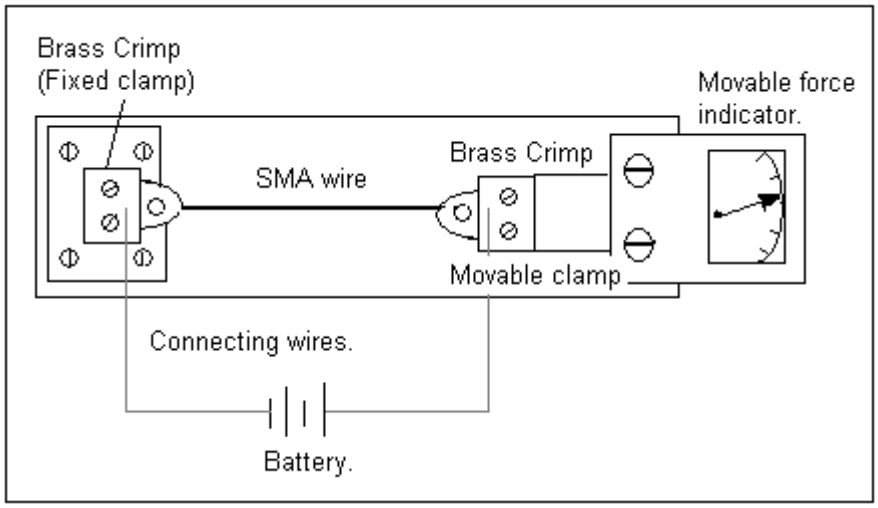


**Figure 4.9 Experimental setup for shape memory alloy.**

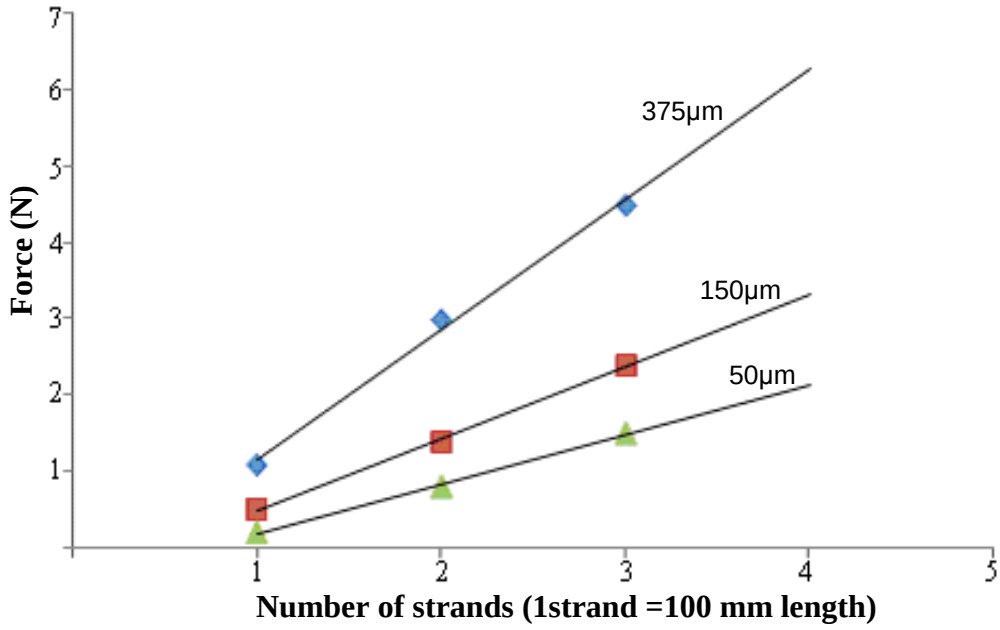


**Figure 4.10 Basic properties of different diameter SMA wires**

Figure 4.10 shows best-fit curves, which indicate that as the diameter and length of the wire increases, so the force produced increased as expected.

An experimental set-up with a load attached at one end of the SMA wire and a J-type thermocouple was used to measure the temperature and the cooling for the wire. This was carried out at room temperature with natural convection. The experiment used 375 µm wire with a constant current of 2.0 A. The time required to heat the wires was measured with a stopwatch. The aim of the experiment was to decide the delay time in sec (t1) discussed in detail in Section 4.5.

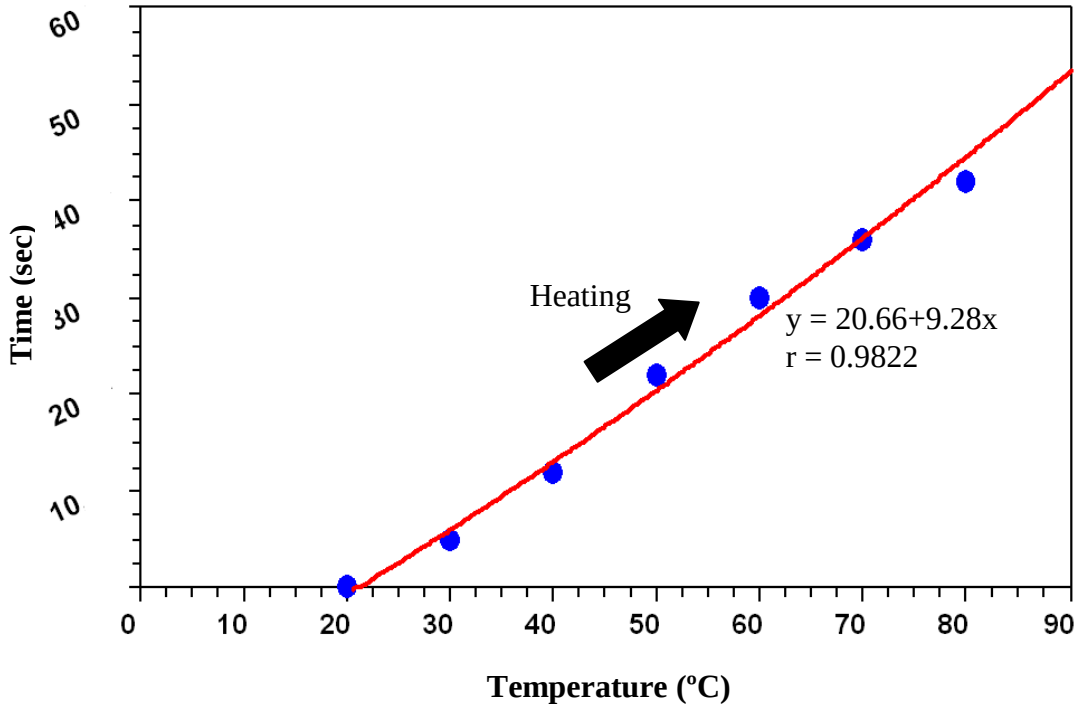


**Figure 4.11 Experimental analysis for time of heating SMA wire**

For testing the properties of the SMA a wire of 375 µm and length 15.25 mm with temperature increasing at 5°C per minute was observed for all experiments. The heating (20 to 90° C) and cooling (90 to 20° C) was observed at room temperature with natural convection. The data sheet provided by the manufacturer Dynalloy (2004), indicates the activation temperature should be between 55 to 90° C.

The displacement analysis produced the temperature / contraction behaviour. Figure 4.12 shows a temperature displacement curve, the slope of this curve is used for calculating the temperature expansion coefficient. Considering figure 4.12 between 55 and 90° C the slope is $13.662 \times 10^{-6}$ m/°C. The heating was constant and the cooling observed was at room temperature with natural convection.

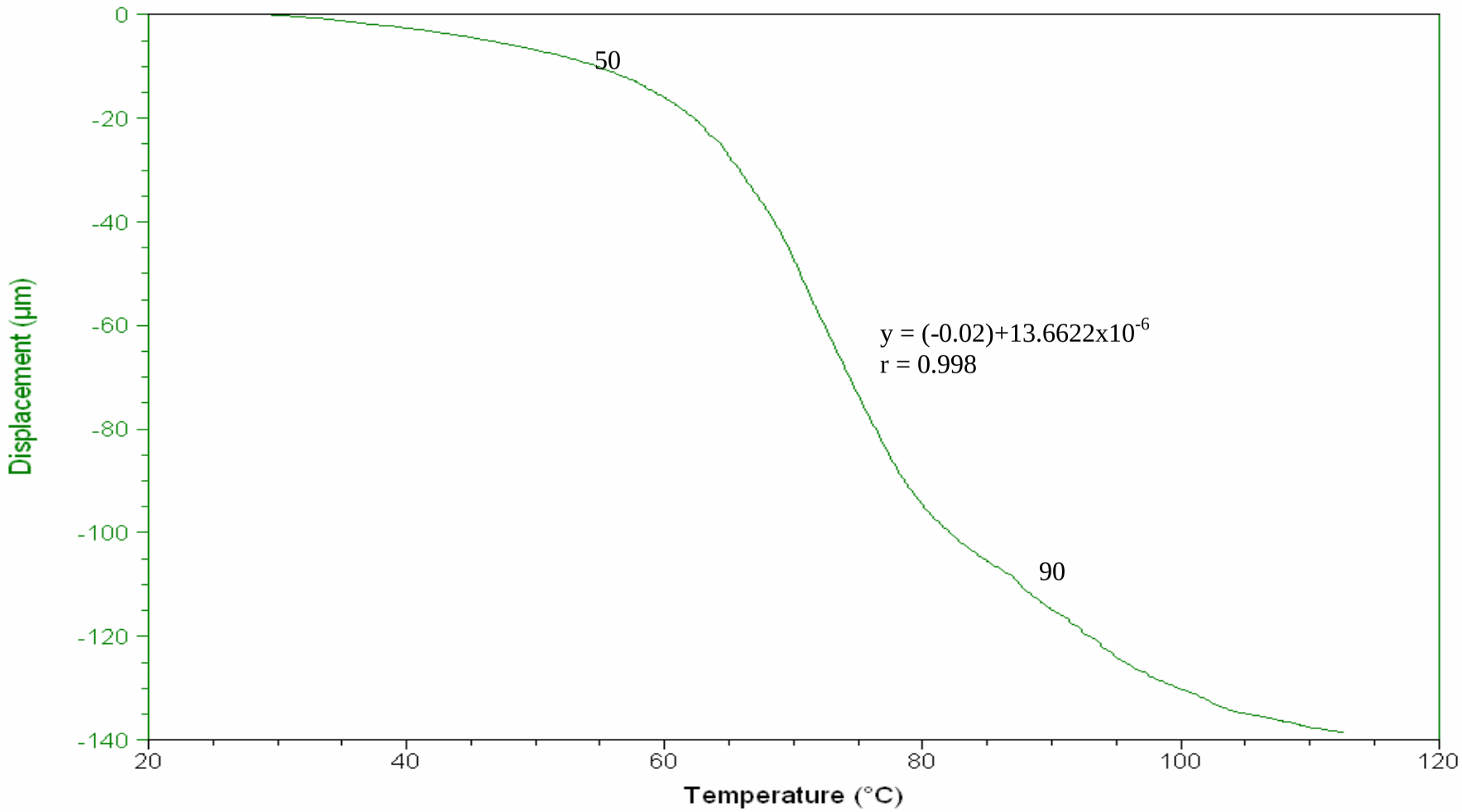


**Figure 4.12 DMA analysis of SMA wire, showing the thermal contraction of the wire.**

The DMA analysis in figure 4.13 shows cyclic heating and cooling (with cooling by natural convection) after a period of 1.5 minutes delay. The test was carried out for a 375 μm diameter wire of length 15.25 mm with a temperature increasing at $5^{o}C$ per minute. Thus the entire repetitive analysis for test number 1 to 5 between activation temperatures 20 to $90^{o}C$ shows that the SMA has a repeatable behaviour with < 20 μm displacement difference.

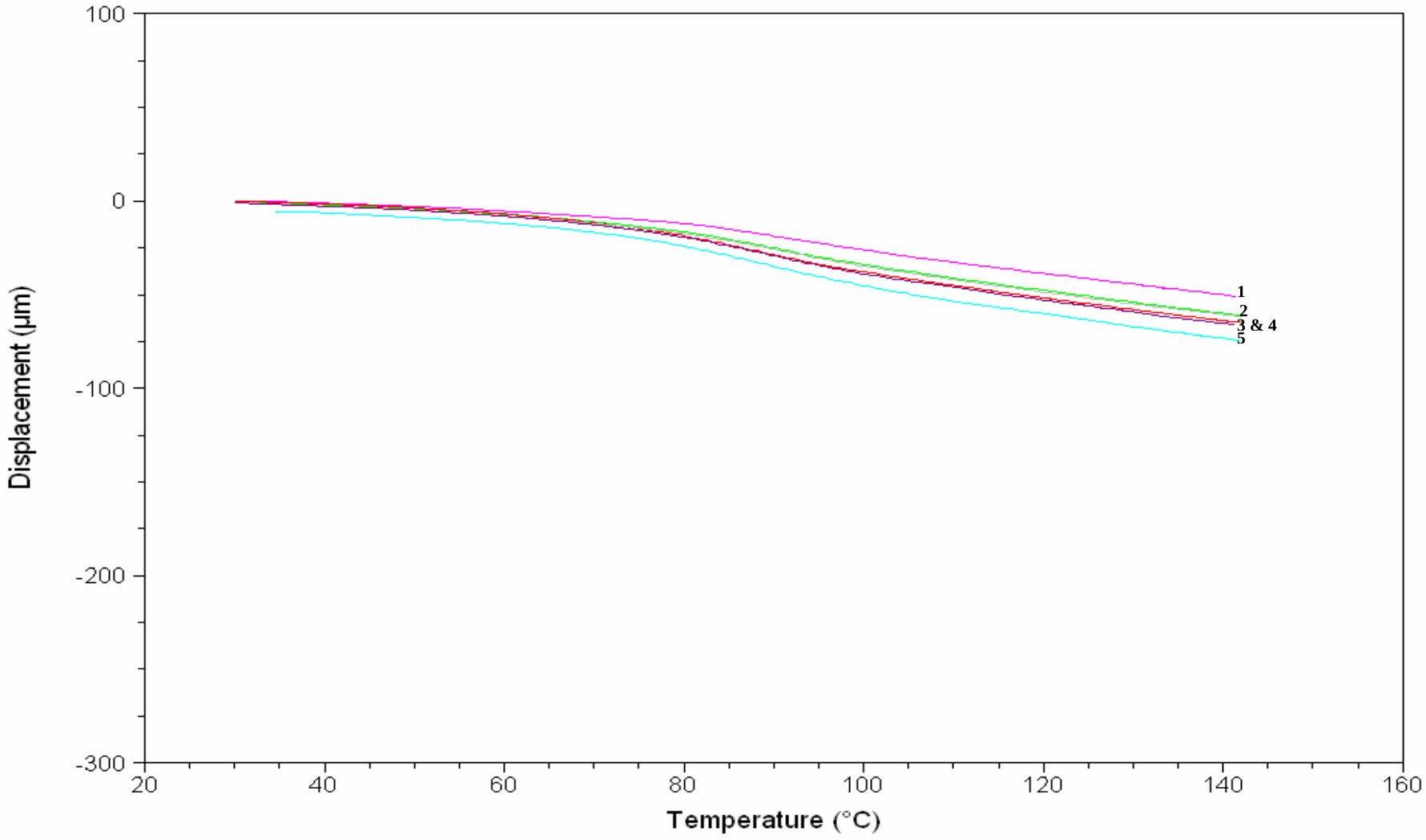


**Figure 4.13 DMA test for repeatability in temperature and displacement curves.**

The results of the DSC test are shown in figure 4.15, and present the variation in heat capacity with temperature. For this study a sample of wire diameter 375 μm and weight of 38 mg was placed in the DSC and heated from 22$^{o}$C (room temperature) to 140$^{o}$C (i.e. the temperature before overheating of wire). This shows that the phase change occurs between 55$^{o}$C to 90$^{o}$C, starting at 55$^{o}$C and reaches it's maximum at 60$^{o}$C, at which time the heat flow is maximum.

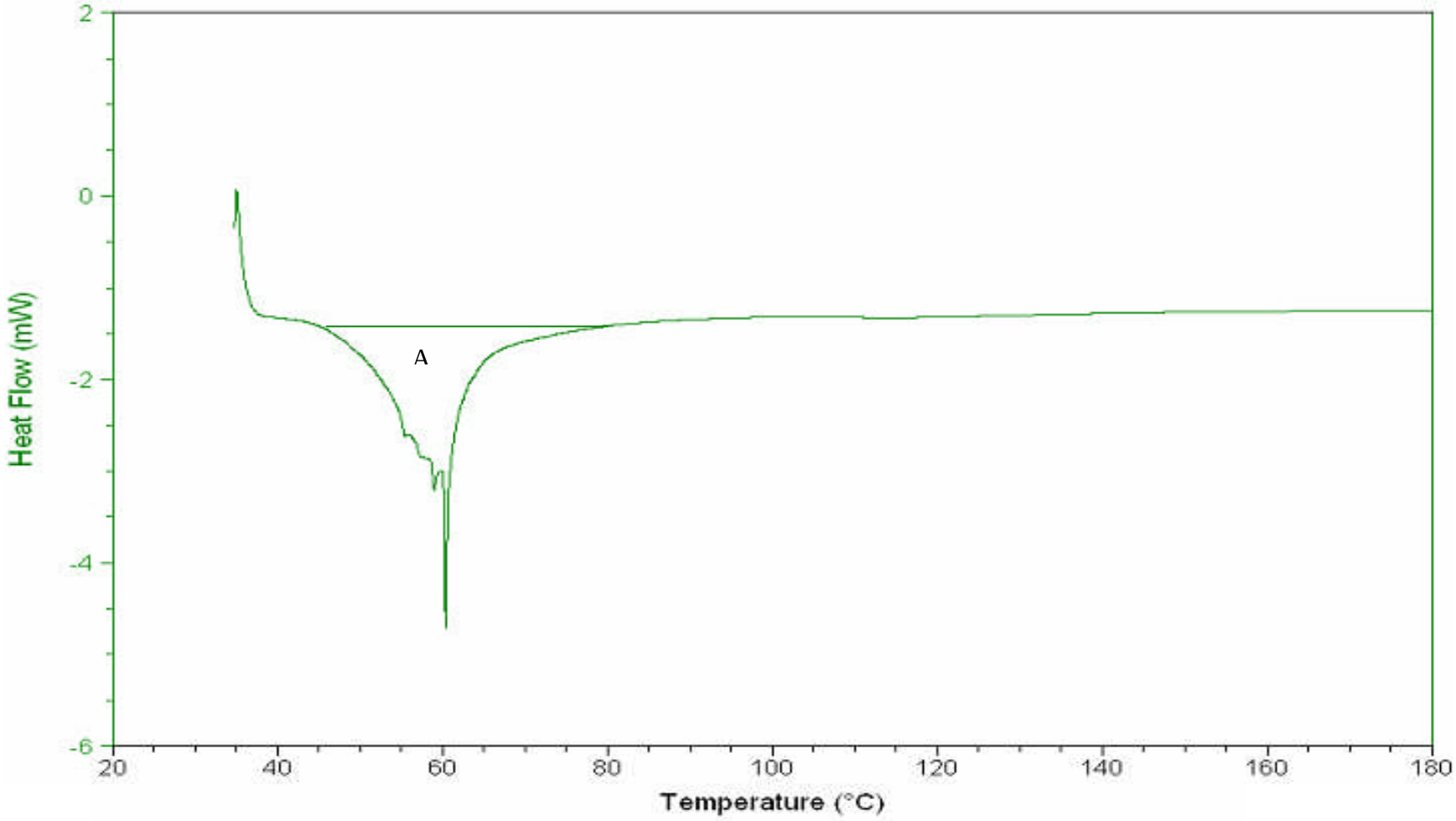


**Figure 4.15 DSC analysis for Shape Memory alloy wire**.

The heat flow graph only considers the austenite cycle, which is the heating cycle, and can be observed as a steep drop in heat flow in the activation range of 50 to 90$^{o}$C. The heat flow becomes constant after the phase change indicating that the heat is absorbed and there is no point increasing the heat further but its always recommended not to overheat the wires which is at 140$^{o}$C.

## 4.5 Development of active muscles for simplified geometry model.

### 4.5.1 Active muscles

The artificial muscles are manufactured from nickel titanium alloy and are attached to each of the processes and can generate a force to overcome the stiffness of the intervertebral disc (i.e. PU-foam). In the actual lumbar spine, the loading is a sum of the body weight, the resisting muscles and the abdominal muscles acting in antagonistic pairs for maintaining different postures. The muscles in the simplified model are divided into several functional fascicles in order to mechanically mimic the real muscle which are arranged parallel to each other.

### 4.5.2 Shape memory muscles and bias springs

Shape memory alloys, when cooled from the high temperature austenite form, undergo a phase transformation in which their crystal structure deforms till the low temperature martensite phase is reached. To overcome the hysteresis a pre-tensioned spring with forced convection must be used.

The muscle wire tension can be adjusted by turning the screw connectors attached to the processes of the simplified vertebral bodies as discussed in Section 4.2. The shape memory actuator with bias spring actuation discussed in Luo et al (2003) is for a model of a transanal endoscopic actuator as shown in figure 4.16, and has initial tension supplied with a spring. Another application in a gastrointestinal monitoring capsule discussed by Menciassi et al (2004) also uses a spring actuator, which acts as a bias mechanism and helps the wire to recover its original shape.

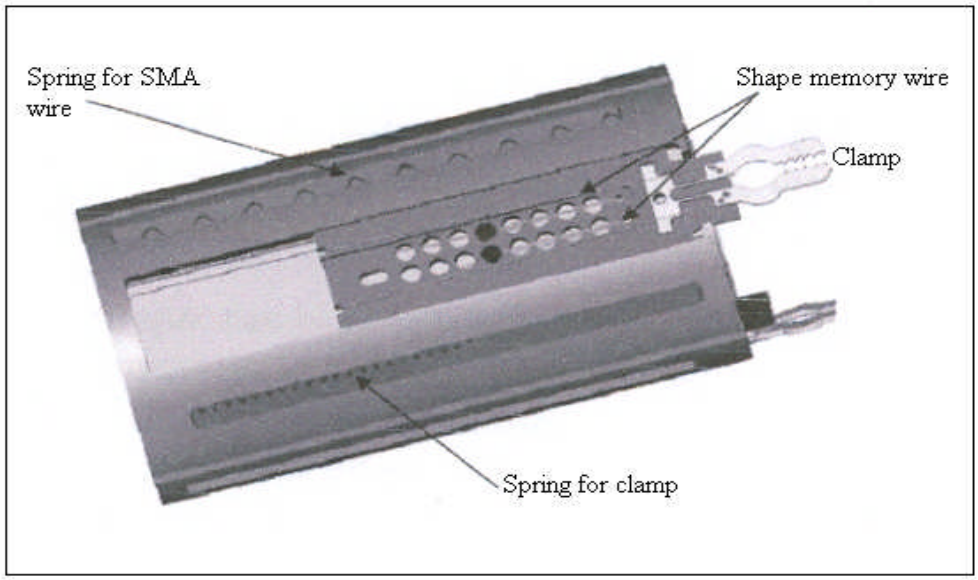


**Figure 4.16 Endoscopic actuator with shape memory alloy**

The above arrangement with pre-extended spring was used in the simplified spine physical model with springs acting as elastic components in antagonistic pairs with the muscle wire. This spring arrangement in the simplified model is used to stabilise the antagonistic motion that acts as retracting force agent, and also helps to provide pretension to avoid slack in the muscular arrangement and apply an offset force during any unbalanced motions. Several spring arrangements were considered before deciding on this configuration but this was decided as the optimum because a torsion spring is considered to satisfy the following assumptions derived from the model:

- The spring should be at an initial pre-stress condition on causing pretension in the muscle wires.
- The spring is reloaded with forces due to contraction applied by muscle wire during phase change.
- The springs should regain its pre-stress position, which is the bias spring force for initial length of wire.

Thus many different arrangements were investigated and a torsion spring was incorporated as shown in figure 4.17.

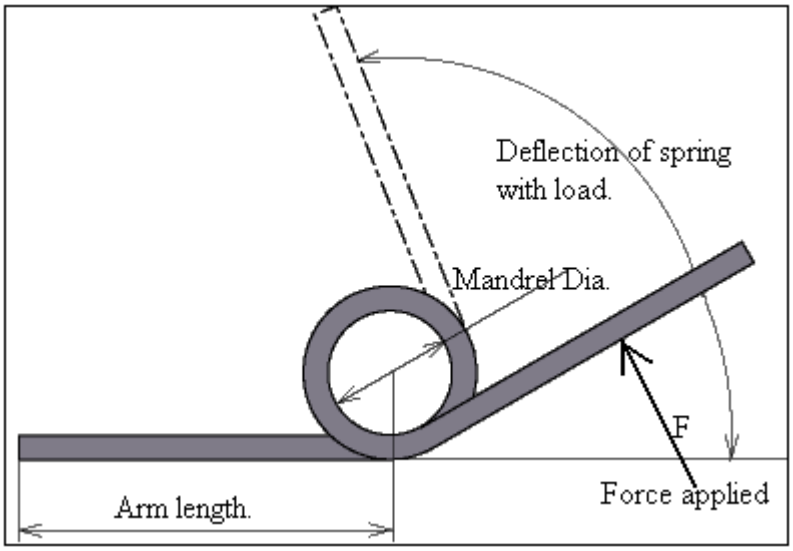


**Figure 4.17 Helical torsion spring**
**(tangential legs at 180$^o$ and material: music wire)**

The effect on the performance of the shape memory alloy wire (diameter 375 μm and length 15.6 mm) with temperature increase of 5$^o$C per minute with and without a bias spring is shown in figure 4.18. The spring that was used with the wire was experimentally tested in the DMA with the wire activation at constant current as shown in figure 4.18. The spring was clamped in parallel with the wire to observe the changes in displacement.

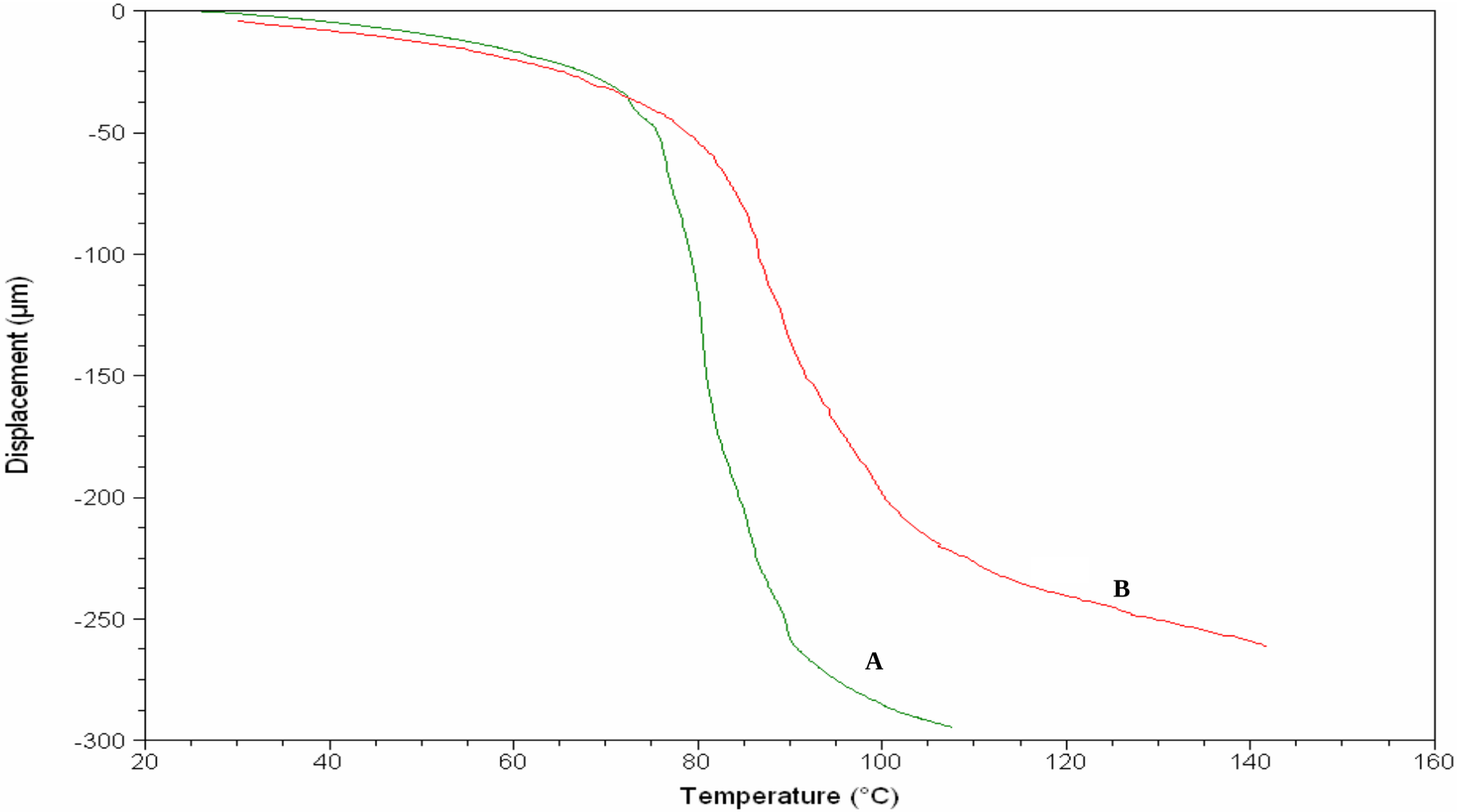


**Figure 4.18 Shape memory wire deformation with (A) and without a spring (B).**

Curve B in figure 4.18 (without a spring) follows the curve previously observed in figure 4.12; while curve A (with a spring) shows how the displacement is increased by the spring producing a much steadier response to the change in temperature.

These experiments with the shape memory wire confirm the force temperature relationship, which combined with the easy handling of wires, makes them suitable for artificial muscles.

In the artificial spine torsion springs are positioned between the transverse and spinious processes as shown in figure 4.19 which exerts force (Fs) to maintain the initial position, provide pretension to wires and provide a biasing force.

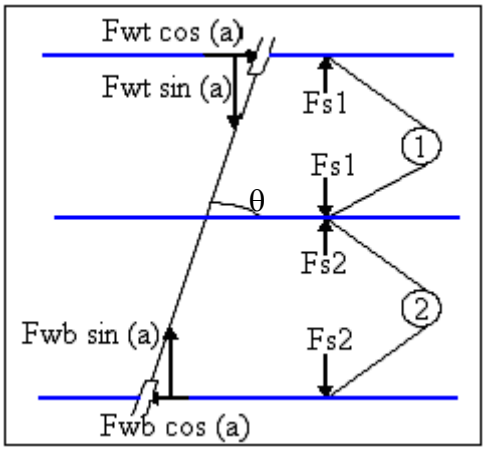


**Figure 4.19 Free body diagram with shape memory alloy and torsion spring.**

The springs were supplied by Lee Springs (LT-025E-4; Wokingham; UK) and had the following dimensions, (Lee Spring, 2005)

Wire radius = 0.32 mm

Length of arm = 25.40 mm (see figure 4.17)

Number of turns = 5

The spring was manufactured using music wire. (Lee Spring, 2005)

The spring force produced in the torsion spring was calculated as,

$$Ko = \frac{c}{c - 0.75}$$

Where, c is a constant for wire diameter 0.64mm. $c = 12.11$, So $K_o = 1.06$

$$\sigma = \frac{32 \times T \times Ko}{\pi d^3} = 2.6 \text{ (Lee Spring, 2005)}$$

$$2.6 = \frac{32 \times F \times 25.40 \times 1.06}{\pi 0.64^3}$$

Thus spring force, F= 2.48 N.

### 4.5.3 An active muscle design.

Activation of the shape memory wires occurs by increasing the wire temperature which is controlled by varying the current supplied, for example if the key characteristics of the wire are:

wire diameter = 375 µm = 0.375 mm.

resistivity (R) = 8 Ω/m. Gilbertson et al. (2003)

maximum current (I) = 2.75A.

Then for a muscle wire of length 100 mm experiencing a current of 2.75 amps, the maximum voltage (V) required will be,

$$V = I \times R = 2.75 \text{ x } 0.01 \text{ x } 8 = 2.2 \text{ volts}$$

The experimental data for a muscle wire of diameter 375 µm has the following properties,

Actuation temperature = 55 $^{o}$C (start) 90 $^{o}$C (finish)

The temperature was measured using a J-type thermocouple attached to the wire.

Young's modulus = 5150 MPa. Gilbertson et al. (2003)

The above data when compared to Gilbertson et al. (2003) was found to be accurate i.e. the voltage = 2.2 volts, Youngs modulus = 5150 MPa and an ideal force produced = 1.10 N, that can be calculated as

Force produced by muscle wire = Maximum recommended stress held x C/S area.

Thus, Force produced by an ideal single muscle wire = 1.10 N.

The above data was used to mathematically model the shape memory wire in Matlab shown in Appendix C, to calculate force and heat transfer coefficient of a single wire.

To increase the force produced, more wires could be applied in parallel or a larger diameter wire could be used.

## 4.6 Designing of the control circuit for the active muscles.

To control the complex arrangement of muscle wires in the artificial spine requires a control system that can not only activate different wires and groups of wire, but can also pulse the signal to the wires to obtain different vertebral movements. This was programmed into Matlab (MatWorks, USA, 2003) with an output to a digital interface card.

### 4.6.1 Control system

The wires were preloaded with springs that kept them under tension when relaxed. The time response of the wires with antagonistic spring depends on the applied heat that can be tuned according to the input current amplitude. In this system the current flow is generated in the form of a square waveform, as shown in figure 4.20. After a delay of time t1 seconds, the current is applied for t2 seconds, followed by a delay of t1 seconds. The time t1 with t2 added is the time required T for one cycle or duty cycle. The advantages of using a pulse width modulation circuit is that it provides a uniform heating of the wire, the duty cycle of the square wave can be varied to generate a degree of proportional control over the contraction.

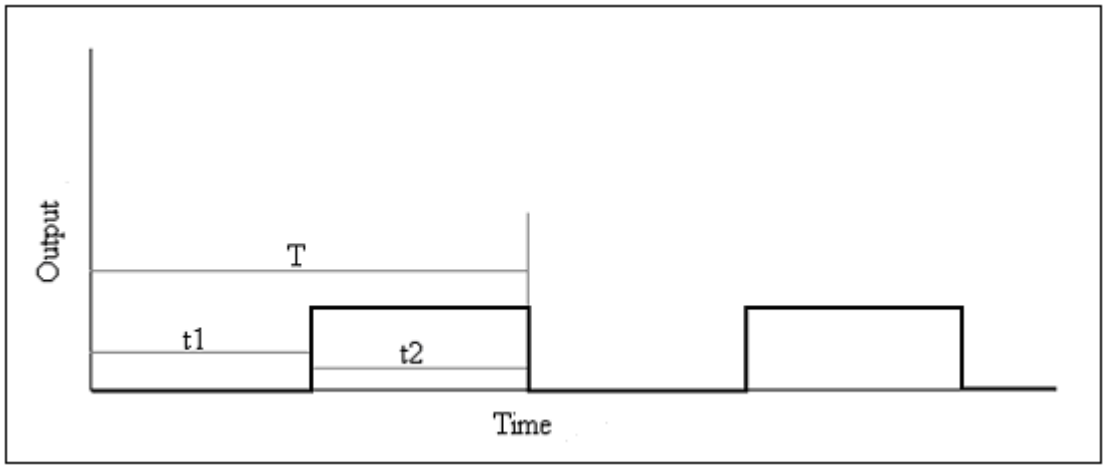


**Figure 4.20 Pulse width modulations (Volt. vs. Time) (t1- off, t2 – on, T-one cycle).**

This can be represented as a simple digital (ON-OFF: 1-0) signal as shown in Table 4.2. The codes were written separately for sequential switching ON and OFF using the decimal numbers shown in Table 4.2, with details of the codes included in Appendix D.

| | Channel number for control | | | | | | | | | | | | | | | |
|---|---|---|---|---|---|---|---|---|---|---|---|---|---|---|---|---|
| **Decimal value for control** | 1 | 2 | 3 | 4 | 5 | 6 | 7 | 8 | 9 | 10 | 11 | 12 | 13 | 14 | 15 | 16 |
| 1 ON | 1 | 0 | 0 | 0 | 0 | 0 | 0 | 0 | 0 | 0 | 0 | 0 | 0 | 0 | 0 | 0 |
| 1 & 7 ON | 1 | 0 | 0 | 0 | 0 | 0 | 1 | 0 | 0 | 0 | 0 | 0 | 0 | 0 | 0 | 0 |
| 1,7&3 ON | 1 | 0 | 1 | 0 | 0 | 0 | 1 | 0 | 0 | 0 | 0 | 0 | 0 | 0 | 0 | 0 |
| 1,7,3 & 9 ON | 1 | 0 | 1 | 0 | 0 | 0 | 1 | 0 | 1 | 0 | 0 | 0 | 0 | 0 | 0 | 0 |
| 1,7,3,9&14 ON | 1 | 0 | 1 | 0 | 0 | 0 | 1 | 0 | 1 | 0 | 0 | 0 | 0 | 1 | 0 | 0 |
| 9 OFF | 1 | 0 | 1 | 0 | 0 | 0 | 1 | 0 | 0 | 0 | 0 | 0 | 0 | 1 | 0 | 0 |
| 14 OFF | 1 | 0 | 1 | 0 | 0 | 0 | 1 | 0 | 0 | 0 | 0 | 0 | 0 | 0 | 0 | 0 |
| 3 OFF | 1 | 0 | 0 | 0 | 0 | 0 | 1 | 0 | 0 | 0 | 0 | 0 | 0 | 0 | 0 | 0 |
| 7 OFF | 1 | 0 | 0 | 0 | 0 | 0 | 0 | 0 | 0 | 0 | 0 | 0 | 0 | 0 | 0 | 0 |
| All OFF | 0 | 0 | 0 | 0 | 0 | 0 | 0 | 0 | 0 | 0 | 0 | 0 | 0 | 0 | 0 | 0 |

**Table 4.2 An example of controlled channel sequence (ON/OFF: 1/0 )** .

The control of the pulse generated by the decimal number entered is shown in figure 4.21, the decimal number 14 entered in (a) has a code to switch ON the 14$^{th}$ wire and can be observed by 14$^{th}$ channel switching ON i.e. 1-ON for the 14$^{th}$ channel and the rest having all 0-OFF. The pulse width modulation square wave at the 14$^{th}$ channel shows ON/OFF control i.e. channel number 14 is switched ON rest is OFF.

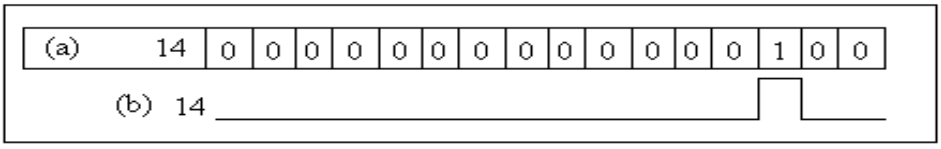


**Figure 4.21 Channel 14 switching sequence**

### 4.6.2 LabJack as a buffer

The LabJack U12 (LabJack, Lakewood, USA) used with a notebook PC is a portable data acquisition and control system when connected with a printed circuit board. The low-power design of the LabJack U12 allows it to draw power from the USB port of the notebook. It is supplied with software provided as a dynamic link library, which can be interlinked with Matlab to generate the control signals.

The LabJack has 8 screw terminals for analog input (AI0-AI7) as shown in figure 4.22. The PC sends a command to the LabJack, which responds with output to one of its 20 digital output channels. These channels can be configured individually as input into a printed circuit board, which drives the shape memory wires.

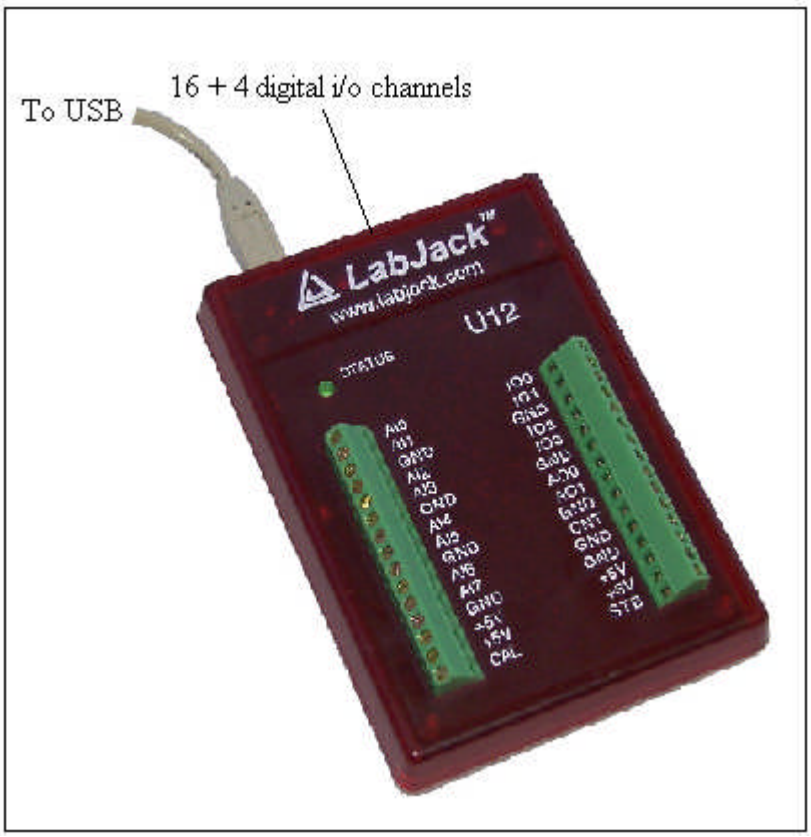


**Figure 4.22 The LabJack interface device used to control the muscle wires.**

### 4.6.3 Programme sequence

The activation regulation of the muscle wires is programmed in Matlab with the sequence flowchart as shown in figure 4.23. The decision variable i can be varied by the user, which uses binary to digital conversion.

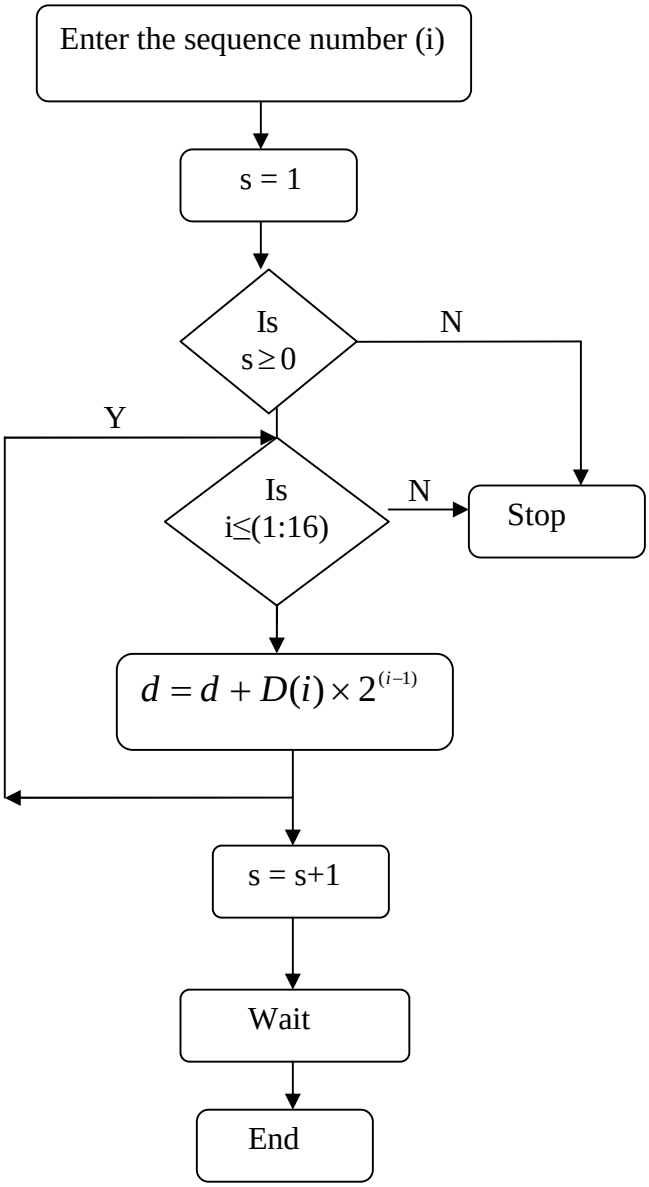


**Figure 4.23 Programming sequence for muscle activation**

The above values are explained in the Appendix D for various codes that were taken from the LabJack data book.

## 4.7 Assembly of the simplified geometry model

### 4.7.1 Simplified model

The final arrangement for the simplified spine model is shown in figure 4.24 with the muscle and bias springs.

The vertebral bodies were glued to the intervertebral discs compressed between two vertebral bodies and a criss-cross fibre cloth glued to the arrangement to increase torsional stiffness as explained earlier. The PU-foam disc wrapped with the cloth has uniform thickness as shown with the dotted lines in figure 4.24.

The active muscles are connected to each vertebral body through brass connectors, which can be tensioned to adjust the tone of the muscle wires. The arrangement also comprises springs connected to processes of the vertebral bodies, which act as stabilizers as described in Section 2.5.3

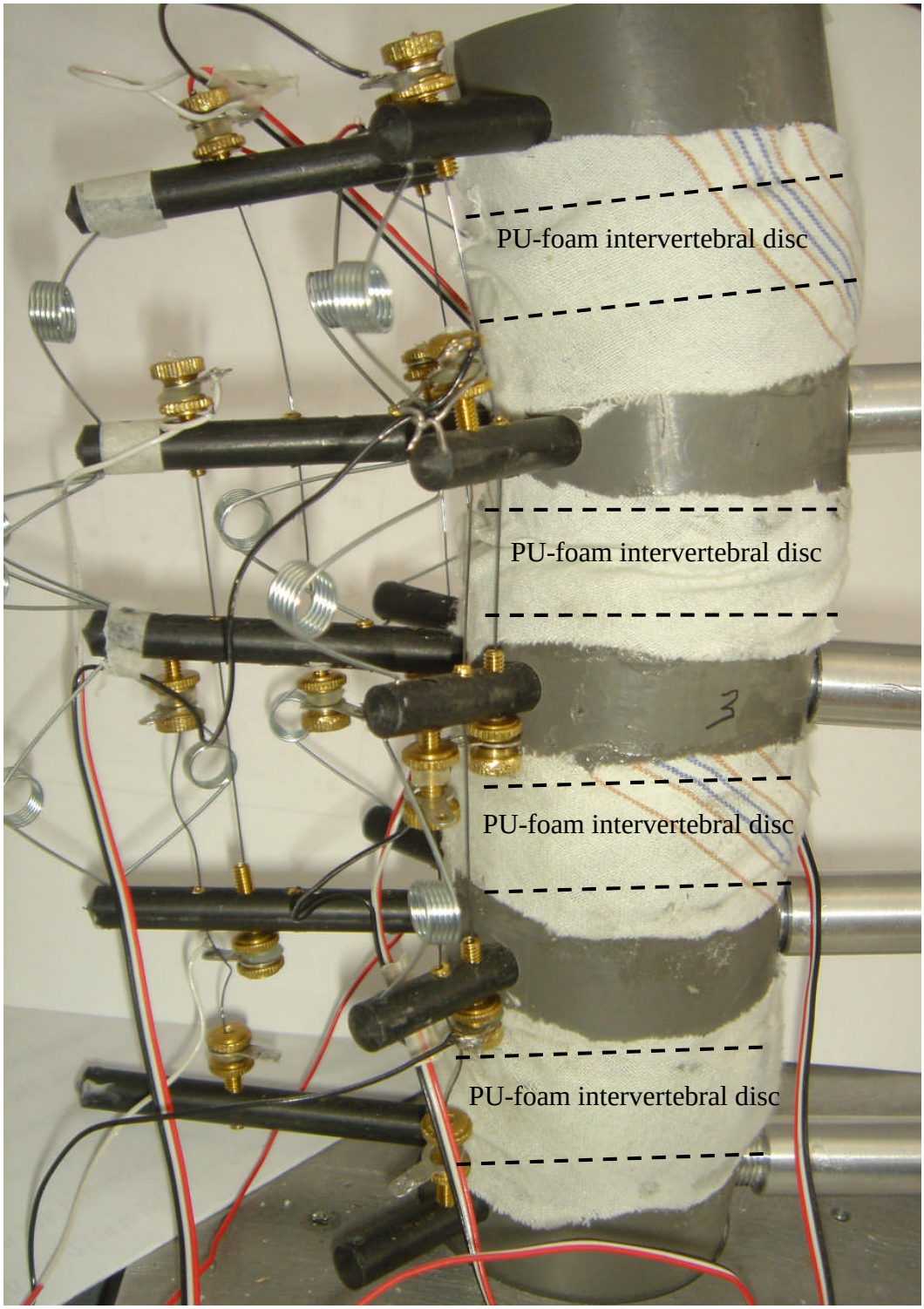


**Figure 4.24 Simplified model with muscle wire, elastic element and PU-foam disc surrounded with criss-cross fibre cloth**.

### 4.7.2 Control system

The block diagram of the control system of the muscles is shown in figure 4.25 and has a switching sequence adapted from the control parameters of the function generator unit i.e. the input.

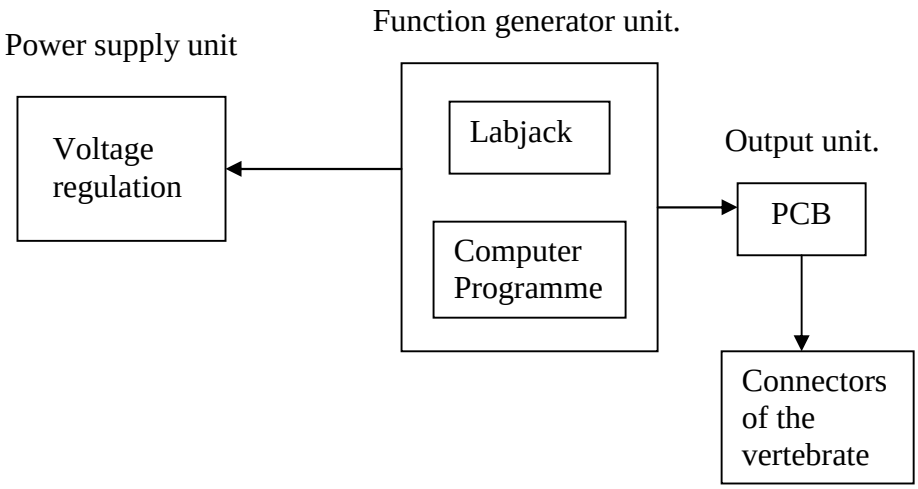


**Figure 4.25 Control system for shape memory alloy**

The control system consist of the following units,

- Function generator unit – The function generator unit (input unit) consists of the computer programme (written in Matlab) with Labjack used as a buffer. The generator creates a sequence of switching operations, which is a response to the activation number, i.e. the switching ON-OFF of the particular wire.
- Power supply unit – The power supply is the main source of power to the control circuit. The power supply supplies a regulated voltage to the parallel circuit board (PCB) to avoid any overheating of the shape memory wire.
- Control circuit unit – This consists of a printed circuit board (PCB), which is the heart of the control system. The main function is to supply the regulated voltage to each muscle wire with the sequence generated by the function generator.
- Output unit – It consists of connectors attached on the vertebral bodies that supply voltage to the artificial muscles.

### 4.8 Discussion

A simplified laboratory spine with simplification in geometry was constructed. The spinal model has a very complex arrangement of muscles and ligaments. Each and every material used for development was analysed and its characteristics plotted.

The complex arrangement of muscles was controlled to physiologically mimic the movements of the actual spine. The laboratory spine is first of its kind, which can perform controlled movements.

The chapter further compares results with a simplified computer model discussed in Chapter 5, which was simultaneously done but written separately.

# CHAPTER 5

# COMPARISION AND VALIDATION OF COMPUTER MODEL AND EXPERIMENTAL MODELS

## 5.1 Introduction

The insufficient data from cadaveric lumbar spine models and forces considering individual muscle architecture reduces the possibility for validation of computer models. Thus the aim of this chapter was to develop a finite element (FE) model that could validate the physical laboratory spine having similar geometry to the simplified physical spine. The comparison in this chapter includes the physical and biomechanical properties of vertebral and intervertebral disc and muscles, while the validation focuses on the movements of motion segments with the active muscle loadings.

## 5.2 The finite element (FE) model

The simplified artificial spine is a surrogate for experimentation with an actual lumbar spine. The finite element computer model is developed to physiologically simulate the movements of vertebral bodies and intervertebral discs, with the muscles surrounding the spine. The entire modelling consists of various parameters are used for the design are discussed in this section. The geometry, material properties and loading constraints of the lumbar spine with stresses in the complex structures are discussed in this section. The simplified spine model is prototyped from actual design data of lumbar vertebral body. It has four intervertebral discs and artificial muscles modelled as linear elements.

The simplified geometry extracted from the actual geometry shown in Chapter 2, has two transverse processes modelled at $45^{o}$ and a longer spinious process attached at the centre. The FE model as compared to the physical models has similar geometrical features. The motion segments as shown in figure 5.1A have simplified vertebral body arrangements similar to the FE meshed model shown in figure 5.1B.

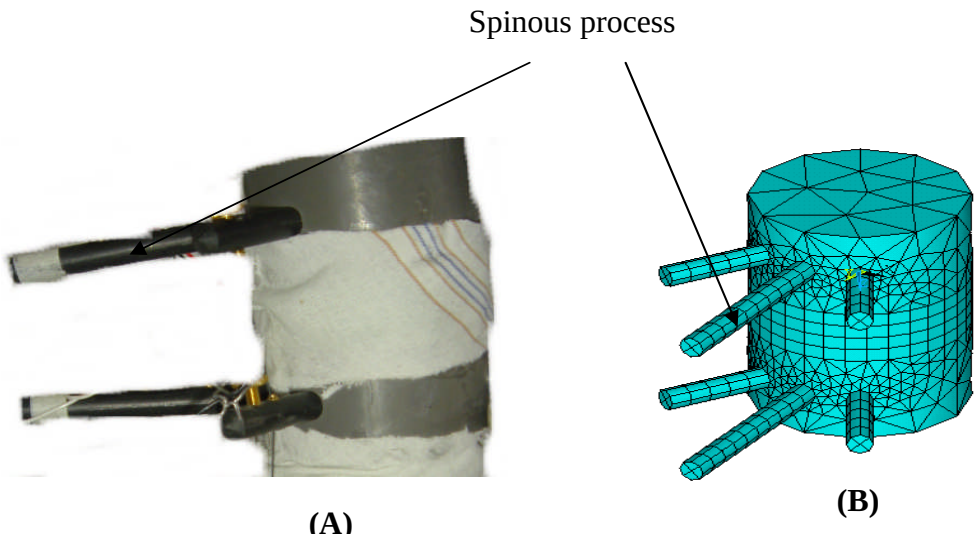


**Figure 5.1 Motion segment for L1 and L2.**

The simplified vertebral bodies shown in figure 5.1A are made from ABS P400 and PU-foam for intervertebral disc. The figure shown in 5.1B is a FE meshed model of the motion segment L1-L2 in the simplified physical model made from similar properties measured in the physical model.

The intervertebral discs used in computer and physical model are simplified versions of the actual intervertebral discs described in Chapter 2. The number of mapped elements for the intervertebral disc was selected with convergence value of 480 elements as shown in figure 5.2.

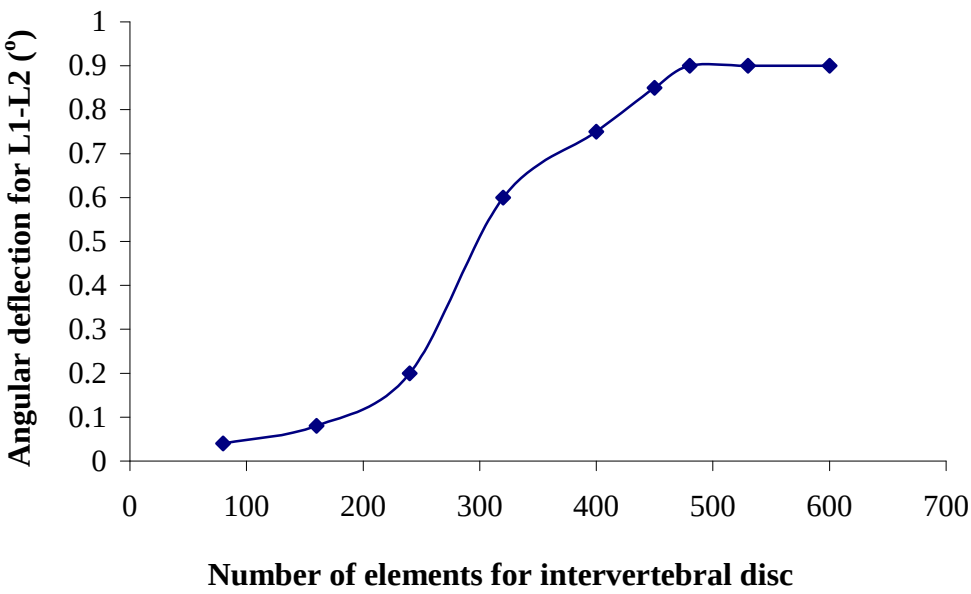


**Figure 5.2 Convergence for FE model of intervertebral disc**.

The discs are designed with a hole in the centre as shown in figure 5.3 and use a PU-foam material discussed in Chapter 4, with a Young's modulus, of 26.67 MPa. (Section 4.2)

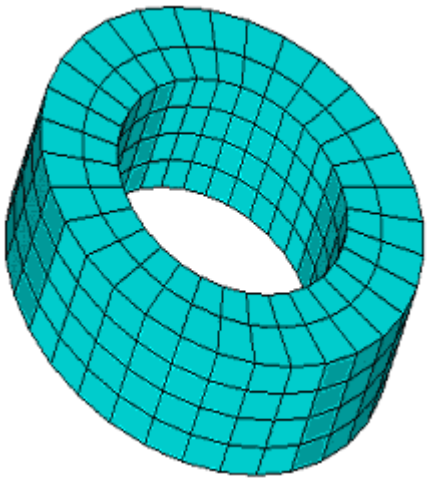

**Figure 5.3 Simplified geometry FE model of intervertebral disc**.

The meshed model of the intervertebral disc with 25 mm circular cavity is shown in figure 5.3. The intervertebral disc is glued between the two vertebral bodies. Table 5.1 shows the properties of the elements and materials used for the physical model. The properties of the material were assumed to be linear elastic for simplification. The table is drawn considering properties from Table 3.1, 3.2 and experimental observations in fig 4.5, 4.12.

| | **Vertebral body** | **Intervertebral disc** | **Active muscles** |
|---|---|---|---|
| **Element type** | Solid 95 | Solid 95 | Link 3D spar cable. |
| **Young's Modulus (MPa)** | 1500 | 26.7 | 51500 |
| **Poisson's ratio** | 0.405 | 0.1 – 0.3 | 0.3 |
| **Coefficient of thermal expansion (m/$^{o}$C)** | -- | -- | $-13.33 \times 10^{-6}$ |

**Table 5.1 Properties of material for FE model.**

In the finite element model the Possion's ratio was varied between 0.1 to 0.3 but shown to have no significant effect on the disc's behaviour. Table 5.2 shows the disc

behaviour when different elastic modulus of the material was varied in FE model. The Young's modulus was calculated from the DMA curve.

| Material | Young's modulus (MPa) | Angular displacement ($^o$) |
|---|---|---|
| Silcoset 101 | 720.5 | 0.05 |
| RTV 940 | 555 | 0.04 |
| AD 25 | 464.7 | 0.08 |
| Silicone gel | 356.3 | 0.1 |
| Cushion | 101.3 | 0.35 |
| PU-foam | 26.6 | 0.9 |

**Table 5.2 Intervertebral disc behaviour for different materials with changing Young's modulus in FE model**.

Artificial muscles were included in the model by cable elements with a specific coefficient of thermal contraction based on the result of the DMA analysis in Chapter 4. So the coefficient of thermal expansion came from the DMA results, with the change in temperature between 55 to 90$^o$C i.e. the activation temperature for 375 μm wire. The loading of the FE model occurred by the muscles which were attached at similar attachment nodes to the physical spine as shown in figure 5.4. The loading configurations i.e. the temperature change from 55 to 90$^o$ was observed for the SMA wires and the following changes in stresses with red (maximum stress) and blue (minimum stress) areas (von Mises) were observed.

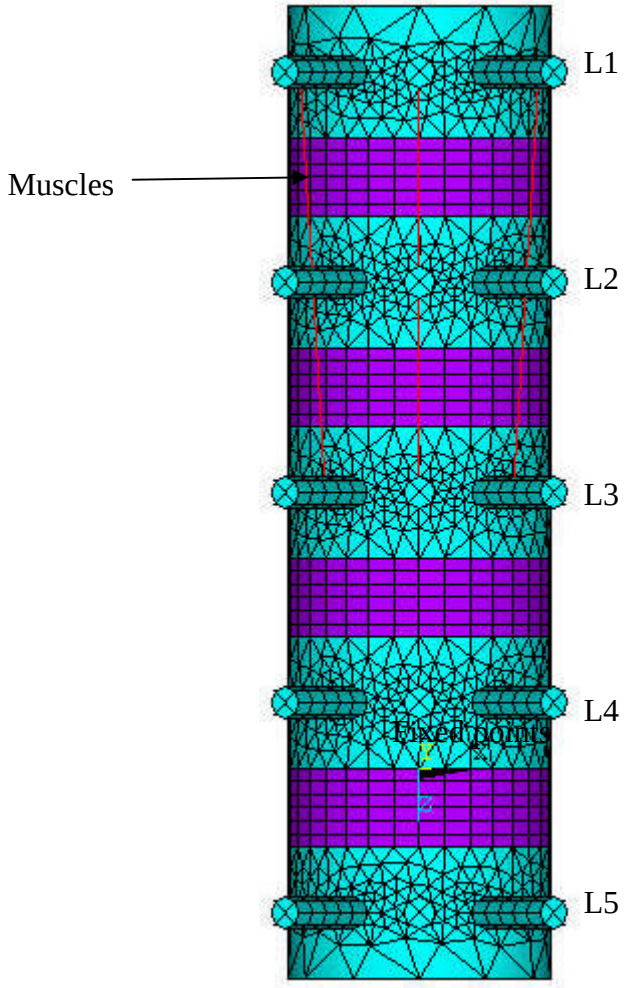


**Figure 5.4 Computer generated finite element simplified geometry model.**

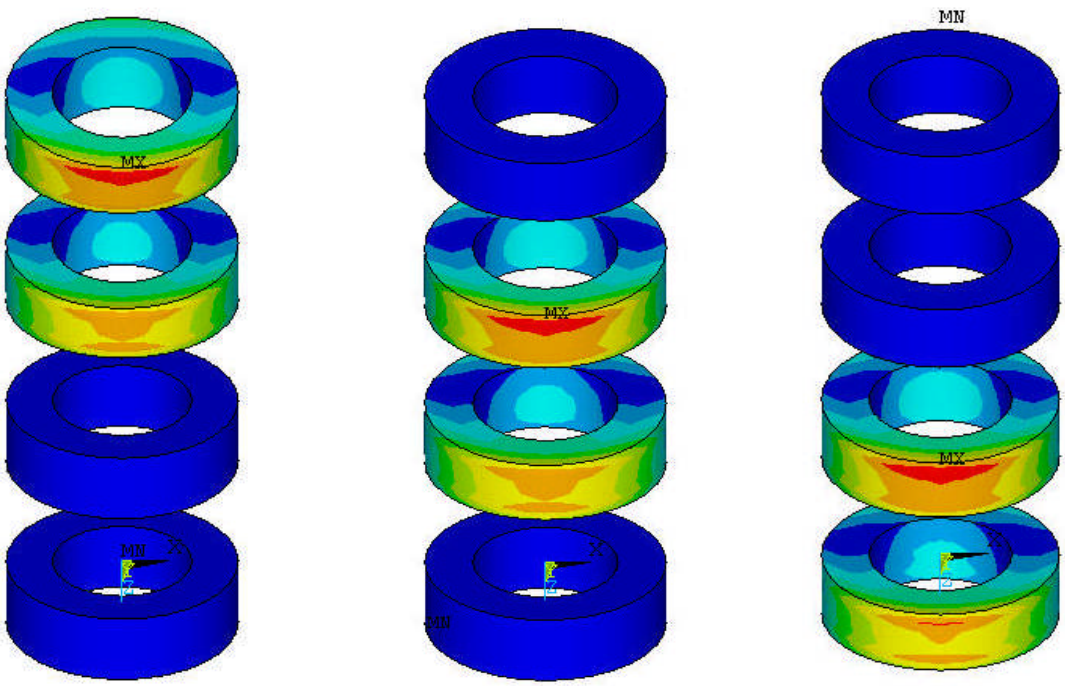


**(A)** **(B)** **(C)**

**Figure 5.5 von Mises stress zones observed in intervertebral disc due to cyclic loading**

The figure 5.5A shows the effect of recruitment of the intersegmental extensor muscles between L1 and L3, which produces the maximum stress zone as shown in red. The figure 5.5B shows the effect of recruitment of muscles between L2 and L4 and similarly for L3-L5 in figure 5.5C.

Figure 5.6 shows the deformation of disc observed in sagittal plane when subjected to similar loading.

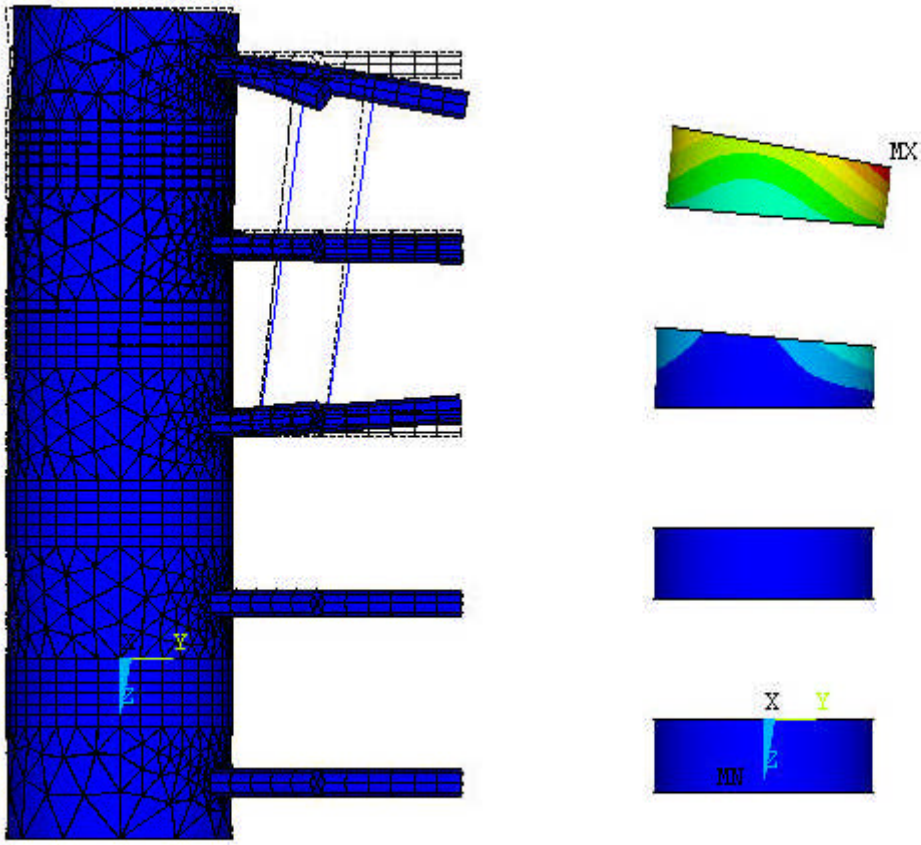


**Figure 5.6 Deformation of intervertebral disc due to cyclic loading.**

In order to test the validity of the FE model, the results of movements of FE model and physical model are compared. The modelling involves equilibrium assumed in three-dimensional space. The angular displacements of the motion segment were recorded from the nodal displacement data using the mathematical inverse-cosine equation [5.1].

The method was therefore used to measure the start and finish locations of the two points on the physical spine, where $X_0$, $Y_0$, $Z_0$ and $X_1$, $Y_1$ $Z_1$ are the initial coordinates of the two points. The final displaced positions are $X_2$, $Y_2$, $Z_2$ and $X_3$, $Y_3$ $Z_3$.

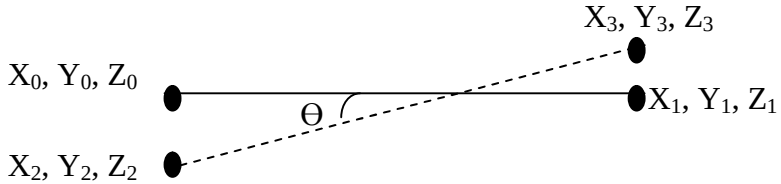


**Figure 5.7 Two lines in space.**

Line 1 has co-ordinates $X_0$, $Y_0$, $Z_0$ and $X_1$, $Y_1$, $Z_1$
Line 2 has co-ordinates $X_2$, $Y_2$, $Z_2$ and $X_3$, $Y_3$, $Z_3$

The coordinate displacements were then converted into an angular rotation by the inverse-cosine angle equation [5.1]. This is derived from simple geometry of two lines in space. The angular rotation 'θ' in degrees is calculated in equation [5.1].

$$\theta = \cos^{-1}\left( \begin{array}{l} ((X_1 - X_0)\times(X_3 - X_2) + \\ (Y_1 - Y_0)\times(Y_3 - Y_2) \\ + (Z_1 - Z_0)\times(Z_3 - Z_2)) \end{array} \Bigg/ \begin{array}{l} \sqrt{\begin{array}{l}(X_1 - X_0)\times(X_1 - X_0) + \\ (Y_1 - Y_0)\times(Y_1 - Y_0) \\ + (Z_1 - Z_0)\times(Z_1 - Z_0)\end{array}} \times \\ \sqrt{\begin{array}{l}(X_3 - X_2)\times(X_3 - X_2) + \\ (Y_3 - Y_2)\times(Y_3 - Y_2) \\ + (Z_3 - Z_2)\times(Z_3 - Z_2)\end{array}} \end{array} \right) \times 180/\Pi$$

---------**[5.1]**

## 5.3 Performance of the simplified spine model

### 5.3.1 Measurement technique

Measurement of the motion of the physical model was undertaken using Microscribe digitiser system. However, before this could be undertaken, the repeatability of the Microscribe in this application was tested as shown in figure 5.8. In this a point marked on the processes of the vertebral body was measured repeatably. The pointer was repeatably measured and the respective X,Y and Z co-ordinates were measured 5 times and the same operation was performed again.

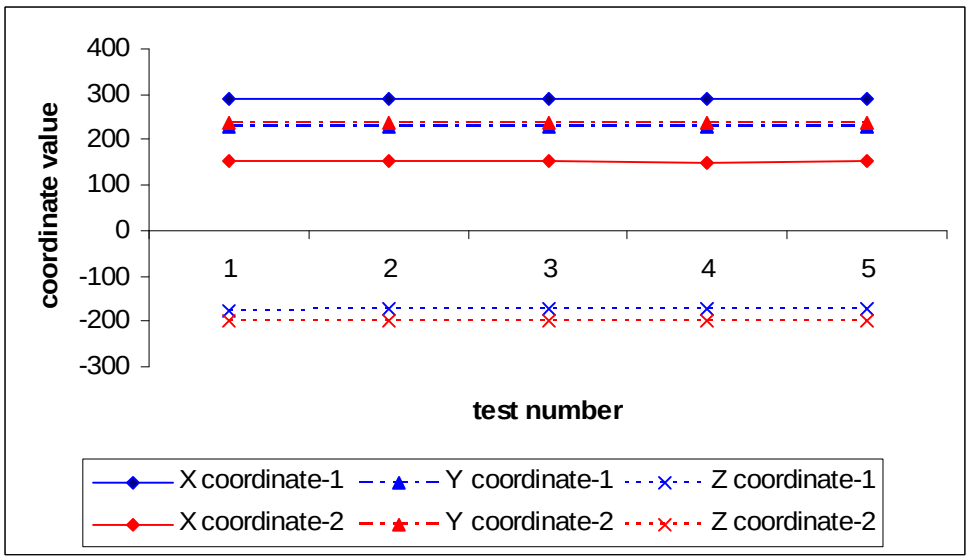


**Figure 5.8 Iterative coordinate values for initial measurement system.**

The experimental results shown in figure 5.9 show variations in iterative values for same point, so it was difficult to get reproducible results using the normal 'point and click' action of the Microscribe. The results showed that just small motions of the operator's hand were sufficient to compromise the results. Therefore a second set-up was developed where the operator's hand would rest on a support. Using this second system, the 3D position of the two points was observed as,

X coordinate 1= 549 ± 0.2 .

Y coordinate 1= 307 ± 0.8 .

Z coordinate 1= - 37 ± 0.3 .

Figure 5.9 demonstrates a second approach in which the user's hand was fixed to measure repeatability of locating the marked point on the vertebral body. This produced very repeatable results.

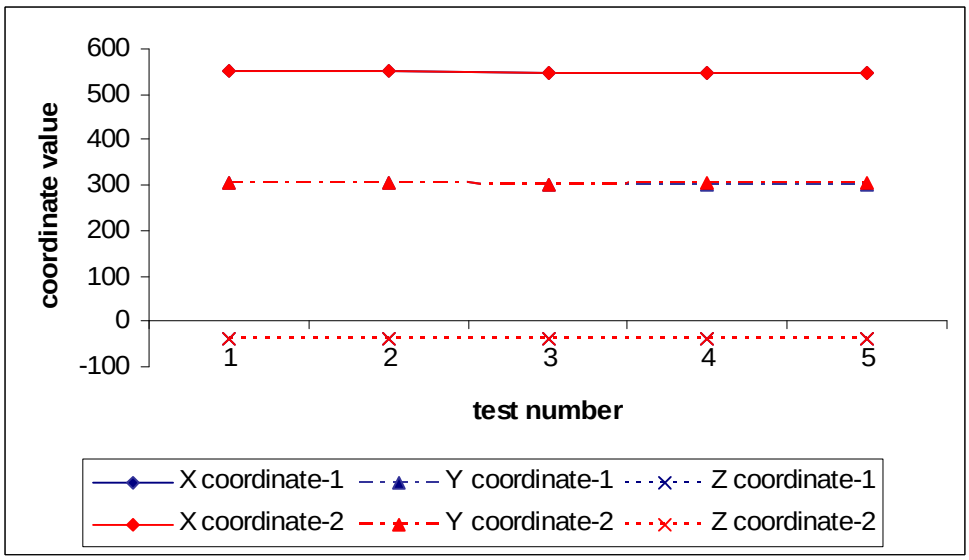


**Figure 5.9 Iterative coordinate values for fixed hand method.**

The accuracy of this whole process was checked by using the Microscribe technique to measure the angular rotation of an engineering mechanist bevel protractor. The location of two points on the protractor were recorded before and after rotation. A comparision of the angles measured by the Microscribe and observed on the protractor is presented in figure 5.10.

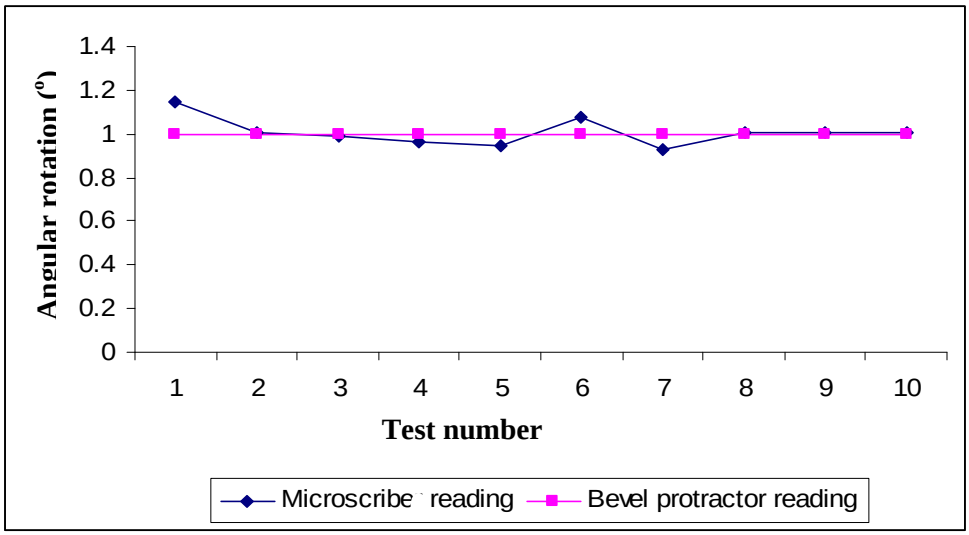


**Figure 5.10 Comparision between bevel protector reading and microscriber reading.**

After the first measurement the angles obtained from the Microscribe do seem reliable, and hence the method can be used with confidence having 100% accuracy depending upon the accuracy of measurements taken. To measure the rotation of the intervertebral bodies, the motion of two points (one anterior and one posterior) were recorded, from which the angle of rotation could be calculated, (see figure 5.7)

### 5.3.2 Performance of the simplified spine

The simple spine was loaded through the activation method described in Section 4.5. The angular displacement was measured by marked points with the Microscribe as described in the previous section.

Figure 5.11 shows the repeatability of the angular measurements of the physical model when muscles are activated between L1-L3. There were 5 measurements that were taken five times to demonstrate the repeatability with two sets which (i.e. a change of hand position after first set of 5 measurements) are shown to produce repeatable results.

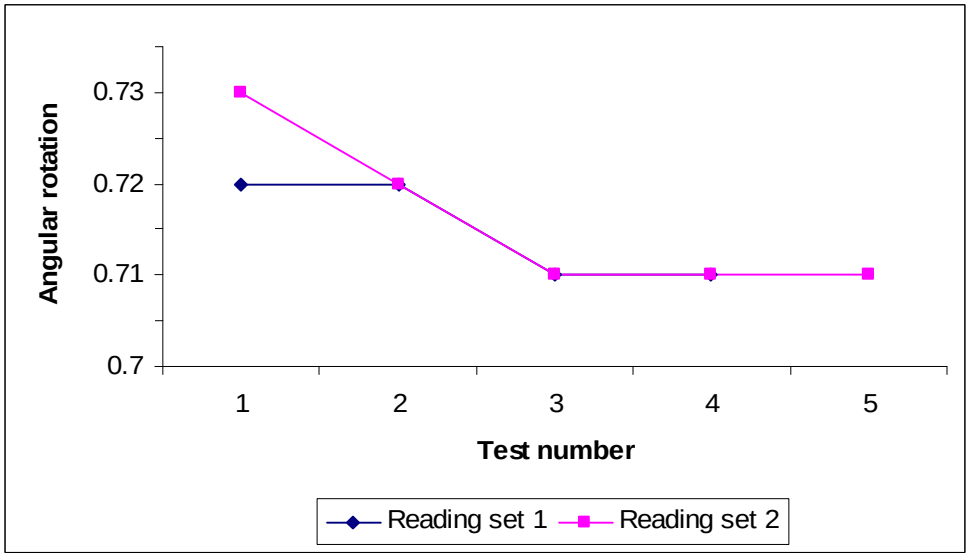


**Figure 5.11 Results for iterative physical measurements on L1-L2 motion segments.**

### 5.3.3 Comparison of the motions of the physical and FE models

Figure 5.12 compares the angular rotations produced by the FE model and physical model. The rotations at three motion segments are presented, where each joint has been tested 3 times. The range of angles produced at each joint is as follows:

L1-L2 = $0.71 \pm 0.03^{o}$

L2-L3 = $0.65 \pm 0.01^{o}$

L3-L4 = $0.56 \pm 0.02^{o}$

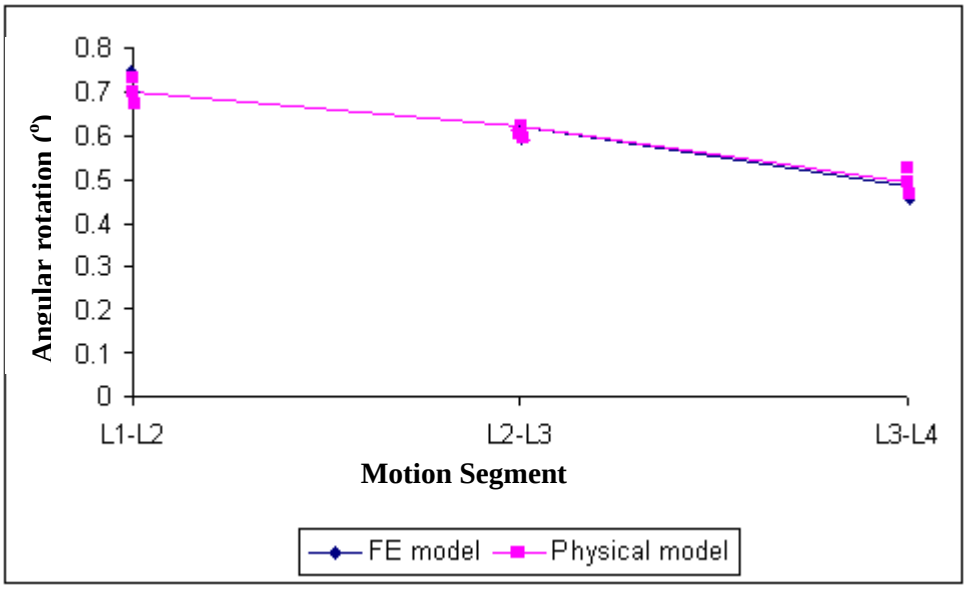


**Figure 5.12 Results for angular displacements for various motion segments**.

The Sagittal plane i.e. Y-axis displacement in figure 5.13 also shows similar translation observed for the different motion segments measured in the Y-axis on the FE model i.e. in sagittal plane.

L1-L2 = 2 ± 0.8 mm

L2-L3 = 1 ± 0.7 mm

L3-L4 = 1 ± 0.5 mm

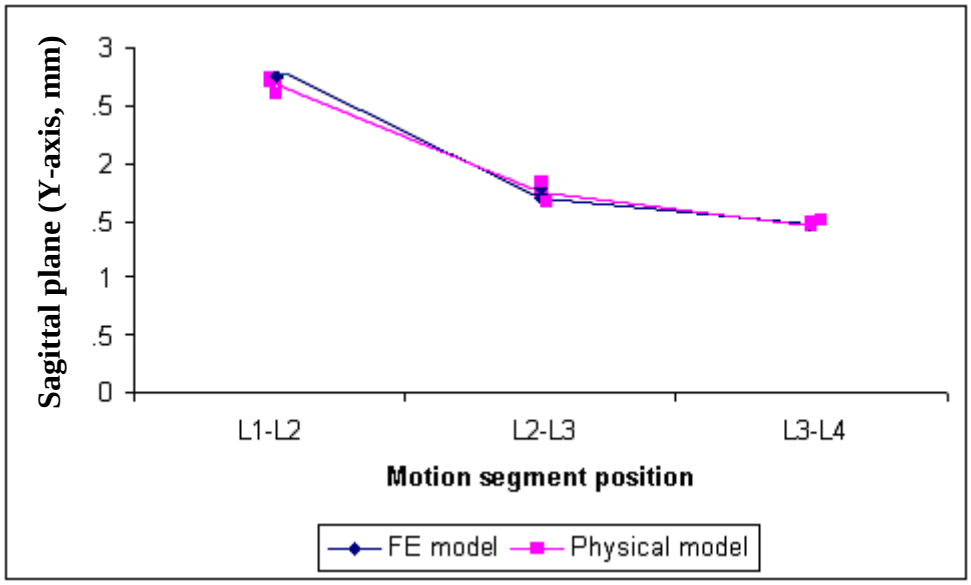


**Figure 5.13 Results for Y-axis translations for various motion segments.**

## 5.4 Discussion

This chapter has shown that the simplified laboratory spine can produce consistent, repeatable results and the FE model of that spine can accurately predict the

performance of that artificial spine. The results in figure 5.12 and 5.13 clearly demonstrate that the FE and physical models are producing comparable and repeatable results with the same and repeatable occurrences using the same technique of measurements. The FE model can therefore be used in the further development of this simplified spine model. It also gives a confidence that an equivalent FE model of the accurate artificial laboratory spine will be similarly accurate and useful. This could then allow finalising the development of the artificial laboratory spine in the future.

# Chapter 6

# Modelling and development of an accurate geometry spine model

The accurate geometry spine model discussed in this chapter includes actual vertebral body geometries and intervertebral discs with a geometrical curve similar to the natural lumbar curve. This chapter discusses the rapid prototyping technique and vacuum casting methods used in its development. Unfortunately the whole development of the simplified and accurate laboratory spine took longer to develop than anticipated, so that more progress could not be achieved with the accurate geometry spine model.

## 6.1 Accurate geometry modelling

The geometry of the lumbar vertebrae was obtained by computer tomography (CT) and the actual lumbar curve presented in Chapter 3 was used for defining the overall model geometry. The intervertebral discs were then defined so that they had the same surface profile as the adjacent bodies. The development of the spine model is explained by figure 6.1.

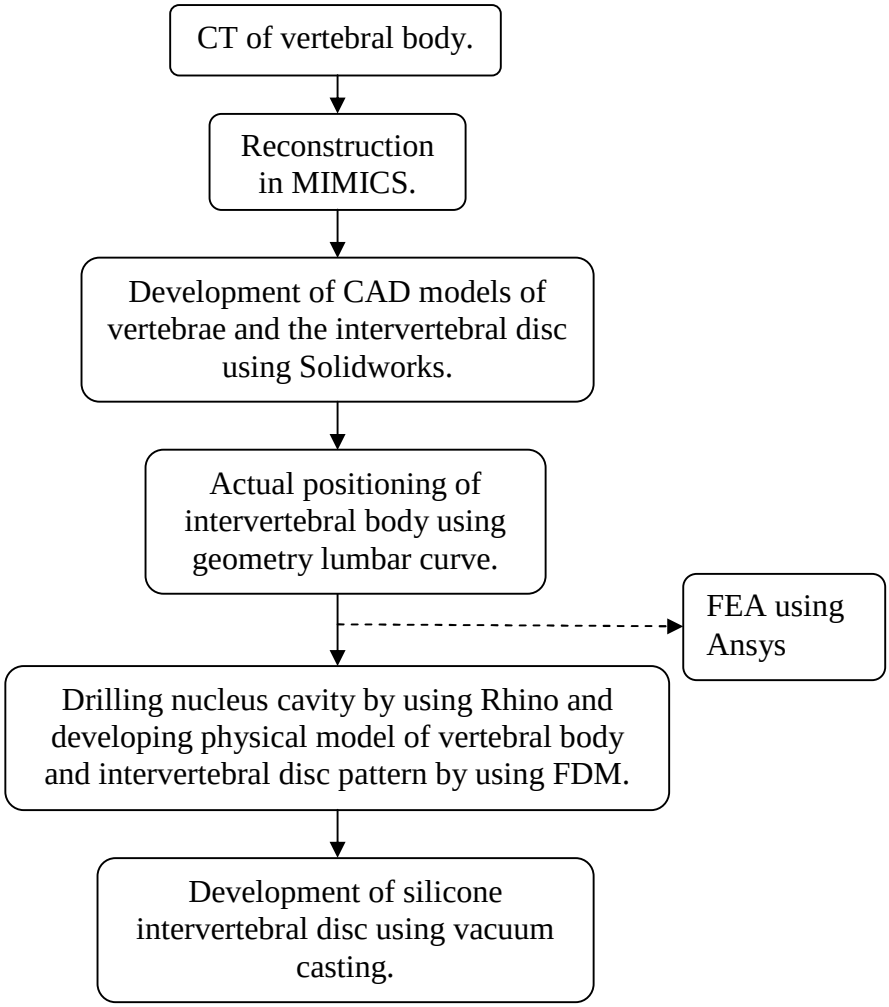


**Figure 6.1 Flowchart for development of vertebral and intervertebral bodies.**

## 6.2 Manufacture of the vertebral bodies.

The CT (Toshiba's Aquilion 32-slice CT scanner, USA; Installed at Hull Royal Infirmary, UK, 2003) images of vertebrae were scanned on the local hospital scanner and the resultant data loaded into MIMICS (Materialise, Leuven, Belgium), which converts the CT images (.tif) into the solid models (.stl). Stereolithography (.stl) files of each vertebrae were then created for input into the rapid prototype, fused deposition method (FDM), as in figure 6.2

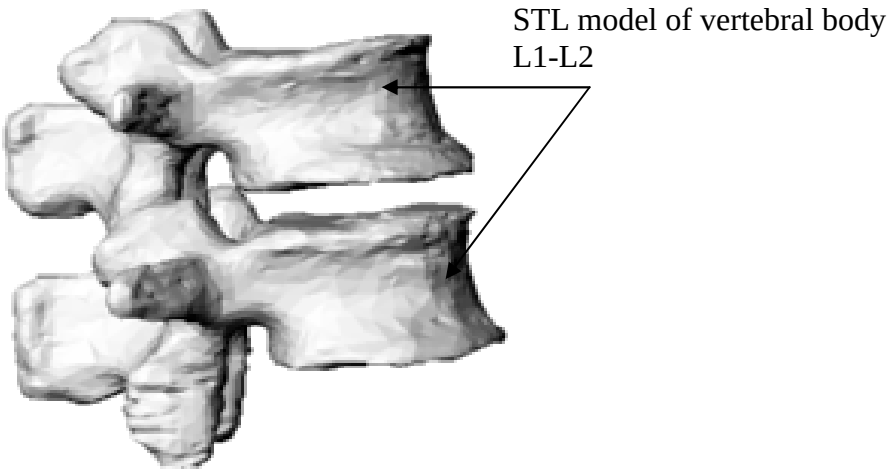


**Figure 6.2 STL models of L1-L2.**

The machine used was a Stratasys (FDM 200mc) provided in the Department of Engineering, Hull University's Design Enterprise Centre (DEC).

Fused deposition moulding (FDM) is a rapid prototyping technique involving the heated marker (i.e. nozzle), which layers the material with the data supplied by the software. The layering takes place in extruded form as compared to other techniques. Figure 6.3 adapted from Zein et al (2002) shows the FDM process.

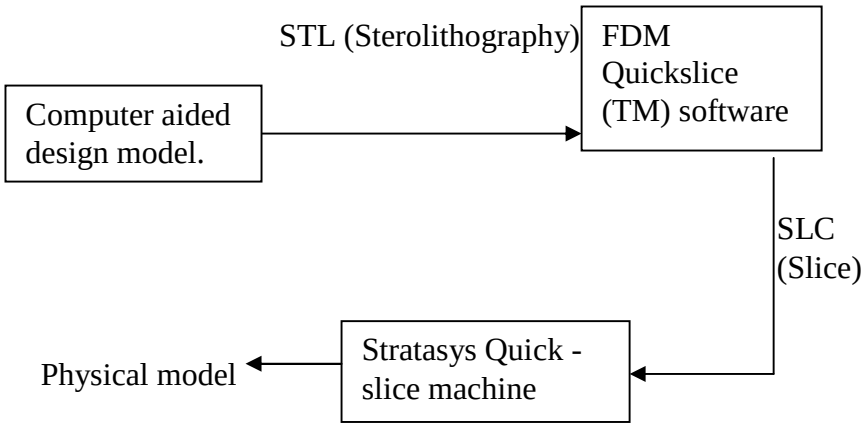


**Figure 6.3 FDM process**.

A three dimensional model was generated using a 3-D CAD package such as Rhino (Rhinoceros, USA, 2002) and Solidworks (Solidworks, USA, 2005) saved in STL

format as a polymesh. The accurate geometry vertebral and intervertebral bodies can be analysed by using Ansys (Ansys, USA, 2003), using the .stl files of the models.

The model was then exported to the FDM Quickslice software (Stratasys, USA, 2003), which generates SLC format data that was imported into the Stratasys Quickslice machine. The SLC file format is a contour representation of a CAD model. It consists of successive cross-sections taken at ascending intervals in which solid material is represented by interior and exterior boundaries. SLC data can be generated from various sources, either by conversion from CAD solid or surface models or more directly from systems that produce data arranged in layers i.e. Quickslice(TM) software. Thus prototypes of Lumbar 1 and 2 as shown in figure 6.4 were developed. The material used was a standard Acrylonitrile-Butadiene-Styrene copolymer, called ABS P-400 used for the simplified model discussed in Chapter 4. For FDM parts using ABS P-400 made with 0.0635– 0.0762 mm overlaps between layers; the tensile strength ranges from 65 to 72% of that of injection moulded ABS P-400 while the compressive strength is 80 to 90 % greater than injection moulded ABS P-400 (Zein et al, 2002). The strength of the vertebral bodies is enough for the application, i.e. to compress the intervertebral discs.

**Figure 6.4 FDM model of L1 and L2**

## 6.3 Manufacture of the intervertebral discs.

The manufacturing of the intervertebral discs was complicated because they needed to have exactly the same shape as the adjacent intervertebral disc. In addition, with a long-term goal to pressurize the discs, they have to make intimate contact with the vertebrae so the surfaces can be sealed. Thus there were various stages in their

development, Stage 1 consisted of a simplified foam model. Stage 2 consisted of a disc with similar geometry to the vertebral body with a flat surface profile that could not perfectly match the irregular surface profile of the vertebral bodies. Finally in stage 3 a rapid prototype process generated the intervertebral discs, so that they had an identical surface profile to the vertebral bodies above and below. The development of stage 3 intervertebral discs took a long time, as the actual lumbar curve was also considered. Firstly an ABS replica of each disc was manufactured, and this was used as a mould for a silicone casting. The vacuum casting process was also carried out in the DEC using vacuum casting machine (MCP 4/01).

The casting process involved the making of a silicone tool that consists of runners (i.e. the channel to supply the resin into the cavity), a gate (i.e. the path which is connected to the runner to supply the resin), air vents (i.e. the small cavity used to make the resin breathe while it fills) and the parting line i.e. the line or area that separates the two regions. The intervertebral disc pattern was held at a set distance with a parting line and runners as shown in figure 6.5, which was a channel located at a parting line between the silicone tool to route the casting material into the cavity. An accurate and detailed description of the manufacture of the silicone tool is included in Appendix A.

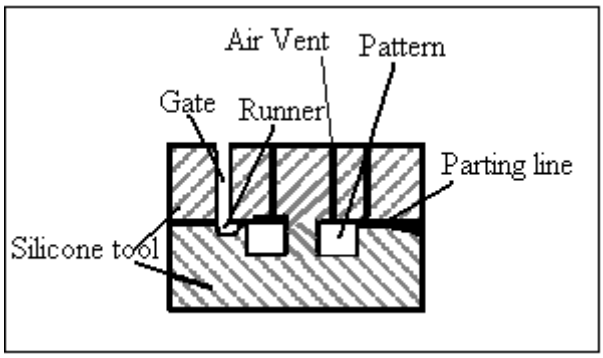


**Figure 6.5 Silicone tool with runner and intervertebral disc pattern.**

A photograph of the final mould for one of the discs is shown in figure 6.6 with the hopper in which the filler material (Silicoset 101) is poured. The entire arrangement is placed on an adjustable table and enclosed in a vacuum chamber. Figure 6.7 shows the two halves of the mould with a Silcoset 101 disc. The silicoset disc is shown in one of the halves, which can be removed smoothly.

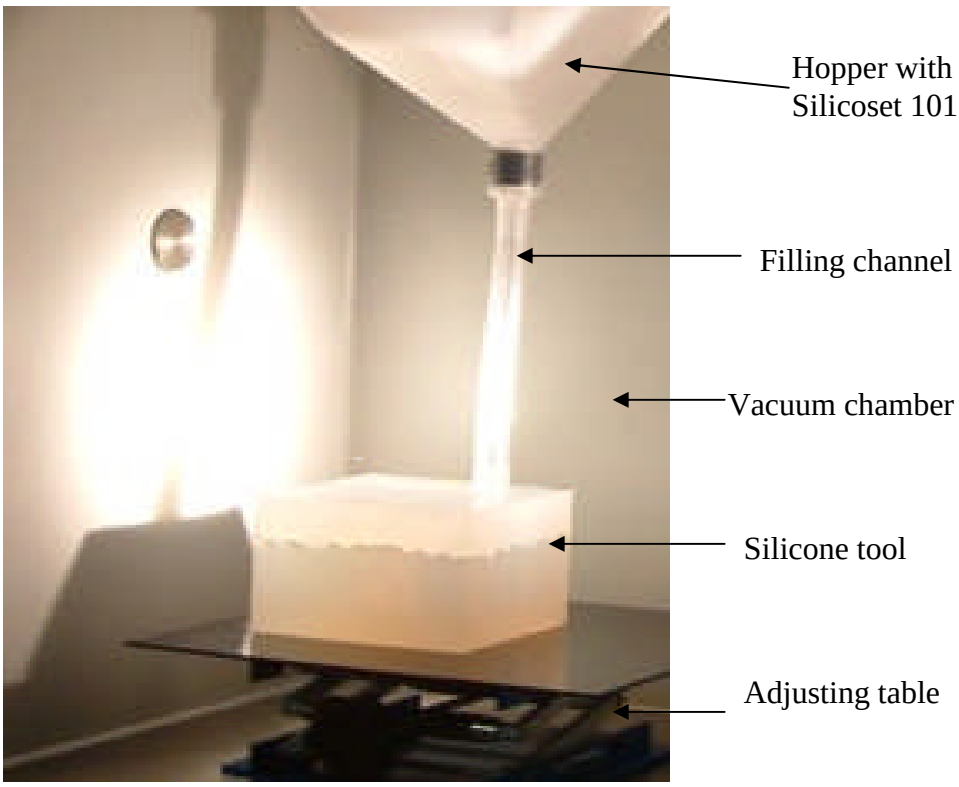


**Figure 6.6 Vacuum casting showing the silicone mould.**

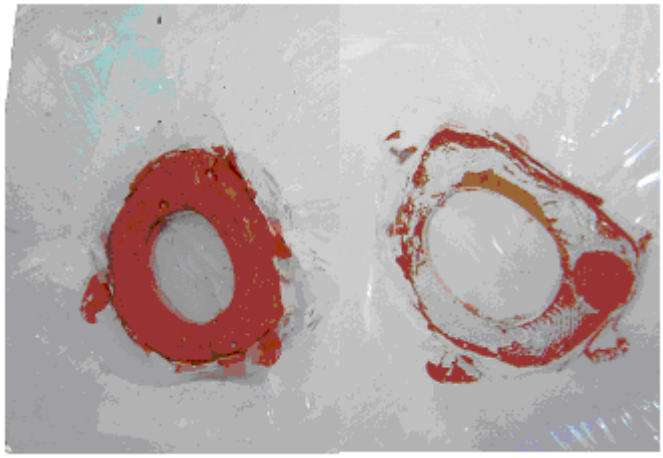

**Figure 6.7 Silicone tool with vacuum cast of intervertebral disc.**

## 6.4 Discussion

Figure 6.8 shows a complete motion segment consisting of two vertebrae and a disc. The intervertebral disc is firmly fixed in between the surfaces of the vertebral bodies.

**Figure 6.8 Vertebral body and intervertebral disc**

Description of figure with material configurations for assembly of vertebral and intervertebral disc.

Material: ABS P400 for vertebral body and Silcoset101 for intervertebral disc.

Processes: Stereolithography (FDM) for vertebral bodies and vacuum casting process for intervertebral disc.

The irregular shape of the intervertebral body was manufactured with the silicone tool shown in figure 6.7 by vacuum casting as discussed in Section 6.4 with the steps mentioned in Appendix A. The entire assembly has an interference fit between the two vertebral bodies due to the identical surfaces between them.

# CHAPTER 7
# DISCUSSION

## 7.1 Introduction

The NHS report (2002) discussed in Chapter 1, describes lower back pain as the most common problem after the common cold, occurring in four out of every five individuals. The pain and disabilities caused by disorders of the spine can range from an inconvenience, to a severe life changing debilitation. The TSSA report (2001) and CSAG survey (1993) showed that lower back pain is not entirely age dependent, and is a major loss to the UK economy, due to the loss of working days.

The structural, mechanical and biological properties of the lumbar spine and muscles were outlined in Chapter 2 with an analysis of lower back problems, showing that the causes are mainly due to intervertebral disc or mechanical tissue failure. The lumbar spine is involved in most of the mechanical movements of the body, and acts as a key building block around which a very complex and intricate network of biological tissue operates. In addition to the tissues, the lumbar spine is also surrounded by very sensitive spinal nerves that form an integral component of the spinal structure. The mechanical failures explained as spinal disorders or lower back problems of the spine are as varied and numerous as its integral components. The extreme degenerative disc discussed in Chapter 3, can produce very significant pain, arising from concentric or radial tears, or possibly producing a pressure on the spinal nerves. The vertebral bodies are also prone to injuries such as spondylolisthesis and spinal stenosis that cause geometrical hindrances, again inducing pressure on spinal nerves. Even the ligaments and muscles attached to spinal elements are innervated, and thus pain can emanate from strains, ruptures and tears within these entities.

Due to the complicated lumbar structure with its integrated musculature and functional complexity, it is not surprising that the current methods of treatment are limited. Currently there are major surgical interventions for treating conditions related to the degenerative disc, namely, discectomy, fusion and replacement. The first two solutions produce relatively acceptable, but short term, results with surgical treatment that alters the biomechanics of the spine, possibly leading to further degeneration of

the adjacent tissues and the discs. Alternatively, the degenerated disc can be replaced with an artificial disc that is designed to replicate the physiological range of motions. So there has been an increasing demand for spinal surgery and a growing number of new spinal implants and surgical procedures being offered by orthopaedic surgeons. The testing of spinal implants and spinal instrumentation is problematic, with testing in cadavers and animals becoming increasingly difficult and both having significant limitations.

Thus the long-term aim of this research is to develop a representative artificial laboratory spine that will have the same physical and biomechanical properties as the human spine, which can eventually be made available for the testing of new implants.

This chapter discusses the progress towards the development of an artificial laboratory spine with the same physical and biomechanical properties as the natural lumbar spine. The results have already been discussed to some extent within the previous chapters and so only a general overview is presented here.

The intervertebral discs for the laboratory spine and the active muscles move the spine in a way similar to that of the actual lumbar spine. When this physical model is operated within the parameters presented in Chapters 4 and 5, it appears that it can perform effectively to produce the necessary output. Chapter 4 presented a simplified model which showed physiologically similar behaviour to other literature showing motion of cadaveric and sheep models which were discussed in Chapter 3. In addition a geometrically more realistic model of the lumbar spine developed from the CT data of patients is discussed in Chapter 6, which includes representative lumbar curves and other parameters.

## 7.2 Simplified laboratory spine

Chapters 4 and 5 focused on the modelling and development of the simplified geometry laboratory spine with different materials, methods and design parameters. The study also dealt with the functional working of the artificial muscle recruitment, generating loading configurations that can be used for validating the models. The muscle forces causing vertebral movements in different directions (discussed in Section 2.5) provide a challenging stability problem. The key mechanical requirement can be considered to be the intervertebral discs of the lumbar spine, with muscle and elastic elements having agonist and antagonist activation. Thus the simplified laboratory spine model consists of vertebral bodies, intervertebral discs, muscle actuators and springs. The literature discussed the antagonistic activation of muscles

and spring elements (as discussed in Chapter 3), which are created in the model as muscle wire with biasing springs attached to the processes.

The simplified vertebral body using ABS (P400) plastic is shown in figure 7.1, with protruding processes, which can be assumed to be beams. The loading applied consists of the muscle forces ($F_m$) inclined at angle α, the stabilizing (spring force) $F_s$, and the horizontal and vertical reactions and moment of the vertebral body. Thus the motion observed for each motion segment of the simplified model is both rotational and translational.

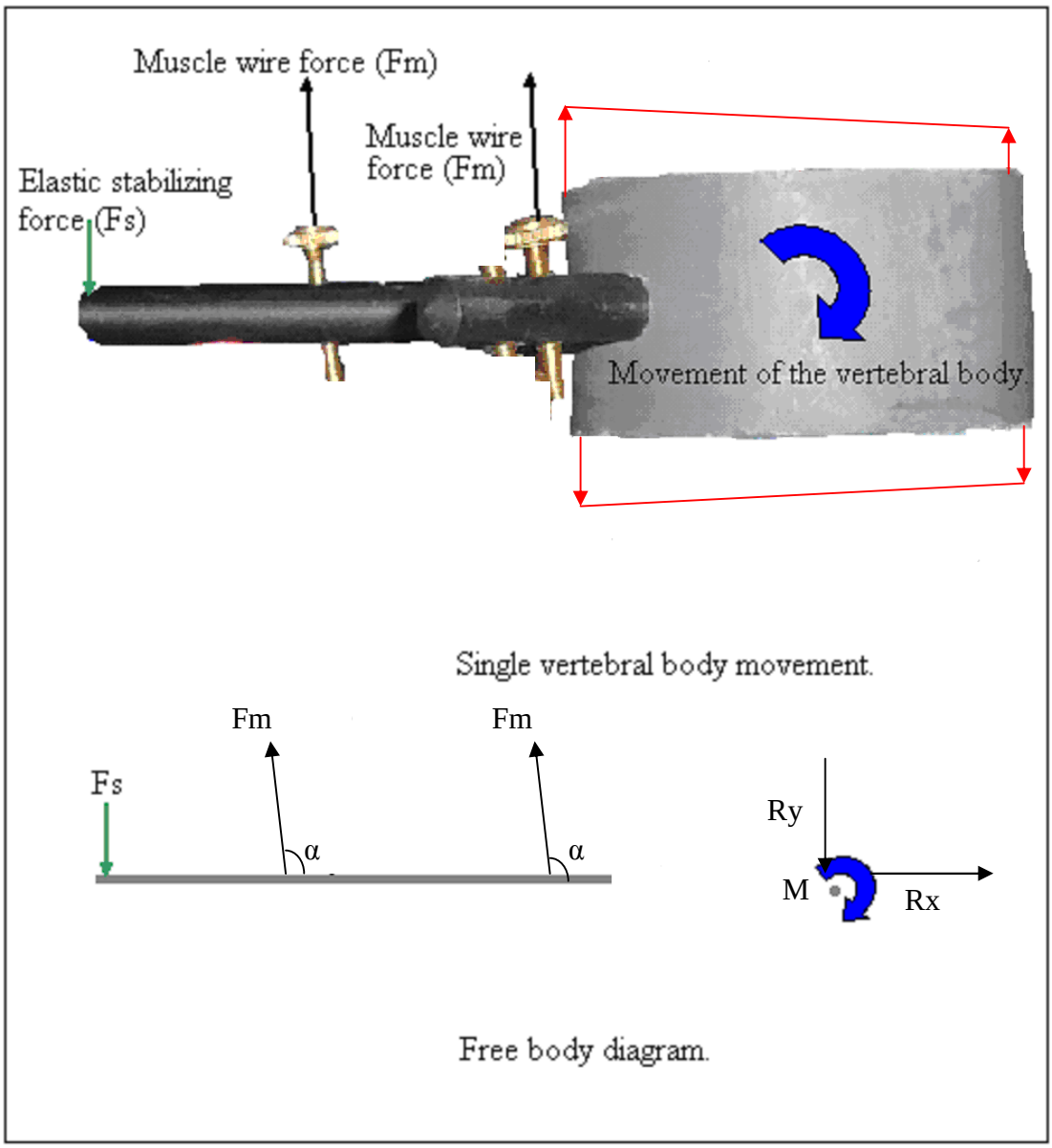


**Figure 7.1 Beam model of vertebral body with FBD.**

The full free body diagram (FBD) of muscle force and biasing spring force is shown in figure 7.1. The model has two reactions and a moment, i.e. vertical reaction Ry and

a horizontal reaction Rx and a moment M. The application of material around the foam increased the stiffness of the foam when in tension, with the criss-cross design limiting the angular rotation for the same loading conditions.

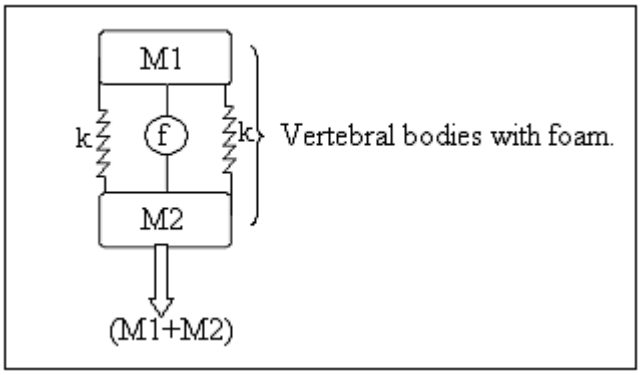


**Figure 7.2 Simplified lumbar spine models with foam acting as intervertebral disc.**

The simplified lumbar spine model shown in figure 7.2, has muscles and spring components (k) causing expansion and contraction that acts in an antagonistic pairing with the dampers or stabilizers of the intervertebral bodies (f) as shown in figure 7.2. The control mechanism has two masses (M1- the top load and M2 – the lower body load), where the muscle causes an unbalanced loading in M1, which is transferred to M2.

Shape memory wire has been used as the active muscles, with different configurations providing variable moments to the vertebral bodies. The force exerted depends on the dimensions of the wires, their pretension and biasing force. During the motion segment testing, in Chapter 5, the control motions were the result of activation of muscles connected to the vertebral bodies. The different muscle recruitment regimes for the shape memory muscle were controlled by a Matlab programme. The antagonistic motion relieves the stress on the intervertebral disc tissue. Although there are anatomical limitations to the overall actual motions and response of the model, it is first of its kind showing simplified lumbar spine with physiologically controlled vertebral bodies.

The performance of the physical and FE model, and the different motion segments, were discussed in Chapter 5, and shown to compare very well. The intervertebral disc behaviour in the physical spine shown in Chapter 4 and FE model in Chapter 5 shows comparable disc behaviour with force causing motion of the nucleus movements. These when compared with placing a spirit level on the physical spine model, the bubble in the spirit level moved as discussed in Chapter 2, which is

from the elastic zone to neutral zone. Also the recorded vertebral bodies in extension showing movements though using single fibre muscles and limited intervertebral disc geometry for physical model; its comparable with the literature discussed in Table 3.2 and 3.3 has angular displacements to human and animal's data with different fibres attached to their vertebral bodies.

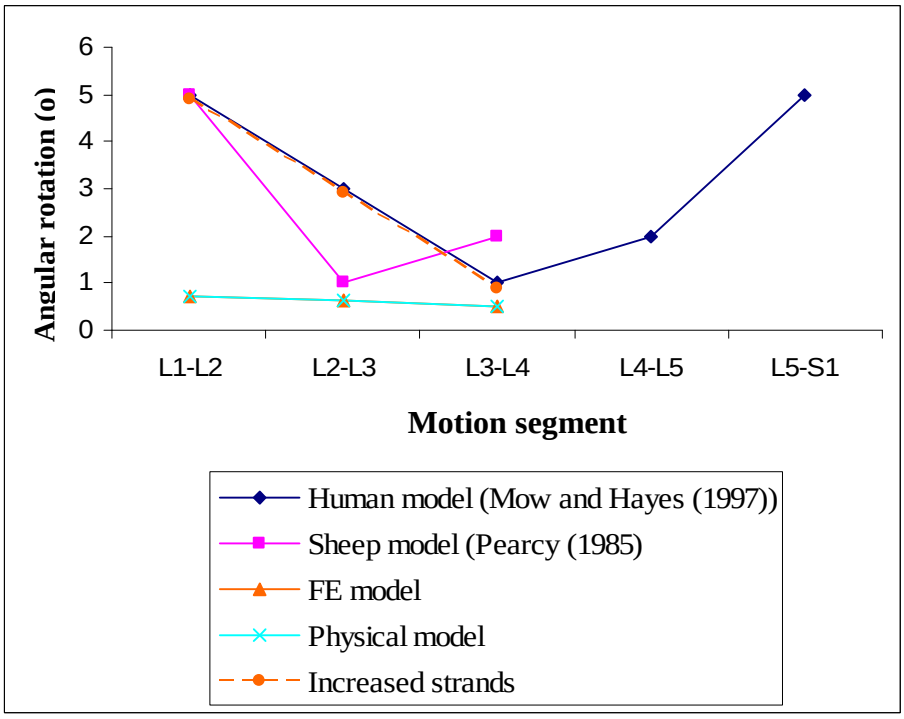


**Figure 7.3 Variations in angular displacements showing extensions in different motion segments of simplified laboratory spine.**

Figure 7.3 shows the behaviour for different motion segments with various loading configurations (i.e. activations of muscles). The FE and physical model displacement, with limited intervertebral disc properties and single wire muscle loading, generate output that is less than the other models – but of the right order. Using more wires in parallel could increase the angular displacement. For example, 5 strands would give a displacement of approximately $5^{o}$, which is similar in the human model shown with the dotted line for an increased strand FE model.

## 7.3 Actual geometry spine

The start of the development of an artificial spine with accurate vertebrae and disc geometries was described in Chapter 6. The vertebral bodies were created by rapid prototyping with the same geometry as the natural human spine. The intervertebral

discs were cast using a vacuum casting technique. This allowed the disc to adopt the complex surface geometries of the end plates of the vertebrae.

# CHAPTER 8
# CONCLUSION

The first part of the thesis discussed the development of a simplified physical model with active muscles. Much of the work was carried out simultaneously with evaluation and testing of the material properties and optimization of the model parameters (Chapter 4) and compared with the FE models (Chapter 5). The second part of the thesis (Chapter 6) focused on the accurate geometry model with realistic geometries for the vertebral bodies and intervertebral discs. It took much longer to develop the simplified spine model than initially expected and analyse the results; and although much of this is applicable to the accurate geometry model, progress with the development of the accurate spine model has only been very limited. It is this model that could then be used to test the implants used for spinal instrumentation.

The intervertebral disc properties and artificial muscles developed for the simplified model from the literature review (Chapter 2) and an overview of the technology (Chapter 3) have helped in the design of the simplified physical model. The material selection for the intervertebral disc from the literature in Table 4.1 and testing was experimentally verified as shown in Chapter 4. In the end PU-foam (polyurethane foam) was selected, with a Young's modulus of 26.67 MPa. The simplified muscle architecture consists of segmented muscles that are connected as single fibres - compared to bundled muscle fibre shown in figure 2.7. These muscles are connected to the various transverse processes and generate perpendicular and parallel components as discussed in Section 2.5 causing the complex motions seen in the natural spine. Springs are applied in parallel to the muscle wires which act as ligament stabilizers, to allow the vertebrae to regain their normal positions and maintain an antagonist mode of action. The biomechanical model of the individual muscle fibres shows the spinal stability depends on the architecture of the loading in which the tissue stability depends on the muscle tone and can be changed in the physical model with the turnbuckle type connectors. The muscle tone in the human spine will be altered with changes in physical fitness and with tissue adaptability depending on age. The muscle adaptability (tone of muscles) for artificial spine

models could be greatly improved by optimizing the angle and the number of fascicle that participate for any activity.

A control system was developed to control the individual muscles of the spine model, while equivalent temperature controlled (thermal contraction) muscles were developed for the FE model. In the FE model the thermal contraction coefficient was calculated from the slope of the temperature displacement curve for the shape memory wire (and found to be $13.662 \times 10^{-6}$ m/$^{o}$C). The effectiveness of the system was examined experimentally with the model's stability. In which the muscle forces acting in an antagonist motions causes the travel of the bubble in the spirit level, which moves around the elastic, zone and returns back to the neutral zone.

The simplified spine model appeared to have a physiologically reasonable response to the loading when applied by the antagonist pairs of shape memory muscles and spring elements, and produced reasonable angular rotations compared to the *in vivo* values reported in the literature, although greater muscle forces are required to produce sufficiently large values. The model also mimics the motion of the spine under repetitive dynamic loading with the switching ON and OFF of the muscles, where the response to extensor segmental muscle recruitment is a transient function depending on the geometrical parameters. This variable transient function reduces the stress in the discs. The stability analysis for the applied loading demonstrated by the observed movements helps to understand the lumbar biomechanics, the soft tissue and control system. These movements in the laboratory model include the muscle wires, in contrast to in vivo studies carried out with cadaveric samples, in which the tissue is dead and stiffer. Thus the simplified model with active muscles should be a better representation of the natural lumbar spine.

The nerve impingement discussed in Chapter 2 was observed to be a direct function of the vertebral foramen and the translatory movement observed by the cosine component ($F_2$) of the muscle force actuators shown in figure 4.15, and the effectiveness of the intervertebral joint is reflected by the maintenance of the contact between the components of the motion segments. Disorders in the form of increased displacement are the main cause of destabilization *i.e.* painful movements. The varying muscle force causes unregulated muscle components, which can be altered by the variable current causing the non-linear stress distribution and unstable motions in the vertebral bones.

The main contribution includes the development of an accurate geometry laboratory spine, with the development of methods for the manufacture of

physiologically accurate intervertebral discs and vertebral bodies. The muscle wire methods, successfully applied to the simplified spine model, now need to be applied to this more accurate model, with braided wires to increase the muscle forces. Once these activities have been completed, a reasonable active laboratory spine with many applications in the development of spinal prostheses and instrumentation as well as surgical education and training will be available.

# CHAPTER 9
# FUTURE WORK

The development of an accurate geometry laboratory spine has started, but still there are many options for its development. The next step is to attach larger muscles to the processes of the simplified vertebral bodies and to combine the modelling discussed in this thesis, to produce a more realistic model of the lumbar spine. This can then be used to model the accurate movements and optimise the configuration and control of the laboratory spine models.

The method of attaching the muscle wires in the simplified model could be applied to the vertebral bodies. Also, this could be easily modelled using finite elements with material properties representing the bone, disc and muscle materials. All these results can then be validated by the production of stereolithography (STL) models of the structures. Additionally, more vertebral and intervertebral bodies can be manufactured using the technique discussed. The intervertebral disc can also be developed further and pressurised to make it more realistic and allow the effect of aging to be examined in the future.

Other developments include the attachment of the flexor muscles and more extensor muscles as shown in Figure 2.6, and researching and addressing the comparison of variation in the model and the literature.

Finally, detailed modelling plans have been discussed so that the spinal devices can be tested to quantify the behaviour (Chapter 3).

# REFERENCES

**Achuthan A. Kengkok A. Ming WC. 2001.** Shape control of coupled nonlinear piezoelectric beams. Smart Material and Structure, 10, 914-924.

**Back.com. 2001.** Anatomy (Retrieved: 15 Nov. 2004)- ww.back.com/anatomy.html

**Back Care 2004**, (Retrieved: 19th Nov. 2004) Back pain can affect us all, The prevalence of back pain in Great Britain, 1998. Department of Health. www.backcare.org

**Benner G. Morris JM. Lucas DB. 1962.** An elecromyographic study of the intrinsic muscles of the back in man. Journal of Anatomy, 4, 509-520.

**Belytschko T. Kulak RF. Schultz AB. Galante JO. 1974.** Finite element stress analysis of an intervertebral disc. Journal of Biomechanics, 7, 277-285.

**Bhattacharyya A. Lagoudas DC. Wang Y. Kinra VK. 1995.** On the role of thermoelectric heat transfer in the design of SMA actuators, theoretical modelling and experiment. Smart Materials and Structure, 4, 252-263.

**Biomechanics BME/ME. 2003.** (Retrieved: 10th Oct. 2003) Structure and function of ligaments and tendons. www.engin.umich.edu/class/bme456/ligten/ligten.htm

**Biomechanics of lifting. 2004.** (Retrieved: 15th Dec. 2004) Effects of force on L5-S1 joint surface. University of Oklahoma, Health Science Centre. http://moon.ouhsc.edu/dthompso/namics/lift.htm

**Bogduk N. and Twomey LT. 1997.**Clinical anatomy of the lumbar spine and sacrum, (3rd Edition), Churchill Livingstone publication. ISBN 0-443-06014-2.

**Bogduk N. Johnson G. Spalding D. 1997.** The morphology and biomechanics of latissimus dorsi. Clinical Biomechanics, 13, 377-385.

**Briggs JP. and Ostrowski JP. 2002.** Experimental feed-forward and feedback control of a one dimensional SMA composite. Smart Materials and Structure, 11, 9-23.

**Brown T. Hansen RJ and Yorra AJ. 1957.** Some mechanical tests on the lumbosacral spine with particular reference to the intervertebral disc. Journal of Bone and Joint Surgery, 39-A, 1135-1164.

**Burcsu E. Ravichandran G. Bhattacharya K. 2003**. Large electrostrictive actuation of barium titanate single crystals. Journal of the Mechanics and Physics of Solids, 16, 643-650.

**Burnett AF. Barett CJ. Marshall RN. Elliott BC. Day RE. 1998.** Three-dimensional measurement of lumbar spine kinematics for fast bowlers in cricket. Clinical Biomechanics, 13, 574-583.

**Choi JB. Lee YJ. Choi BY. 2004.** Fast Preisach modelling method for shape memory alloys actuators using major hysteresis loops. Smart Material and Structures, 13, 1069-1080.

**Cholewicki J, Juluru K, McGill S. 1999.** Intra-abdominal pressure mechanism for stabilizing the lumbar spine. Journal of Biomechanics, 32, 13-17.

**Cohen YB. 2001.** Transition of EAP material from novelty to practical applications- are we there yet? EAPAD, SPIE's 8th Annual International Symposium on Smart Structures and Materials. 4329-4402.

**Crone WC. Yahaya AN. Perepezko JH. 2002.** Bulk shape memory NiTi with refined grain size synthesized by mechanical alloying; Material Science Forum, 386: 388, 597-602.

**CSAG (Clinical Standards Advisory Group) report on back pain, 1993,** (Retrieved: 12th Jan. 2004) Available: www.osteopathonline.com/backpain.htm

**Dean C. and Pegington J. 2002.** Core Anatomy Vol:1- The limbs and vertebral column. W B Saunders Publication. ISBN 0-7020-2040-0.

**DEC. 2004.** (Retrieved: 25th Jan. 2004) Rapid prototyping, FDM user manual. Mike Poole, Design enterprise centre. http://www.hull.ac.uk/dec/rapid_prototyping.htm

**Dieen JH. Selen PJ. Cholewicki J. 2003.** Trunk muscle activation in low back pain patients, an analysis of literature. Journal of Biomechanics. 13, 333-351.

**Dynalloy Technical report. 2004**. Technical characteristic report of Flexinol actuator wires, Dynalloy Inc. of Dynamic Alloys.

**Eberlein R. Holzapfel GA. Frohlich M. 2004,** Multi-segmental FEA of the human lumbar spine including the heterogeneity of the annulus fibrosus. Computational Mechanics. 34, 147-163.

**Fagan MJ. Julian S. Siddall DJ. Mohsen AM. 2002.** Patient-specific spine models. Part 1: Finite element analysis of the lumbar intervertebral disc-a material sensitivity study. Proceedings of the Institution of Mechanical Engineers, Part H, Journal of Engineering in Medicine. 216, 5, 299-314.

**Fazey PJ. Song S. Monsas A. Johansson L. Haukalid T. Price RI. 2006.** An MRI investigation of intervertebral disc deformation in response to torsion. Clinical Biomechanics. 21, 538-542.

**Floyd WF. and Silver PH. 1955.** The function of the erectors spine muscles in certain movements and postures in man Journal of physiology. 129, 1, 184-203.

**Fung YC. and Pinto J. 1993.** mechanical properties of muscles. (Retrieved on 26 March 2005). http://www.exb.ucdavis.edu/faculty/hawkins/126site/chp7.pdf.

**Gilbertson RG. Miranda C. Tuchman M. 2003.** Muscle wire project book, Mondo-tronics Publication. ISBN 1-879896-14-1.

**Gillespie P. Siddall DJ. Fagan MJ. 2001.** A finite element analysis of the lumbar invertebral disc – a material sensitivity study. Fifth International Symposium of computer methods in Biomedical engineering in Rome 2001.

**Goel VK. Gilbertson LG. Kim YE 1995.** Effects of injury on the spinal motion segments in the axial compression model. Clinical Biomechanics. 4, 161-167.

**Gorbet RB. and Russell AR. 1995.** A novel differential shape memory alloy for position control . Robotica, 13, 423-430.

**Gracovetsky SA. Zeman V. Carbone AR. 1987.** Relationship between lordosis and the position of the centre of reaction of the spinal disc. Journal of Biomedical Engineering, 9, 237-248.

**Grant D. and Hayward V. 1998.** Vibration isolation with high strain shape memory alloy actuators: case of the impulse disturbance. Proc-Intel. Mechanical Engineering Congress and Exposition. 229.

**Gray H. Pick TP. 1987.** Gray's anatomy, (15th edition) Chancellor Press, London.
ISBN 0-517-22365-1

**Gregg H. 2000.** A new work-seat for commerce and industry: Design and evaluation strategies. PhD thesis for University of Nottingham.

**Heidari B. FitzPatrick D. Synnott K McCormack D. 2004.** Modelling of annuls fibrosus imbalance as an aetiological factor in adolescent idiopathic scoliosis. Clinical Biomechanics, 19, 3, 217-224.

**Heremans J.1983.** A capacitive instrument for the measurement of magnetostriction in pulsed control. . (Retrieved on 28 March 2005) Journal of Physics for Engineers: Scientific Instruments. 16. www.npl.co.uk/materials/functional/magneto/magneto_index.html.

**Hill D. 1938.** The heat of shortening and dynamic constants of muscle. Journal Physiology, 136-195.

**Holman JP. White PRS. 1993.** Heat transfer. McGraw Hill publications. ISBN 0-07-112644-9.

**Hoppenfeld S. 1976.** Physical examination of the spine and extremities. Retrieved on 26 March 2005. Prentice Hall publications, London. ISBN 0-8385-7853-5.

**Hyo JL. and Lee JJ. 2003.** Time delay of a Shape memory alloy actuator. International Journal of Robotic Results, 10:1, 13 - 20.

**Iida T. Abumi K. Kotani Y. Kaneda K. 2002.** Effects of aging and spinal degeneration on mechanical properties of lumbar supraspinous and interspinous ligaments. The Spine Journal, 9, 95-100.

**Ikuta K. Tsukamoto M. Hirose S. 1991.** Mathematical model and experimental verification of shape memory alloy for designing micro actuators. Journal for Institute of Electrical and Electronic Engineers . 10, 103-108.

**Jackson RP. Peterson MD. McManus AC. Hales C. 1998.** Compensatory spinopelvic balance over the hip axis and better reliability in measuring lordosis to the pelvic radius on standing lateral radiographs of adult volunteers and patients. Spine, 23, 16, 1750-1767.

**Jaink TJ. Harrison DD. Cailliet R. Troyanovich SJ. Harrison DE. 1998.** Can the sagittal lumbar curve be closely approximated by an ellipse? Journal of Orthopaedic Research 16, 6, 766-770.

**Jaink TJ. Harrison DD. Cailliet R. Troyanovich SJ. Harrison DE. Holland B. 1998.** Elliptical Modelling of Sagittal Lumbar Lordosis and segmental rotation angles as a method to discriminate between normal and low back pain subjects, Journal of Spinal Disorders, 11, 5, 430-439.

**Janda S. Valenta J 2000.** Mathematical model of the lumbar spine Journal of Mechanical Engineering, 51, 2, 1-6.

**Jemmett RS. MacDonald DA. Agur AMR. 2004.** Anatomical relationships between selected segmental muscles of the lumbar spine in the context of multi planar segmental motions: a preliminary investigation. Manual Therapy, 9, 203-210.

**Jorgensen MJ. Marras WS. Gupta P. 2003.** Cross-sectional area of the lumbar back muscles a function of torso flexion. Clinical Biomechanics, 18, 280-286.

**Kahn H. Huff M A. Heuer A H. 1998.** The TiNi shape-memory alloy and its applications for MEMS. Journal of Micro-Engineering, 8, 213-221.

**Kuribayashi K. 1991.** Improvement of the response of an SMA actuator using a temperature sensor. International. Journal of Robotic Results, 10,4, 18 - 24.

**Kulak RF. Belytschko TB. Schultz AB. 1976.** Non linear behaviour of the human intervertebral disc under axial load. Journal of Biomechanics, 9,6, 377 - 386.

**Lagoudas DC. and Bhattacharyya A. 1998.** A modelling of thin layer extensional thermoelectric SMA actuators. International Journal Solid Structure, 35, 331-362.

**Lee Spring. 2005.** Engineering guide. Design and specification manual for springs. BS 1726.

**Lueder RK. 1993.** Humanics ErgoSystem report. Virginia Polytechnic Institute and State University. . (Retrieved on 29 December 2005) http://humanics-es.com/humanics.pdf

**Lavaste F. Skalli W. Robin S. Camille RR. Mazel C. 1992.** Three-dimensional geometrical and mechanical modelling of the lumbar spine. Journal of Biomechanics. 10, 1153-1164.

**Luo H. Abel E. Hewit J. Steele RJC. Slade A. Wang Z. 2003.** Development of a two way shape memory actuator for transanal endoscopic surgery. Applied Simulation and Modelling. Conference proceedings in Spain 2003. 573-577.

**Ma N. and Song G. 2003**. Control of shape memory alloy actuator using pulse width modulation. Smart Material and Structure, 12, 712 – 719.

**Nae M. Song G. Lee HJ. 2004.** Position control of shape memory alloy actuator with internal electrical resistance feedback using neural network. Smart Material and Structure, 13, 777-783.

**Machado LG. Savi MA. 2003.** Medical applications of shape memory alloy. Brazilian Journal of Medical and Biological Research, 36, 683-691.

**Madden JD. Vandesteeg N. Madden PG. Takshi A. Zimet R. Patrick A. Lafontaine SR. Wierenga PA. Hunter IW. 2004.** Artificial muscle technology physical principles and naval prospects. Report from Naval research group report, USA, 2004.

**Madill DR. 1993.** Modelling and stability of shape memory alloy position control system. Masters thesis, University of Waterloo, Canada.

**Martini FH. Ober WC. Garrison CW. Welch K. Hutchings RT. 2001.** Fundamentals of Anatomy and Physiology. Prentice Hall Publication, ISBN 0-13-017292-8.

**Mow VC. and Hayes WC. 1997.** Basic Orthopaedic Biomechanics. Raven Press, New York.

**McGill SM. Hughson RL. Parks K. 2000.** Changes in lumbar lordosis modify the role of the extensor muscle. Clinical Biomechanics. 15, 777-780.

**Menciassi A. Gorini S. Pernorio G. Dario P. 2004.** (Retrieved: 1st Feb. 2005) A SMA actuated artificial earthworm. IEEE International Conference on Robotics and Automation ICRA 2004. http://www.ics.forth.gr/bioloch/docs/Bioloch_ICRA04.pdf

**Molly MM. Blume. 2001.** (Retrieved: 25 Jan. 2004) Oh my aching back! Vertebral disc and the effect of aging. EN 175.
http://www.engin.brown.edu/courses/en175/project%2001/miller.htm

**Moore KL. Agur AMR. 2002.** Essential Clinical Anatomy, Lippincott Williams & Wilkins Publication, ISBN 0-7817-2830-4.

**Morra F. Molfino R. Cepolina F. 2004.** (Retrieved: 1 Nov. 2004) Miniature gripping device. IEEE International conference on intelligent manipulation and grasping IMG 04, Italy. www.cepolina.com

**Nachemson AL. and Evans JH. 1968.** Some mechanical properties of the third human lumbar interlaminar ligament (ligament flavum). Journal of Biomechanics.1, 211- 220.

**Najarian S. Dargahi J. Heidari B. 2005.** Biomechanical effects of posterior elements and lingamentous tissues of lumbar spine on load sharing. Bio-Medical Materials and Engineering. 15, 145-158.

**NHS report. 2002.** (Retrieved: 15 Dec. 2004). The prodigy guidance – lower back pain. www.prodigy.nhs.uk/guidance.asp?gt=backpain-lower.

**Noordeen H. Elsebaie H. Crockard A. Winter R. Lonstein J. Taylor B. Soames R. Renton P. Tucker S. and Crisco J. 2001** Interactive spine: Primal Pictures Ltd. London, ISBN 1-902470-32-X.

**Noordeen H. Elsebaie H. Crockard A. Winter R. Lonstein J. and Crisco J. 1997**. Primal Pictures Ltd. London.

**NPL.2003.** Magnetostrictive materials. (Retrieved: 12th Nov. 2004). www.npl.co.uk/materials/functional/magneto/magneto_index.html.

**Panjabai M. 2003.**Clinical spinal instability and low back pain. Journal of Electromyography and Kinesiology.13, 371-379.

**Pearcy MJ. Tibrewal SB. Portek I. Spivey J. 1985.** A prospective study of lumbar spinal movements before and after discetomy using biplanar radiography. Correclation of clinical and radiographic findings. Spine. 10, 5, 455-460.

**Polikeit A. Lutz LP. Nolte P. Stephen SJ. Ferguson J. 2003.** Simulated influence of osteoporosis and disc degeneration on the load transfer in a lumbar functional spinal unit. Journal of Biomechanics.37, 1061-1069.

**Potvin JR. Stephen HM. Brown. 2005.** An equation to calculate individual muscle contributions to joint stability. Journal of Biomechanics, 30, 973-980.

**Rathel. RS. McCrary WS. Callahan NR. 2007.** Gauge repeatability and reproducibility studies and measurement system analysis: a multi exploration of the state of practice. Journal of Industrial Technology, 23, 1.

**Ren J. Liew KM. 2005.** Mesh free modelling and simulation of the thermo-mechanical behaviour of shape memory alloys.. Smart Material and Structure, 14, 302-311.

**Reuber M. Schultz A. Denis F. Spencer D. 1982.** Bulging of lumbar intervertebral disc. Journal of Biomechanical engineering, 104, 3, 187-192.

**Reference planes. 2007.** National institute of technology and evaluation. Top Human characteristic database, Basic matters [Reference planes]. Retrieved: 12th Nov. 2007. http://www.tech.nite.go.jp/human/eng/contents/cindex/referencedevelop.html

**Roglin RL. and Hanagud SV. 1996.** A helicopter with adaptive rotor blades for collective control. Smart Material and Structure. 5, 76- 88.

**Rohlmann A. Wilke HJ.Neller S. Graichen F. Claes L. Bergmann G. 2005.** A novel approach to determine muscle forces during flexion and extension**.** Spine, 28, 23, 2585-2593.

**Rohlmann A. Bauer L. Bergmann G. Zander T. Wilke HJ. 2006.** Determination of trunk muscle forces for flexion and extension by using finite element model of lumbar spine and measured in vivo data. Journal of Biomechanics, 39, 6, 981-989.

**Rohsenow WM. and Hartnett JP. 1973.** Handbook of heat transfer, 7-20. ISBN 0-07-053576-0.

**Sasaoka R. Azegami H. Murachi S. Kitoh J. Ishida Y. Kawakami N. Makino M. Matsuyama Y. 2003.** Investigation of buckling phenomenon induced by growth of vertebral bodies using a mechanical spine modal, Japan Society of Mechanical Engineers International Journal, Series C (JSME Int.). 46, 4,1382-1387.

**Schmorl G. and Junghanns H. 1971.** The human spine in health and diseases. 2nd American Education for Grune & Stratton, New York, 18-20.

**Seroussi RE. Karg MH. Muller DL. Pope MH. 1989**. Internal deformations of intact and decneuleated human lumbar discs subjected to compression, flexion and extension loads. Journal of Orthopaedic Research. 7, 122-131.

**Shekelle PG. and Delitto AM. June – 2005.** Treating low back pain. The Lancet 365: 9476, 1987-1989.

**Shirazi-Adl A. 2006.** Analysis of a large compression loads on lumbar spine in flexion and in torsion using a novel wrapping element. Journal of Biomechanics, 39, 267-275.

**Shirazi-Adl, Sadouk S, El-Rich M, Pop DG, Parnianpour M. 2002.** Muscle forces evaluation and the role of posture in human lumbar spine under compression. European Spine Journal, 11, 519-526.

**Shirazi-Adl. Shrivastava SC. Ahmed AM. 1984**. Stress analysis in the lumbar disc body unit in compression. Spine, 9. 120-134.

**Shu SG. Lagoudas DC. Hughes D. and Wen JT. 1997.** Modelling of a flexible beam actuated by shape memory alloy wires. Smart Material and Structure, 6, 265-277.

**Shirley D. Hodges PW. Eriksson AE. and Gandevia SC. 2003.** Spinal stiffness changes throughout the respiratory cycle. Journal of applied Physiology, 95, 4, 1467 - 1475.

**Siddall DJ. 2003**. Patient specific spine models: The development of a laboratory validation spine. PhD disst., University of Hull.

**Simon BR. Wu JSS. Carlton MW. Evans JH. Kazarian LE. 1985.** Structural models for human spinal motion segments based on a poroelastic view of the intervertebral disc. Journal of Biomechanical Engineering,107, 327-335.

**Snell RS. 2004.** Clinical Anatomy. Lippincott Williams and Wilkins publication.

**Song C. Campbell PA. Frank TG. Cuschieri A. April – 2002.** Thermal modelling of shape memory alloy fixator for medical application. Smart Materials and Structure, 11, 312-316.

**Spencier D. ScM Pe. Greene D. Paiva J. Palumbo M. Crisco. 2006**. The multidirectional bending properties of the human lumbar intervertebral disc. The Spine Journal, 6, 248- 257.

**Spine Universe. 2004.** Ligaments support the spine. (Retrieved: 06 Nov 2005). http://.spineuniverse.com/displayarticle.php/article1303.html

**Spine-health. 2005.** Back muscles and low back pain. Spine health.com. (Retrieved: 07 Nov 2005). www.spine-health.com/topics/anat/a005.html

**Sterkenburg SWP. 1992.** The electrostriction of silicon and diamond. Journal Physics D: Applicational Physics, 25, 996-1003.

**Steuwer A. Hall DA. Withers PJ. Mori T. 2006**. Analysis of domain switching and elastic lattice strain in ferroelectric ceramics. SRMS -5 Conference, Chicago July 30 to August 2, 202.

**Stokes IAF. Morse GM. 2004.** Muscle activation strategies and symmetry of spinal loading in the lumbar spine with scoliosis. Spine, 29, 19, 2103-2107.

**Thomas LC. 1980**. Fundamentals of heat transfer, Prentice-Hall, Inc, ISBN 0-13-339903-6.

**Thompson RE. Pearcy MJ. Barker TM. 2004.** The mechanical effects of intervertebral disc lesions. Clinical Biomechanics.19, 448-455.

**Troisfontaine N. Bidaud P. Larnicol M. 1999.** Optimal design of micro actuators based on SMA wires. Smart Material Structure. 8, 197-203.

**Tsai KH. Chang GL. Lin HT. Kuo DC. Chang LT. Lin RM. 2003.** Differences of lumbosacral kinematics between degenerative and induced spondylolisthetic spine. Clinical Biomechanics. 18, S10-S16.

**TSSA Rep's bulletin. 2001. (Ref: H& S / 011 / May2001.).** Technical standards and safety authority report on back pain**.**

**Valdevit A. and Errico TJ. 2004.** Design and evaluation of the FlexiCore metal-on-metal intervertebral disc prosthesis. Spine, 4, 9, 276S-288S.

**Valerie I. 1998.** The Penguin Dictionary of Electronics. Penguin books,(3rd Edition) ISBN 0-14-051402-3.

**Van CM. and Hayes CW. 1997.** Basic Orthopaedic Biomechanics. Lippincott Raven Publication, ISBN 0-397-51684-3.

**Velazquez R. Pissaloux E. 2005.** (Retrieved: 11th Nov. 2005) Design of shape memory alloy helical springs using force and time response criteria. http://www.jussieu.fr/publications

**Wagner H. Andres Ch. Puta Ch. Petrovitch A. Morl F. Schilling N. Witte H. Blickhan R. 2005.** Musculoskeletal support of lumbar spine stability Pathophysiology, 12, 257-265.

**Wang Q. and Arora J. 2004.** Optimization based formulations for simulation and design of dynamic digital human models. University of Iowa, Phd thesis.

**Wayman CM. RW Cahn. P Haasen. 1983.** Phase transformation, no diffusive physical metallurgy. New York: North Holland, 1031-1075.

**Weinstein JN. Rydevik BL. Sonntag VKH. 1995.** Essentials of the spine. Ravens Press, New York.

**Whiting WC. and Zernicke RF. 1998.** Biomechanics of musculoskeletal injury. Human Kinetics, Publications. ISBN 0-87322-779-4.

**Xiao DC. Case K. Acar BS. Porter JM. 1998**. Computer Aided Modelling of human spine. Presented in 14th National Conference of Manufacturing Research, USA' 98.

**Yang S. and Kam B. 2002**; Finite element analysis of lumbar spine: linear and nonlinear static analysis. Louisville University thesis.

**Yamamoto I. Panjabai M. Oxland T. Crisco J. 1989.** How does posture affect coupling in the lumbar spine? Spine.14, 1002-1011.

**Zee M. Hansen L. Andersen TB. Wong C. Rasmussen J. Simonsen EB. 2006**. On the development of a detailed rigid body spine model. Journal of Biomechanics International Congress on Computational Bioengineering, USA 2006.

**Zein I. Hutmacher DW. Tan CK. Teoh SH. 2002**. Fused deposition modelling of novel scaffold architectures for tissue engineering applications. Biomaterials. 23, 1169 – 1185.

**Zhou LM. and Lau KT. 2001**. Investigation of strengthening and strain sensing techniques for concrete magnetostrictive structure using FRP composites and FBG sensors. Material and structure. 34, 42-50.

# APPENDIX

## Appendix A

Casting silicone with the MCP vacuum casting machine.

Method

To prepare the mould for the disc.

1. The cardboard box or a wooden box with (30-40 % more area than the basic pattern size is built). The box should have a required height for sustaining the rise and fall of silicone, during degassing is described in activity 1.
2. The box is taped with magic tapes at all ends so that no leakages are left in the box.
3. The box should fit the cavity inside the machine (lower chamber).
4. The pattern for the intervertebral disc is sprayed with the release agent.
5. The pattern is glued with the gate and is placed at the centre of the box. The various air vent rods are glued at edges of the pattern.
6. The silicone rubber is mixed and the crystallization state is changed by putting it inside the oven at 70$^{o}$C for 2 hrs.
7. The component A and B are mixed together in a jar.
8. The mixing jar is then degassed in the chamber. The operation is carefully monitored as the rubber rises and falls five times its original height.
9. Casting the rubber in the moulding box.
10. The moulding box is then, kept in the vacuum chamber for degassing. Until the air bubbles are completely released.
11. Then the mould is cured in the oven at 40$^{o}$C in the box overnight.
12. After the overnight cooking the box is opened and the pattern of the intervertebral disc is removed.

The moulding and casting procedure used by the MCP vacuum casting machine is divided into the following segments.

Activity 1.

1. The disc replica is manufactured using a FDM process.
2. The cardboard box or a wooden box. (30-40 % more area than the basic pattern size is built) The box should have a required height for sustaining the rise and fall of silicone, during degassing. The size of the cardboard box used for making one disc is 125x115x110 mm. The box is taped at all ends and corners so that theirs no leakage left in the box. The box should fit the cavity inside the machine (lower chamber).
3. The cleansing spirit is used to clean the surfaces of the disc and the release agent is sprayed on the disc surface.
4. Establish the disc's surface with a parting line using clear adhesive tape (magic tapes) and colour the tape edge with a marker pen to later assist in removing the disc from the silicone tool.
5. Casting gates are attached to the disc and the disc is suspended in the cardboard box or casting frame and venting rods are attached.

Activity 2.

1. The silicone rubber K E 1300 T is generally poured out from the container.
2. Weight of silicone,
   The weight of silicone = $Volume \times (allowance = 1.1)$ = 1.739375 ~ 2 Kgs.
3. The catalyst used, generally in the ratio of 10: 1. The weight of the catalyst calculated was 0.173 ~ 0.2kgs or 200gms.
4. The bucket is wiped with the catalyst into the inner periphery, using the pro food hand gloves only with a little cloth. Careful not to spill it over your self.

5. Scale the bucket before scaling the silicone rubber.
6. Mix the silicone rubber and catalyst thoroughly in the bucket for 4 to 5 min.
7. The size of the bucket should be always 5 times the size of silicone and catalyst in the bucket.
8. *Primary Degassing* Place the container in the vacuum chamber and apply the vacuum. As the silicone rubber will expand approximately five times in volume, it is essential to watch the operation carefully until primary degassing is complete. When the level of rubber reaches the top of the container, press the 'Fast leak' control once or twice to reduce the level in the container. Generally, the primary degassing is done for 8 to 10 min after the level of liquid in the container suddenly collapses.
9. After the degassing, pour the degassed mixture slowly, allow it to flow at the bottom and then slowly on the top.
10. *Secondary Degassing* Place the mould in the vacuum chamber and carry out the same degassing procedure as described above in segment 2 (8). The secondary degassing time is generally 10 to 25 min.
11. The lower furnace temperature should be at 40$^{o}$C. For e.g. keep the furnace for nearly an hour, and then the doors are kept open to allow it to cool down for about 5 to 10 min.
12. The silicone rubber is the kept in the oven at 40$^{o}$C for over night cooking to melt all the silicone.
13. Separate different part of the box for e.g. the box is then removed apart. To make it more convenient for a user it is better to draw a line just around the parting line and by carefully using the scalpel and mould openers the silicone rubber tool is cut into two halves. Remember to cut only once just up to the parting line.

Activity 3.

1. The silicone tool is taped tighter and prepared for casting.
2. The amount of resin can be calculated as per the weight of disc.

$$Weight = (disc, weight) \times (specific, gravilty) \times (allowance = 1.5)$$

3. Silcoset and its catalyst are mixed in ratio of 10:1 and are placed in the cups A and B. They are precisely measured by weight into their respective containers. Always remember to add the Silicoset premier.
4. When the resin is ready, place the mould in the vacuum chamber and the cups are placed in the upper chamber.
5. Attach to the funnel by means of the flexible hose connectors to the gate of the tool.
6. Raise and lower the mould to the correct position by means of the lift.
7. Ensure both the cups are positioned correctly and the blending whisk is securely located.
8. Before starting make sure that the upper and lower doors are properly closed.
9. The exact procedure for manual working is given as below,

Pump (speed 2)

↓

Degas (Run 10 min)

↓

Run

↓

Cup A Down (8 sec) and Cup A Up (Speed 3)

↓

Mixing Run Degas (1min)

↓

Cup B Down (8 sec) and Cup B Up (Speed 3)

↓

Fast (2 min)--- Slow Pump (3 min)

↓

End.

10. After carrying out the casting operation, lower the lift and remove the plastic horse tube.
11. The mould is then cooked in the oven between 65 to 70$^{o}$C for 8 to 10 hrs or may be overnight.
12. While the component is removed to avoid the deformities the casted disc is cooked for nearly 30 min between 65 to 70$^{o}$C.

Activity 4.

Different resins have different perpetration technique, the material data and safety data sheet should be read before the preparation procedure is read and then compared.

1. The resins component B is liable to crystallise at low temperature. So they are both stored at 25$^{o}$C.
2. Check for crystallization in data sheet, generally component B seems to be more crystallised.
    - If component A and B does not seem to be more crystallised then replace the plastic stoppers and place both cans in oven for 2 hrs at 65 to 70$^{o}$C.
    - If component B is crystallised then keep in the furnace or oven for 4 hrs at 65 to 70$^{o}$C.
3. Primary degassing is done in the vacuum chamber.
    - Remove the cans from the oven or furnace and shake it or stir it.
    - Empty each cans into a cup of vacuum casting, fitted with cup liners, and place as far as possible, to avoid any cross contamination. Remember to indicate A and B marks.
    - Switch on the vacuum and leave the materials for approximately two hours.
    - Degassing is complete when bubbles are no longer visible.
    - After degassing the components are stored in the oven at 40$^{o}$C.
    - Due to delay as of any reason, then degassing is carried out again.
4. Calculating the amount of resin: (to calculate the amount of resin required for the disc the disc is measured (Similar to segment 3, 2)).
5. The data sheet should be referred for the resin temperature.

<u>Precautions:</u>

a. Remember to apply a load on the casted silicone foams.
b. The mixture should be handled with utmost care.
c. Aqueous soap solution should be applied for cups and cavity.
d. Always check that both resin components and the mould are in position before attempting to mix and cast.
*e.* Keep your hands out of the vacuum chamber while any of the mechanisms are operating.
*f.* Proper cleaning solvents should be used to remove any stains.

## Appendix B

Casting of silicone foam using Med-6382S (Mat M), R-2370 (Mat R).
Method and time:

| | |
|---|---|
| 1. Silicone material is poured and thoroughly stirred with a stirrer.<br>Mat R = 7gms. | 40 sec |
| 2. Silicone material is poured and mixed continuously. Mat M = 7 gms. | 40 sec |
| 3. Both are mixed together with continuous stirring.<br>Mat M&R = 8 & 2 gms respectively. | 50 sec |
| *Remember:* Be as quick as possible and keep stirring continuously. | 120 sec |
| 4. All apparatus should be systematically arranged.<br>(The handling time is just 300 sec. Once the catalyst is mixed) | 10 sec |
| 5. Mixing and continuous stirring are required. | 30 sec |
| 6. Addition of release agent into the cavity | 10 sec |
| 7. Pouring of the mixture into the cavity for casting. | 40 sec |
| 8. Settling down time for optimum physical properties. | 24 hrs. |

Precautions:

1. Remember to apply a load on the casted silicone foams.
2. The mixture should be handled with utmost care.
3. Aqueous soap solution should be applied for cups and cavity.

## Appendix C

/*Calculation of heat transfer coefficient for one SMA wire of 375 μm wire with operating temperature between 70 and 90°C*/

```
clear all
 velocity_fluid = 1;
 t_surr = 20+273;
 number_of_wires = 1;
 % enter the value of which force, n the exerted force value.
 tmartenite = 70+273;/* in Kelvin*/
 taustenite = 90+273;
 t=150;
 tdiff = (taustenite-tmartenite);
 diameter_wire = 375E-3;
/*Force calculations equation
Force produced by muscle wire = Maximum recommended weight wire can hold x C/S area.
Thus, Force produced by an ideal single muscle wire = 1.10 N */
force = number_of_wires*(pi/4)*diameter_wire*diameter_wire*10;
/* Now, the heat transfer calculations, refer Chapter 3*/
 t_init_wire=tmartenite;
 t_film=(t_surr+t_init_wire)/2;
 length_wire=0.093;
 k_wire=1.5E01;
 cp_wire=770;
 rho_wire=6450;
 rho_air=1.224;
 area_wire=(0.25*pi*diameter_wire^2);
 vol_wire=number_of_wires*(area_wire*length_wire);
 surface_area_wire=number_of_wires*pi*diameter_wire*length_wire;
 k_air=0.0253;
 cp_air=1005;
 t_lookup=[250 290.00 330 400];
 dens_air_lookup=[1.413 1.224 1.076 0.883];
 dyn_vis_air_lookup=[1.61e-5 1.807E-5 1.99E-5 2.294E-5];
 spec_heat_air_lookup=[1003 1005 1007 1013];
 thermal_conduct_air_lookup=[0.0223 0.0253 0.0283 0.0331];
 rho_air=interp1(t_lookup,dens_air_lookup,t_surr);
 mhu_air=interp1(t_lookup,dyn_vis_air_lookup,t_surr);
 k_air=interp1(t_lookup,thermal_conduct_air_lookup,t_surr);
 k_air_film=interp1(t_lookup,thermal_conduct_air_lookup,t_film);
 cp_air=interp1(t_lookup,spec_heat_air_lookup,t_surr);
 rey_lookup=[4 40 4000 40000 40E4];
 c_lookup=[0.989 0.911 0.683 0.193 0.027];
 m_lookup=[0.330  0.385  0.466  0.618 0.805];
 re=rho_air*velocity_fluid*diameter_wire/mhu_air;
 pr=cp_air*mhu_air*rho_air/k_air;
  n=(1/3);
 c=interp1(rey_lookup,c_lookup,re);
 m=interp1(rey_lookup,m_lookup,re);
nud=c*(re^m)*(pr^n);
h_air_film=k_air_film*nud/diameter_wire;
 power=((h_air_film * surface_area_wire * (tdiff))-(rho_wire*cp_wire*vol_wire*(t_film -
t_surr)*1/t))*1e-3;
 fprintf('\n\n Thus, shape memory wire dia = %d  with heat tranfer coefficient = %d Watt/mm^2 K and
number of wires = %d, Force produced =  %5.2f N \n , power =%5.2f mWatt \n', diameter_wire,
h_air_film, number_of_wires, force, power);
```

/*Interpolation for air properties*/ [1]

/*Example for Matlab programme with simplified calculation for heat transfer coefficient (hc). Activation of the shape memory wires occurs by increasing the wire temperature, wire

diameter = 375 µm = 0.375 mm. The heat transfer coefficient can be calculated considering the temperature difference and the heat convected to air. There are some interpolations for calculating the properties of air as shown above in [1].

These properties are then feed into equation, which results out the Nusselt number (a constant) further using, $hc = k/d \times Nu$.

Thus, shape memory wire dia = 375 with heat transfer co-efficient =7.02 Watt/mm$^2$ K and number of wires.= 1, Force produced = 1.10, Power = 1.12 Watt*/

## Appendix D

/*Mat-lab programme for activation of wires as shown in figure 4.23.*/

```
function z=wireON(s)
[a,b]=EdigitalOut(-1,0,s,1,1);
disp(['Wire ' num2str(s) ' ON'])
function z=wait(2)
disp(['wait ' num2str(s) 's'])
t=clock;
while(etime(clock,t)<(2))
end
function z=wireAllOFF
disp('All Off')
for s=1:16
   [a,b]=EdigitalOut(-1,0,s,1,0);
end
wireAllOFF
wireON(1)
wait (1)
wireON(2)
wait (2)
wireON(3)
wait (3)
wait (1)
wait (2)
wait (3)
wireOFF(1)
wireOFF(2)
wireOFF(3)
wireAllOFF
```

/*For switching on wires 1,2 and 3 */

For switching on wires 1, 2 and 3 with a waiting time of 16 sec between each wire.

# Development of an active artificial laboratory lumbar spine

A Swamy, M J Fagan
Medical Engineering, Department of Engineering, University of Hull, HU6 7RX.

## Abstract

Low back pain is an extremely common condition, but very difficult to diagnose and to treat. Computer models may help in the diagnosis, but need validation. This paper describes the development of an artificial laboratory spine to be used in validation of these computer models.

The vertebrae of the artificial spine are exact replicas of vertebral bodies, manufactured by rapid prototyping methods; the intervertebral discs are manufactured from silicone rubber and can be pressurized to simulate normal intra-discal pressure, while the muscles are manufactured from Flexinol wire, a shape memory alloy. The spine is currently being assembled and should be ready for testing in the laboratory soon.

## Introduction

Low back pain is seen in different age groups as a major cause of absenteeism, physical disability and one of the highest contributors to compensation claims across the globe. In the UK over 1 million people are disabled by it, and in 1997-8, over 119 million days a year were lost due to registered disability caused by back problems. 13% of unemployed people say that back pain is the reason they are not working. The cost of back pain to the NHS and through lost production is in excess of £5M. (Department of Health, 1999).

Diagnosis of back pain requires detailed imaging of the patient's spine in realistic positions and loading conditions, but with the current technology this is currently possible. The scans have to be taken with the patient in supine position, when the spine is unloaded. The long term goal of this research is to develop a new technique whereby patient specific spine models are developed from standard scan data, loaded and then used to modify the original images of the spine and surrounding soft tissues to reveal the movement of patients spine under loading.

Validation of this approach is difficult and hence an active artificial laboratory spine is being developed to assist in this process. In the first instance, work is concentrating on the lumbar spine, since that is where the majority of back pain occurs. It is anticipated that the laboratory spine will have a number of other applications in particular in assessment of spinal instrumentation.

## Development of the artificial spine

The lumbar spine consists of five vertebral bodies with an intervertebral disc between each pair of vertebral bodies and follows a lumbar curve. Changes in the lumbar curve and pelvic orientation affect the distribution of gravity and other external loads acting on the spine, and influence its stability and loading of its components and the surrounding soft tissues. The intervertebral disc is the most critical component of the spine, as it provides the means by which the spine can move.

The development of laboratory spine is taking place in two steps, involving the development of a model with simplified geometry and an anatomically accurate model. Both models incorporate silicone-based (Silcoset-101) intervertebral discs which have previously been shown to provide a reasonable representation of the actual discs (Siddall 2003, Fagan et al. 2001). The intervertebral discs can also be pressurised, as occurs in the natural disc.

The vertebral bodies are generated from CT data by a rapid prototyping technique using a Stratasys Fused Deposition Modelling (FDM) machine with ABS P-400 resin (figure 1). Generation of the discs also uses rapid prototyping, with the disc models produced so that they perfectly replicate the inferior surface and superior surface profiles of the vertebral bodies. A casting of the disc is then taken in an MCP vacuum casting machine which produces an accurate silicone copy of the disc, which sits perfectly on the adjacent vertebrae (figure 1).

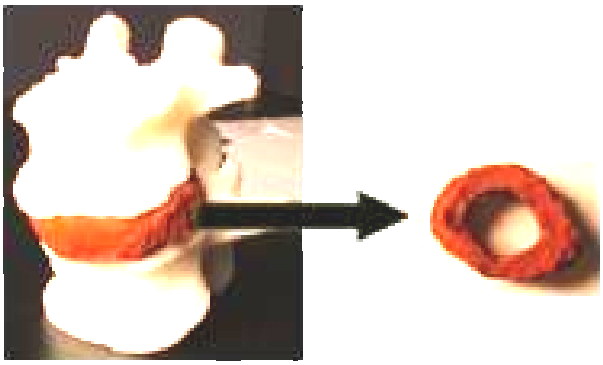

**Figure 1.**
Picture of part of the accurate laboratory spine model. With ABS vertebrae and a Silicone intervertebral disc.

Artificial muscles are now being developed and attached to the vertebral bodies. These are developed from Flexinol wire, a nickel–titanium shape memory alloy, which contracts when an electric current is passed through it. This occurs because a change of phase from austenite to martensite occurs when it is heated. The maximum force that a wire can exert depends on its cross-sectional area, length, convection heat transfer coefficient, the alloy composite and its refined grain size (Troisfontaine 1993 et al). The wires are available in a range of sizes, and a series of studies has been undertaken to quantify and calibrate the wires to be used in the artificial spines. Figure 2 shows the force generated by different muscle wire configurations.

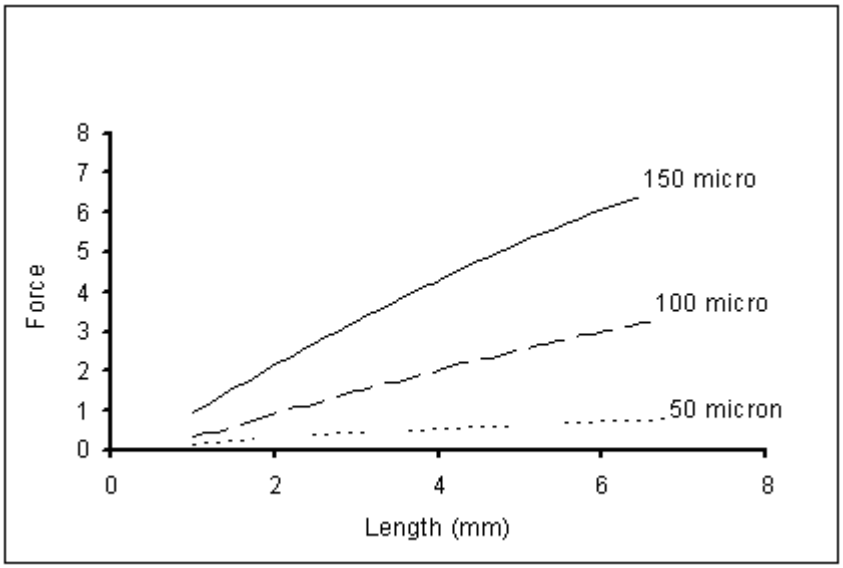


**Figure 2.**
Variation of Flexinol (muscle) forces with different wire diameters and number of strands length.

## Discussion

Development of the vertebrae and intervertebral discs of the simplified and anatomically accurate spine models is nearing completion. Characterisation of the Flexinol muscle wires is complete and work has started on the attachment of the muscles to the simplified spine model. Design of the electronic control mechanism to actuate the different muscles of the spine is now underway so that different spinal motions can be achieved. It is anticipated that testing of the spines in the laboratory should start soon.

## References


- Fagan MJ, Gillespie P, Julian S, Siddall S, Mohsen A. 2001. Development of an artificial intervertebral disc for a laboratory test spine. Journal of Biomechanics 34:S1, 58-59.
- Siddall DJ, 2003. Patient specific spine models: The development of a laboratory validation spine. PhD Thesis, University of Hull.
- The Prevalence of Back Pain in Great Britain in 1998, Dept. of Health Statistical Bulletin 1999/18.
- Troisfontaine N, Bidaud P, Larnicol M, 1999, Optimal design of micro-actuators based on SMA wires. Smart Mart. Struct. 8, pp 197-203



**Acknowledgements**
We are grateful to Mike Poole, formerly of the Design Enterprise Centre, for his assistance in manufacturing the components of the spines.